ACRONYMS, ABREVIATIONS, NAMES OF SATELLITES/INSTRUMENTS

This list is far from complete in the field of satellite meteorology but hopefully contains the most frequently encountered terms.

APT	Automatic Picture Transmission. Generally refers to low spatial resolution imagery directly broadcast by a satellite. Such imagery usually has lower grey-scale resolution than digital data.
ARGOS	The French automatic location and data collection system carried on the TIROS-N spacecraft.
ASDAR	Aircraft to Satellite Data Relay. A system for automatically transmitting observations of wind and air temperature made on commercial aircraft via the data-collection system of a geostationary meteorological satellite.
ATN	Advanced TIROS-N. An enlarged version of the TIROS-N spacecraft, to carry research instruments.
AVHRR	Advanced Very High Resolution Radiometer. The visible and infra-red imaging instrument on the TIROS-N satellites.
CTH	Cloud Top Height. An image product from Meteosat in which grey-scale relates directly to height of highest cloud tops.
CZCS	Coastal Zone Colour Scanner. A very high resolution multi-channel visible (and infra-red) imager, flown on NIMBUS-7.
DCS	Data Collection System. The telecommunications system on a satellite for receiving messages from DCPs. Often refers to the system on GOES and other geostationary satellites, but can refer to satellite instrument for ARGOS.
ERB	Earth Radiation Budget. Normally refers to an instrument for measuring incoming solar radiation and outgoing fluxes with wide and narrow field-of-view in many spectral channels. Flown on Nimbus 6 and 7 (See ERBE and ERBS).
ERBE	Earth Radiation Budget Experiment. A planned experiment to fly ERB instruments on two ATN spacecraft and ERBS, in order to investigate sampling problems in satellite measurements of radiation budget (particularly diurnal variations).
ERBS	Earth Radiations Budget Satellite. An experimental satellite which forms part of ERBE. It will carry an ERB and be placed in an orbit which processes, to obtain observations at varying local solar time.
ESA	European Space Agency.
ESOC	European Space Operations Centre. The ESA facility at Darmstadt which includes the Meteosat central ground station.
DCP	Data Collection Platform. A telecommunications package for transmitting environmental data to a satellite.

GAC	Global Area Coverage. A reduced resolution form of AVHRR which is tape-recorded, replayed in USA, and used to produce mosaics etc.
GMS	(sometimes GEMS) Name of Japanese geostationary meteorological satellite. GMS-1 launched July 1977, still operating.
GOES	Geostationary Operational Environmental Satellite. The USA geostationary met satellite(s). GOES-1 to -4 are in orbit.
GOSSTCOMP	Global Operational Sea Surface Temperature Computation. NOAA/NESS's operational scheme for retrieving SSTs from polar orbiting radiometer data.
HCMM	Heat Capacity Mapping Mission. A NASA satellite, launched 1978, carries a high resolution infra-red (and visible) imager in an orbit such that observations are at 02 and 14hr local time (ie near minimum and maximum of diurnal temperature cycle.).
HIRS	High resolution Infra-red Radiation Sounder. Infra-red temperature sounding instrument, flown on Nimbus-6.
HIRS/2	"Mark 2" version of HIRS (and normally now just called HIRS), which is the infra-red temperature sounder on TIROS-N.
HRPT	High Resolution Picture Transmission. The high spatial resolution image data stream directly broadcast by the US polar orbiting satellites.
IFOV	Instantaneous Field of View. The angular field of an instrument or the area on the earth surface defined by this angle. Normally applies to an instrument which can scan its field of view (eg with a rotating mirror).
IR	Infra-Red
ITOS	Improved TIROS Operational Satellite. The US polar-orbiting meteorological satellites prior to TIROS-N. Last member was called NOAA-5.
JMA	Japanese Meteorological Agency.
LIMS	Limb Infra-red Monitor of the Stratosphere. A cryogen-cooled limb-scan radiometer for obtaining profiles of temperature and minor constiuents, 15-70km. Flown on Nimbus-7.
MDMD	Meteosat Data Management Department, of ESDC at Darmstadt, F.R. Germany. Central facility for Meteosat.
METEOSAT	European geostationary meteorological satellite.
MSU	Microwave Sounding Unit. The 4-channel microwave passive radiometer which forms part of the temperature sounding instrumentation on TIROS-N.
METEOR	Series name for USSR polar orbiting meteorological satellites. Current series METEOR-2. Also refers to experimental satellites.

NASA — National Aeronautics and Space Administration. US Department responsible for research and development in space etc. Funds experimental satellite and prototypes of operational series.

NASDA — National Space Development Agency. Japan's NASA.

NEΔT — Noise equivalent temperature difference. A measure of random noise on the output of a radiometer. That change in scene temperature which produces a change in output equal to the rms noise.

NESS — National Earth Satellite Service. The part of NOAA which is responsible for providing and operating operational satellites for remote sensing of the atmosphere and Earth's surface.

NIMBUS — The series name for NASA experimental atmospheric research satellites. Used to test and develop operational meteorological instruments. Last member NIMBUS-7 launched 1978; primarily stratospheric composition measurements.

NOAA — National Oceanic and Atmospheric Administration. Part of the US Dept of Commerce, responsible for meteorology, oceanography etc.
Also the name given to US operational polar-orbiting meteorological satellites since 1970 (ie NOAA-2 to NOAA-5 were the follow-on ITOS; NOAA-6 and subsequent numbers are TIROS-N series satellites).

NOSS — National Oceanic Satellite System. A proposed joint NASA/NOAA/Dept of Defense satellite system to demonstrate operationally the ability to monitor ocean surface conditions and ice.

PDUS — Primary Data User Station. A user reception facility for digital image transmissions from Meteosat. (A PDUS is being installed at Met O RRL).

PMR — Pressure Modulated Radiometer. An experimental infra-red vertical temperature sounding instrument for stratosphere and mesosphere. Developed at Oxford, flown on Nimbus 6.
Is also used as a general name for radiometers which exploit gas filters in which the pressure is modulated as the spectral selective element (ie the SSU is a PMR).

RU — Radiance Unit. $1 mW/(m^2\ sr\ cm^{-1})$.

SAGE — Stratospheric Aerosol and Gas Experiment. A NASA satellite experiment to determine profiles of aerosol, ozone and nitrogen dioxide by occultation techniques. Launched 1979.

SAMS — Stratospheric And Mesospheric Sounder. An infra-red limb sounding instrument to measure temperature and minor-constituent profiles. Developed by Oxford University Atmospheric Physics Dept. Flown on Nimbus-7.

SAR — Synthetic Aperture Radar. An imaging radar in which signals obtained with a moving antenna are combined to produce spatial resolution consistent with a much larger antenna. Also used to refer to a specific instrument of this type (eg on SEASAT).

SASS — Seasat-A Scatterometer System. An active microwave sensor, flown on SEASAT, which measures ocean surface roughness. Its output can be interpreted as surface wind speed and direction.

SATEM — Satellite Temperature. WMO code used to distribute atmospheric layer temperatures, humidity, total precipitable water, derived from satellite radiances (eg from TOVS).

SATOB — Satellite Observation. Name of WMO code used to distribute satellite derived winds, sea surface temperatures, cloud information etc.

SBUV — Solar Back-scatter Ultra Violet. An instrument to measure vertical distribution of ozone, flown on Nimbus satellites.

SCAMS — Scanning Microwave Spectrometer. A 5-channel microwave temperature sounder, flown on Nimbus-6.

SCR — Selective Chopper Radiometer. Experimental Infra-red temperature sounding instrument, which includes channels in stratosphere. Developed at Oxford University. Last model flown on Nimbus-5.

SDUS — Secondary Data Users Station. A user reception facility for analogue image transmissions from Meteosat. (The Office uses an SDUS at Lasham).

SEASAT — An experimental NASA satellite for ocean studies (winds waves, ocean SAR imagery). Operated for 3 months in 1978.

SMMR — Scanning Multichannel Microwave Radiometer. A microwave imaging instrument. Sensitive to sea-surface temperature wind, atmospheric liquid water, rain, snow and ice cover. Flown on Nimbus-7 and Seasat.

SMS — Synchronous Meteorological Satellite. SMS-1 and SMS-2 are NASA prototypes of the US operational meteorological geostationary satellites (GOES 1-3).

SR — Scanning Radiometer. The visible and infra-red imaging instrument used on the ITOS polar orbiting satellites, up to and including NOAA-5.

SSP — Sub-satellite point. The point on the earth's surface vertically below the satellite. Most commonly used for geostationary satellites.

SST — Sea Surface Temperature.

SSU — Stratospheric Sounding Unit. An infra-red 3-channel temperature sounding instrument, using carbon-dioxide PMR channels. Forms part of temperature sounding instrumentation on TIROS-N. Developed by Meteorological Office.

TIROS-N — Name of series, and first member , of current US polar-orbiting meteorological satellites. Subsequent members, NOAA-6...

TOMS	Total Ozone Mapping System. An ultra-violet instrument for determining total-column ozone. Flown on Nimbus-7 in conjuction with SBUV.
TOVS	Tiros Operational Vertical Sounder. The instrument package (HIRS/2, MSU, SSU), for measuring atmospheric temperature and water vapour profiles, on the TIROS-N series of satellites.
UARS	Upper Air Research Satellite. A planned experiment, involving one or two satellites in the late 1980s to study dynamics and chemistry of the 10-100km region.
UTH	Upper Tropospheric Humidity. A Meteosat quantitative product derived principally from the WV channel.
VAS	VISSR Atmospheric Sounder. An extension of the imager on the US geostationary satellites to provide temperature and humidity data with high spatial resolution. Has additional infra-red channels to VISSR. First flown (experimentally) on GOES-4. Perhaps operational on later models.
VHRR	Very High Resolution Radiometer. High resolution (1km) visible and infra-red imaging instrument used to provide HRPT service on ITOS-series, up to NOAA-5.
VIS	Visible. The channel of an imaging instrument which responds to reflected sunlight, and whose response overlaps the spectral response band of the human eye.
VISSR	Visible and Infra-red Spin Scan Radiometer. An imaging instrument on a geostationary satellite, which uses rotation of the satellite to scan the telescope view in the east-west direction and a secondary mirror to step the scan in the north-south direction. Normally refers to the specific instrument on SMS/GOES.
VTPR	Vertical Temperature Profile Radiometer. The infra-red temperature sounding instrument used operationally on the ITOS series up to NOAA-5.
WEFAX	Weather Facsimile. Often used to refer to broadcasts in analogue format of weather information (eg processed image data) by GOES satellites.
WV	Water Vapour. Used to refer to the 6.3 micron channel of the Meteosat image data.

ADVANCED LECTURES, 1981

SATELLITE METEOROLOGY

Lecture 1. (Miller)

AN INTRODUCTION TO SATELLITE METEOROLOGY

1 General Introduction

The purpose of this series of lectures is to discuss ways in which satellite techniques can be applied to meteorology. The aim is to provide an appreciation of potential applications of satellite data, including their strengths and short-comings.

Satellite meteorology is a young subject. The first meteorological observations were made from a satellite only 22 years ago. The subject is already wide-ranging. Satellites are the basic vehicles for space research and have become the major source of observations of the upper atmosphere. This series of lectures will concentrate on applications of satellite techniques to studies of the lower atmosphere, the realm of operational meteorology. Useful review papers on satellite meteorology can be found in the list of references (below).

Most conventional meteorological observations are made by in-situ techniques, in which the measuring instrument is in direct contact with the atmosphere. Instruments may be carried aloft by a balloon to observe the troposphere and stratosphere. Rockets can carry instruments to higher levels. A satellite can provide measurements over greater horizontal distances and for longer periods than a single rocket. But satellites cannot remain in orbit at heights much below 150km, so in-situ techniques cannot be used from satellites to study the atmosphere below that height. However, satellites can play a role, through provision of reliable rapid and economic telecommunication channels for collecting data from in-situ sensors on the ground, on buoys, on ships and on aircraft. They can also locate a sensor from its transmissions (useful for drifting buoys).

There are ground-based instruments which make observations at a distance. Radar provides information on the spatial distribution of rain by detecting back-scattering of an emitted pulse of rf radiation from raindrops. Such remote sensing techniques, exploiting the processes of scattering, absorption and emission of radiation, are the basic tools of satellite meteorology. To date operational satellite techniques have been confined to exploiting "natural" radiation (ie sunlight, thermal 'blackbody' emission). Instruments have been flown experimentally which generate microwave radiation to illuminate the scene and detect the back-scattered radiation. Sensors using natural and artificial radiation are refered to as "passive" and "active" respectively.

Following lectures will describe examples of these remote sensing techniques and go into details of the theory of the methods. At this point it may be useful to provide a reminder of some of the terminology and basic laws of radiation.

2 Radiation

a) Units of wavelength and frequency

Radiation may be described by its wavelength (λ) or frequency (ν), which are related by:

$$C = \nu\lambda$$

where C is the velocity of light, $3\ 10^8\ ms^{-1}$.
In the visible and infra-red spectral regions, radiation is normally refered to be its wavelength, in nanometers (nm = 10^{-9}m) or microns (10^{-6}m). In the infra-red wavelength is often expressed as the number of wavelengths per cm, the wavenumber, in units of cm^{-1}. Thus

$$1000\ nm \equiv 1\ micron \equiv 10000\ cm^{-1}$$
$$10\ micron \equiv 1000\ cm^{-1}$$

In the microwave region it is more common to refer to radiation by its frequency. Thus a frequency of 30GHz (1 gigahertz = 10^9 cps) corresponds to a wavelength of approximately 1 cm.

b) emission: some definitions.

A 'black body' absorbs all radiation which falls upon it. In general a body absorbs only a fraction of incident radiation, known as the absorbtivity; this is wavelength dependent. Similarly, the efficiency for emission is known as the emissivity.
At a given wavelength:

Emissivity = Absorptivity (KIRCHHOFF'S LAW)

Power emitted per unit area, steradian and wavenumber is known as radiance.

c) emission from a blackbody.

Flux (ie energy per unit area) per unit wavelength interval emitted by a blackbody at temperature T at wavelength λ is given by:

$$B(\lambda) = \frac{2\pi hc^2 \lambda^{-5}}{\exp(hc/k\lambda T) - 1}$$

$B(\lambda)$ and its equivalent in frequency units, $B(\nu)$, are known as the Planck Function.
$B(\lambda)$ peaks at wavelength λ_m given by:

$$\lambda_m . T = 0.29\ deg.\ cm \quad \text{(WIEN'S LAW).}$$

For the Sun: T = 6000K; λ_m = 0.48 micron
For the Earth T = 290K ; λ_m = 10 micron
Total energy emitted by a blackbody:

$$= \int B(\lambda)\, d\lambda = \sigma T^4$$

σ, STEFAN'S CONSTANT

B is proportional to T at microwave and far infra-red wavelengths.
Typical dependence of B on T for λ at or below λ_m is shown in Figure 1.

d) atmospheric absorption.

Atmospheric absorption in the infra-red is dominated by "absorption bands" of water, carbon dioxide, ozone etc. Studies of radiation within these bands enables us to determine characteristics of the atmosphere; its temperature and the concentration of the absorber. However, there are

regions of the spectrum where absorption is low, providing the possibility for a satellite sensor to view the surface and to determine its temperature or other characteristics. Such spectral regions are called "windows". There is a particularly important "window" near the peak of the earth/atmosphere emission curve, around 11 microns.

3 Satellite orbits

An artificial satellite moves in an eliptical orbit, with the earth's centre at one focus of the ellipse. The size, shape and orientation of the orbit are defined by a set of parameters known as orbital elements. For various practical reasons meteorological satellites are placed into circular orbits (or as nearly so as possible). The angle between the orbital plane and the earth's equatorial plane is termed the inclination, i (see Fig.2). The point at which the orbit crosses the equator with the satellite going north is called the ascending node. The orbital period, P is given by:

$$P = 2\pi\sqrt{\frac{a^3}{\mu}}$$

where a is the semi-major axis of the orbit (in practice the radius, ie earth's mean radius plus satellite's height above the surface) and $\mu = 3.986\ 10^5\ km^3\ s^{-2}$. The orbital period of a satellite at a height of 900 km is about 102 minutes.

For an orbital height of 36000 km (ie $a \simeq 42400$ km), P=24 hr. If the orbital inclination is zero, the satellite is travelling vertically above the equator. The angular velocity of a satellite at this height is equal to that of the earth and the satellite remains above the same point on the equator; the satellite appears stationary relative to an observer on the earth's surface. Such an orbit is termed geostationary. In practice, the inclination of such an orbit will be non-zero (even if inserted into an i=0 orbit, inclination will change as a result of the influence of the moon). In this case the more general term, geosynchronous orbit, applies and the satellite will appear to move in the sky through a narrow 'figure 8', bounded in latitude by angles of i and -i, each day.

In Fig 2 the angle Ω defines the position of the ascending node with respect to a conventional fixed reference direction (the intersection of the equator and ecliptic planes, the 'first point in Aries'). King-Hele (1964) shows that, contrary to simple theory, Ω changes at a rate given (approximately) by:

$$\dot{\Omega} = -10.0\left(\frac{R}{a}\right)^{3.5}\cos i \quad \text{deg/day}$$

where R is the earth's equatorial radius. (This effect is caused by the oblateness of the earth). Thus, unless i=90° (a true polar-orbit), the plane of the orbit precesses about the earth's axis (see Fig 3).

To achieve good quality visible imagery from near-earth orbit, it is desirable to be able to select the local solar time at which observations are made and to keep this constant (or at least to avoid substantial long-term changes) throughout the satellites's life. This means that the orbital plane of the satellite should remain fixed in orientation to the earth-sun direction. The latter rotates in the ecliptic plane, through 360°/year (approx 1°/day). For $i < 90°$, the precession of the orbital plane adds to this relative rotation. However, if i is increased beyond 90° to the point where $\dot{\Omega} = +1°$/day, then precession of the plane will, over a year, balance out the effect of the motion of the earth around the sun.

Such an orbit is termed sun-synchronous.

For an orbital height of 850 km, the necessary value of i is about 99°. Thus the orbit is still near-polar and by using instruments which scan either side of the satellite track one may obtain observations from pole to pole.

Satellite orbital-height controls the radius of the contact circle for direct reception of data transmitted in real-time and the width of swath which can be observed by a satellite sensor. Both are improved by increasing satellite height.

Sat series	ht (km)	period (min)	telecom range (km, 5° elev)	swath width (km, edge elev 25°)	separation of equat. cross. (km)
HCMM	620	96.7	2200	2000	2680
TIROS-N	850	101.5	2600	2600	2820
ITOS	1450	114.5	3420	3800	3180

Note that the current US operational series (TIROS-N), unlike its predecessor (ITOS), does not provide overlap between successive swaths at the equator. Whilst greater orbital height has its advantages there are practical difficulties. Satellite orbits above 1100 km encounter a much increased flux of charged particles (which can degrade performance of solar cells and other materials). Increases in satellite height also require more sensitive instruments to maintain the same ground resolution.

4 General classes of meteorological satellites

There are two major classes of satellites, distinguished by their orbits: geosynchronous and sun-synchronous near-polar.

THE TWO MAJOR CLASSES OF WEATHER SATELLITE

	POLAR-ORBITER	*GEOSTATIONARY*
Orbit and consequences	height~1000 km sun-synchronous fixed local solar time	Height 36000 km equatorial plane fixed sub-satellite point (ssp)
coverage	global	limited (60° of ssp)
frequency	twice/day	twice/hour
special advantages	—high resolution IR measurements easier —active location of buoys and balloons	—winds from motion of clouds —warnings from remote sensors

A geostationary satellite can produce an image by optically scanning the earth's disc, within 25 minutes; so observations are essentially simultaneous over its complete zone of coverage. Thus these observations are readily compatible with normal synoptic conventional

observations. This is not to say there are no difficulties. Products dependent on visible imagery cannot be available simultaneously from all geostationary satellites.

The low-orbiting satellite makes use of its orbital motion to build up its coverage of observations, taking 12 hours to obtain full global coverage. Its observations are asynoptic. Two satellites working together in orbits about 6 hr apart, can dramatically increase the number of observations of a particular area within the acceptance interval of an analysis. This is the approach adopted in the current US series, TIROS-N.

5 Current operational meteorological satellite series

There are three types of low-orbiting meteorological satellite in operation. These are:

TIROS-N: the US civil satellites. System comprises two satellites (Currently TIROS-N and NOAA-6). They provide image services and carry instruments for temperature sounding and data collection/ location. Products are on GTS.

DMSP: the US military satellites. These provide image and (less sophisticated) sounding data. Their real-time transmissions are encrypted.

METEOR-2: The USSR series; image and sounding services, but lower-quality infra-red imagery. No products on GTS.

Complete coverage of the tropical belt requires five geosynchronous satellites. The current position is:

GOES : the US satellites. Two satellites provide imagery from longitudes 75W and 135W. A third is used for dissemination of imagery (located at 105W). There are other satellites (some only partially workable) available as spares .

GMS: the Japanese satellite. A US-designed and launched satellite operating at 140°E.

Meteosat: the ESA satellite, at 0°E. Meteosat-1 has a fault; only the data-collection system can be operated. Meteosat-2 is due to be launched "this summer".

During the FGGE year, the US provided a spare GOES satellite which was positioned near 60°E and operated by ESA. It was known as GOES-IO.
(Further information is given in the references listed at the end of this lecture).

6. What satellite products are operationally available?

a) Qualitative products

Images from satellites can be used to locate features (cloud bands, fog patches, snow and ice cover) and to estimate the vigour of synoptic systems. Polar-orbiting satellites transmit imagery in real-time. Given suitable reception and display facilities the forecaster can have access to image data over an area of radius about 2500km. Such imagery is available 4 times per day (by day, and by night from each of 2 satellites). Reception of data from a geostationary satellite can provide more frequent pictures of a wider area. In either case images can be available within 10-20

minutes of the time of observation, the delay being associated with addition of geographical location information (eg grids or coastlines). More details of image services will be given in Lecture 2 and their use will be discussed in Lecture 6.

b) Quantitative products.

Images, supplemented by observations of radiance in a range of spectral channels, particularly in absorption bands of carbon dioxide, are used to generate a range of quantitative products. Principal amongst these are:

- winds, derived from the motion of clouds as seen in the frequent images of geostationary satellites. Each satellite operator is providing about 1000 winds per day within the latitude belt 40N to 40°S (see lecture 7);

- temperature profiles, derived from radiances. NOAA are producing about 8000 profiles per day, on a 300 km spacing (Lecture 4);

Other products now available regularly include sea-surface temperatures, cloud and humidity information (Lecture 5).

7 Conclusion

Satellites are providing data which has operational applications. Following lectures will explain the sources of the data, the means by which products are generated and an indication of this quality. The last two lectures will discuss techniques which are still at the research and development stage.

REFERENCES

Recent Reviews (ie sources of references to the literature)

F G Finger & R M McInturff, "Applications of satellite data to aeronautical meteorology", Technical Note 142, WMO No 413 (1975)

J T Houghton, "The future role of observations from meteorological satellites", Quart. J R Met Soc (1979) 105, 1-23

J T Houghton & F W Taylor, "Remote sounding from artificial satellites and space probes of the atmospheres of the earth and the planets", Rep Prog Phys (1973) 36, 827-919

D S Johnson & I P Vetlov, "The role of satellites in WMO programmes in the 1980s", WWW Planning Report No 36, WMO No 494 (1977)

B J Mason, "The role of satellites in the global weather experiment", Radio & Electronic Eng, (1979) 49, 604-610

D E Miller, "Weather satellites", J R Soc of Arts, (1980) 128, 813-825

J S Winston (editor), "Quantitative meteorological data from satellites", Technical Note 166, WMO No 531 (1979)

H W Yates & W R Bandeen, "Meteorological applications of remote sensing from satellites", Proc IEEE (1975) 63, 148-163

Orbit theory

D King-Hele "Theory of satellite orbits in an atmosphere" London, Butterworths, 1964.

Information on satellite systems and products

BASIC INFO "WWW GOS-satellite sub-system: Information on meteorological satellite programmes operated by members and organisations" WMO No 411 (1975, but up-dated annually).

TIROS-N "The TIROS-N/NOAA A-G satellite series", A Schwalb, NOAA Technical Memorandum NESS 95, (1978)

"Data extraction and calibration of TIROS-N/NOAA radiometers", L Lauritson, G L Nelson and F W Porto, NOAA Tech Memo NESS 107, (1979)

DMSP "Defense meteorological satellite program (DMSP) Users Guide", Washington Air Weather Service, Technical Report 74-250 (1974)

"The Defense Meteorological Satellite Program", D A Nichols, Optical Engineering 14 273-278 (1975)

METEOR "Soviet Meteor satellite imagery", B C Diesen III and D L Reinke, Bull. Amer Met Soc (1978) 59, 804-807

GOES "Central processing and analysis of geostationary satellite data" C F Bristor, NOAA Tech Memo NESS 64 (1975)

"Geostationary operational environmental satellite/data collection system", NOAA Technical Report NESS 78 (1979)

METEOSAT "Introduction to the Meteosat system", ESA Darmstadt (1978)

GMS "The GMS users' guide", issue 1, Tokyo Meteorological Satellite Centre, (1980)

T-N/GOES "National Environmental Satellite Service. Catalogue of Products, 3rd edition." D C Dismachek, A L Booth & J A Leese, NOAA Tech Memo NESS 109, (1980)

A LIST OF ACRONYMS, ABBREVIATIONS etc IS AVAILABLE

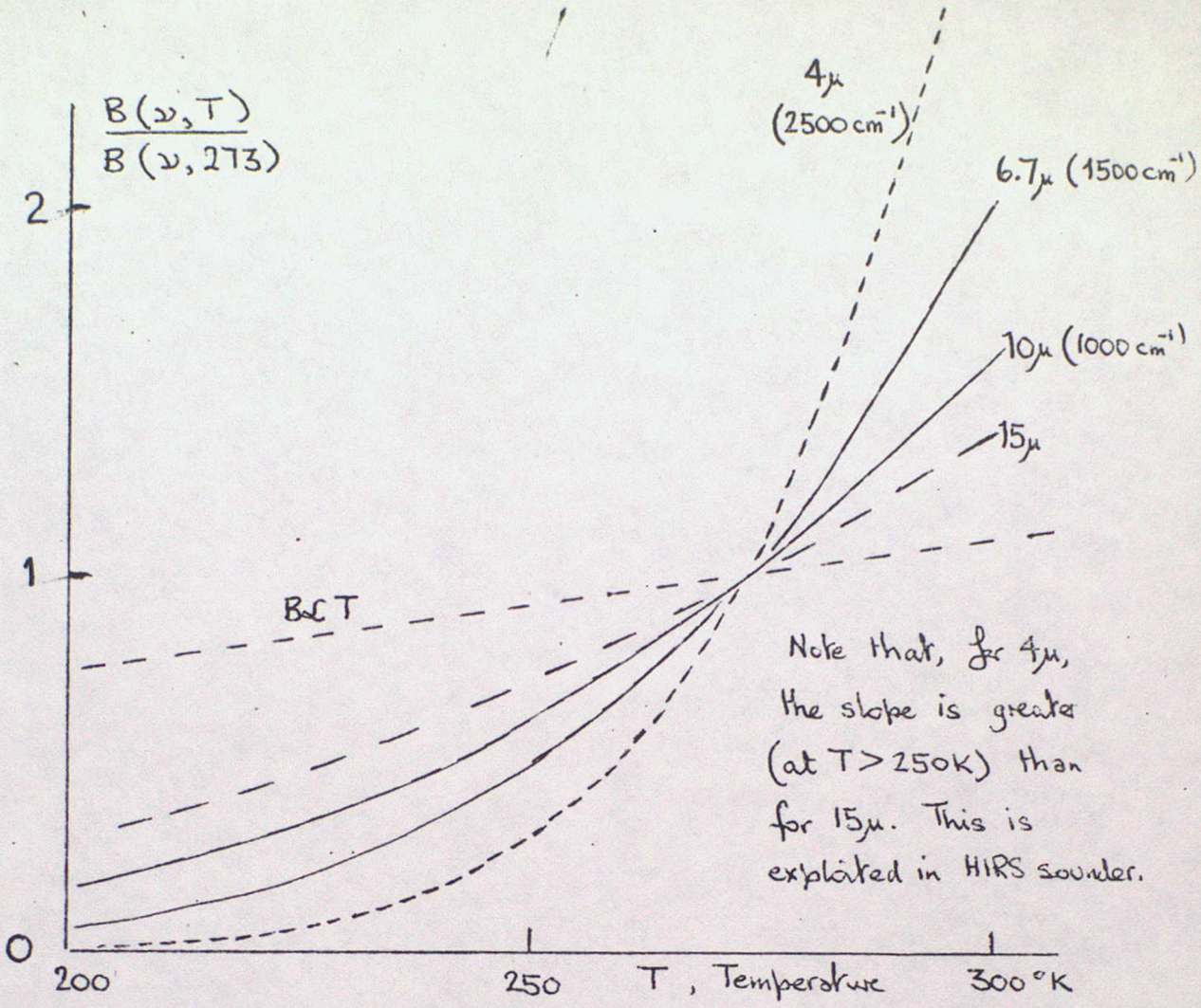

Figure 1. Temperature dependence of Planck function.

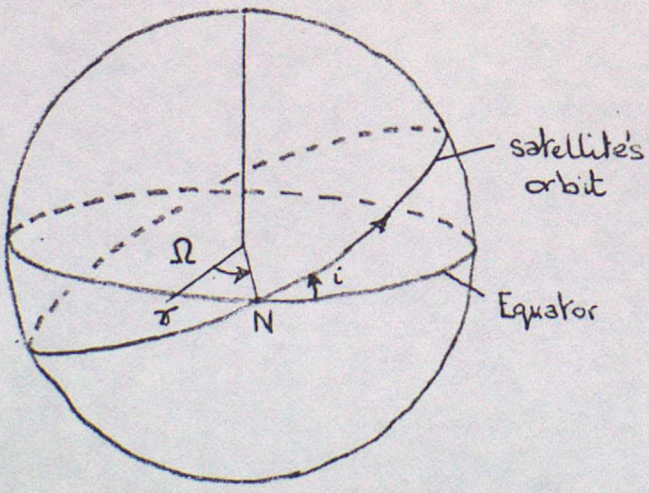

Figure 2. Satellite orbit.
- N, ascending node
- i, inclination of orbit
- γ, first point in Aries
- Ω, Right ascension of node.

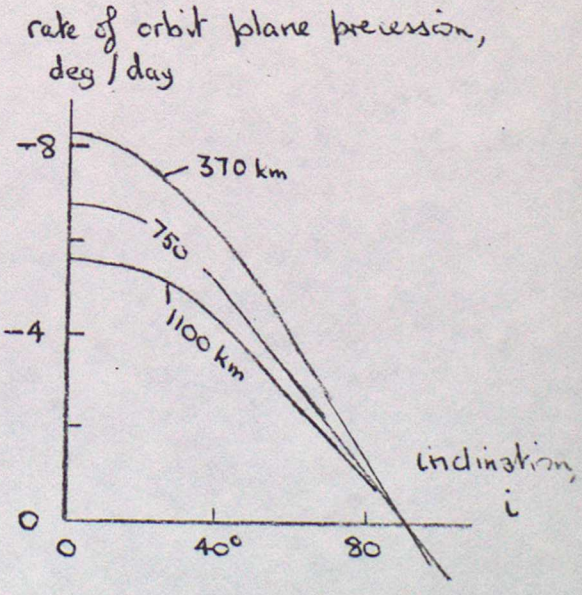

Figure 3. Precession of orbit plane for three orbit heights.

ADVANCED LECTURES 1981

Satellite Meteorology - Lecture 2 Satellite Instruments and Data Transmission (Brownscombe)

Introduction As discussed in Lecture 1, satellites provide remote observing platforms on which instruments can be placed to make or relay "observations" of the state of the earth's atmosphere and surface. In this lecture I shall be concentrating on satellite instruments designed to make observations (eg imagers or atmospheric sounders) but will briefly mention some data relaying instruments.

There are fundamental limitations on the type of information about the atmosphere that can be derived from remote sounding instruments (whether land or satellite based) and these will be described in later lectures. (particularly in Lectures 3 to 5).

In addition there are severe limits placed on the design of instruments for use on satellites by the requirement to minimise size, mass and power consumption because of the very high cost of launching large objects into space. A further obvious design constraint is that the instruments must be designed to have excellent long term reliability and stability in order to operate unattended in a space environment for several years. These practical design problems have delayed the use of "active" instruments such as radars and lidars on satellites. Their use is still in its infancy but some applications of active instruments will be discussed in Lectures 8 and 9. These limitations also require design trade offs between spatial resolution, spectral resolution, minimum detactable signal change, area of coverage and data transmission rates for instruments passively observing radiation at various wave lengths emitted from the top of the atmosphere.

In this lecture I propose to cover the following areas

1 Explain the basic design representative of most current passive remote sensing instruments, identifying limitations on ultimate performance and resulting trade offs.

2 Discuss in some detail the Instrument pay load of the current polar orbiting NOAA satellites and describe the ways in which the data are made available to users. Describe similarly the European Geosationary satellite, Meteosat.

3 Summarise the relative performance of the current satellite passive sensing instruments. Outline the impact of improvements in absolute conventional meteorological parameters from the measured radiances. Discuss the problems of maintaining a consistent series of observations from satellite passive radiometers.

1 Basic design of a radiometer for measuring emitted or reflected (scattered) radiation emerging from the top of the atmosphere

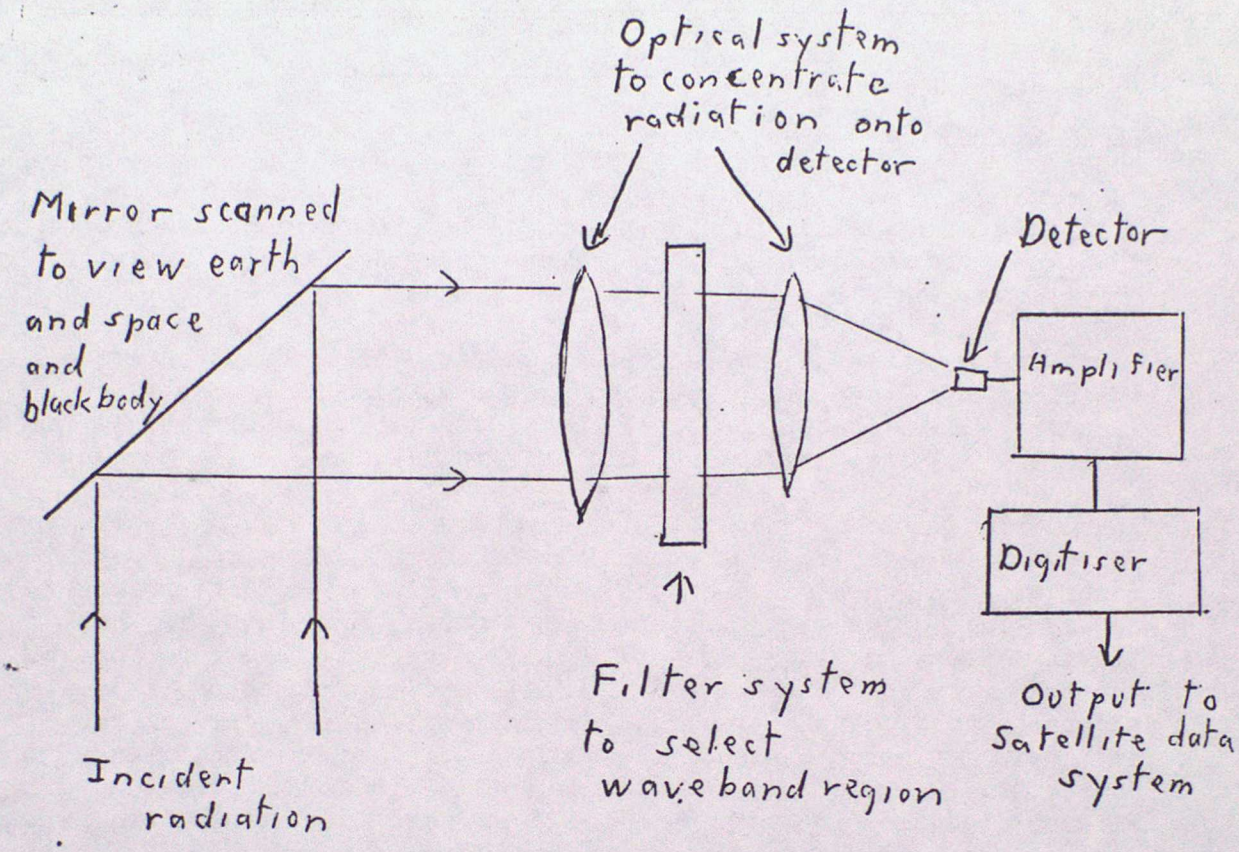

Fig 1

The basic elements are shown schematically in Fig 1. The exact arrangement and type of components will vary with the type of orbit (geosynchronous or low orbiting), the wavelength region to be used (visible, infrared or microwave) the size of field of view and the total geographical coverage required. The spectral region chosen will determine whether the radiometer will be looking mainly at reflected (scattered) solar radiation or radiation directly emitted from the earth's surface or atmosphere. Generally the longer the wavelength chosen the larger the fraction of emitted radiation observed. The three atmospheric "windows" (ie regions of good atmospheric transmission) normally used for surface/cloud observation are 0.4 → 1.1 μm (visible and near infrared) 3.5 →4.0 μm and 10–12 μm (Thermal infrared), other wavelengths are used for observation of atmospheric emission or absorption eg 4.3 μm and 15 μm absorption bands of CO_2, 5.5 mm oxygen bands. In general in order to minimise the range of the heights in the atmosphere (or the type of emitting gas) from which the observed radiation comes it is necessary to use very narrow wave length regions for these instruments.

However, even using a vanishingly narrow waveband (monochromatic) the sounder will still observe radiation from a wide range of heights. It is possible to improve vertical resolution of radiance (and hence temperature of gas content) by limb scanning (ie looking $\sim$ horizontally through the atmosphere instead of $\sim$ vertically) or (to some extent) try combining many measurements from different wavelength regions.

The distinction between Images and Sounders is based partly on whether observations are made in window regions or of atmospheric emission and partly on the size of each individual field of view of the instrument (km $\gg$ 100s of km).

To design a radiometer to observe radiation emitted from the earth/atmosphere we must first specify:

1 Spatial resolution required - this determines instrument acceptance angle and mirror scanning rate to achieve complete coverage once orbital parameters are given eg 1 km resolution from orbital height of 1000 km (corresponding to a satellite velocity of $\sim$7km/sec) would require a regular acceptance angle of 1 milli radion or ($\sim$0.05°) and a scan repitition rate of $\sim$400 rpm resulting in a time available to observe each IFOV of $\sim 2 \times 10^{-5}$ sec. Thus we must digitise at a rate $\sim$ 50000 words per sec if we wish to retain full spatial resolution. If we require a resolution of radiation intensity of 1 part in 10^3 of full scale (ie digitisation of 10 bits) this results in a data flow per channel of 500,000 bits per sec. (Of course from an altitude of 1000 km the radiometer scanning perpendicular to its direction of motion would only observe the earth for $\sim \frac{1}{3}$ of its scan time. Thus data buffering on the satellite before transmission would reduce the data rate to $\sim$170,000 bps for each channel.

2 Spectral band location and width required This will determine the region of the atmosphere or earth's surface from which the radiation observed by the instrument is mainly emitted. Instrumentally it will determine the size of "optics" required to obtain a given spatial resolution (diameter $\propto \lambda$) and a given rate of radiant energy collection and hence the signal to noise ratio (S/N) for a given instrument detectivity. If a certain S/N is required this will determine the time required for one observation and hence for a low orbiting satellite set a minimum field of view size.

It is obvious that all these decisions are related and that trade offs between spatial resolution, area of coverage, signal to noise ratio and spectral band pass will be required. The data rate which can be handled both for satellite processing, satellite to ground transmission and ground processing will also be a limitation on ultimate performance.

Essential features of instrument operation

The instruments measure radiance (units normally used mW m^{-2} $st^{-1}(cm^{-1})^{-1}$) emitted from the top of the atmosphere at whatever angle to the earth's surface the instrument is looking.

Spatial Resolution

Although spatial scanning maybe accomplished by either stepwise or smoothly rotating motion, each instrument will have an "Instantaneous Field of View" (IFOV) which will determine the ultimate spatial resolution. In general the instrument output will be digitised. Each digital sample will represent data from 1 (or if averaging is done, more) IFOV. The distance of separation of these samples may be less or greater than the size of the IFOV. In the case of Images the basic image sample is given the name "Pixcell" and sampling is usually done at a finer resolution than the IFOV (Oversampling). For sounders the separation of samples is often greater than the IFOV (undersampling).

Calibration

In general the relationship between radiance and instrument output in "counts" (after digitisation) is arranged to be essentially linear. Calibration is undertaken by allowing the instrument to view space and a black body of measured temperature during part of its scan. Hence the constants A and B in a calibration equation of the type

$$R = A\,C + B,$$

where R= radiance (mW m^{-2} sr^{-1} $(cm^{-1})^{-1}$)
and C= Instrument counts,
can be determined.

The radiance can then if required be converted into an effective brightness temperature using the Plank function calculated for the wavenumber region concerned, taking into account the transmission function of the instrument. The relationship is generally nonlinear $R \propto T^n$ where $n > 1$ for infrared instruments, but becomes more linear as wavelength increases → microwave, The radiances or brightness temperatures can then be used as inputs for the derivation of surface or atmospheric temperatures or variable constituent (eg H_2O) concentrations by methods discussed in later lectures. Calibration of "visible" radiances is more difficult but targets of known brightness can be used in place of the "black" body.

It is clearly vital that instuments should be well calibrated on the ground before launch and that changes in calibration during use in space should be carefully monitored. Both of these are tasks of some difficulty since we must be able to measure linearity and offsets to better than 1 in 10^3. The possibility of tranferring calibration standards over a sequence of instruments and hence maintaining "climatological" satellite records has now arisen with the overlapping nature of the TIROS-N series of US polar orbiting satellites. However comparison of satellite and conventional data is still very necessary to check (and "adjust") the calculated atmospheric transmissions used to obtain "real" temperatures from radiances.

2.1 The NOAA system of polar orbiting satellites (TIROS-N series)

The first prototype satellite (TIROS-N) was launched on Friday 13 Oct 1978 and the second (now called NOAA 6) in June 1979. A launch failure occurred for the next satellite in May 1980 but another satellite launch is planned for May 81. This series will continue until the late 80s with additional instruments to be added later.

The TIROS-N series of satellites is a cooperative effort of the United States, the United Kingdom and France. The UK Meteorological Office provides a Stratospheric Sounding Unit (SSU), one of three sounding instruments for each satellite. The Centre National d'Etudes Spatial (CNES) of France provides the Data Collection System (DCS) instrument for each satellite and provides the facilities necessary to process and make available to users the data obtained from the system (ARGOS system). The Centre d'Etude de la Meteorologie Spatiale (CEMS) of France at Lannion provides ground facilities for reception of sounder data during blind orbit periods.

A schematic drawing of the satellite is shown in Fig 2 with 'meteorological' instruments outlined.

The primary environmental sensors are:

i) A TIROS Operational Vertical Sounder (TOVS). The TOVS is a three instrument system consisting of:

a) The High Resolution Infra-red Sounder (HIRS/2) - a 20 channel instrument making measurements primarily in the infrared region of the spectrum. The instrument is designed to provide data that will permit calculation of

1) temperature profile from the surface to 10mb
2) water vapour content in three layers of the atmosphere and
3) total ozone content

A list of the channel specifications is shown is table 1

b) The Stratospheric Sounding Unit (SSU) is designed to provide data for the upper stratosphere (~20mb to 1 mb). Selective absorption techniques using CO_2 filled cells as fillers are employed to make measurements in 3 channels around 15 μm in the infra-red.

c) The Microwave Sounding Unit (MSU)- a 4 channel Dicke radiometer making passive measurments in the 5.5 mm oxygen absorption band. This instrument, unlike those making measurments in the infra-red region is little affected by clouds.

Data from the TOVS are broadcast continually for local reception as part of the HRPT transmission and on the spacecraft beacon transmission as well as recorded on board to provide world coverage to NOAA from tape-recorder replay. A summary of the TOVS instruments is given in Table 2

ii) The Advanced Very High Resolution Radiometer (AVHRR) - a 4 channel (5 channels on later satellites of the series) radiometer sensitive in the visible, near infra-red and infra-red window regions. Details are given in Table 3. Data from this instrument are recorded for central processing and broadcast as HRPT (full resolution of 1.1 km in all channels) and APT (reduced resolution of 4 km in 2 selectable spectral channels).

iii) The Data Collection System (DCS): a random access system to acquire data from fixed and free floating terrestial and atmospheric platforms. Platform location (to an accuracy of 5 to 8 km rms in position and 1 to 1.5 mps rms in velocity) is accomplished by ground processing of Doppler measurements of carrier frequencies. Data collected by this system are also included in the HRPT and beacon transmissions. Data can be received and processed locally but the ARGOS system provides central processing of recorded data in France; receiving data via links with the USA and outputting processed data (including location if desired) via post, telex or dedicated communication systems.

Scanning

All the sounding (TOVS) instruments and the AVHRR imager scan perpendicular to the direction of spacecraft motion. Looking in the direction of the spacecraft velocity vector, the AVHRR scans the earth from right to left by a continuously rotating mirror; the TOVS instruments from left to right in a variety of step scan modes. Details of the scan patterns of the HIRS 2, MSU and SSU are shown in Figs 3 and 4. Although the AVHRR scans the earth from horizon to horizon and beyond, only data from within $\pm$ 55° of the nadir are digitised together with space and black body calibration views.

Orbits and Data Acquisition

The TIROS -N satellite series has been designed to operate in a Sun-synchronous orbit at 833 ±90km (450 ±50 n.mi). Two nominal altitudes have been chosen: 833 km (450 n.mi) and 870 km (470 n.mi). The choice between nominal altitudes will be made to keep the orbital periods of two operational satellites in similar orbits sufficiently different (1 minute) so that they do not both view the same point on the Earth at the same time each day.

Nominal orbital parameters are shown in the table below

TIROS-N series orbital parameters

Parameter	833 km orbit	870 km orbit
Inclination	98.739 degrees	98.899 degrees
Nodal period	101.58 minutes	102.37 minutes
Nodal Regression	25.40 degrees/orbit W	25.59 degrees/orbit W
Nodal Precession	0.986 degrees/day E	0.986 degrees/day E
Orbits per day	14.18	14.07
Equator crossing times (local solar time)	1500 north bound	0730 south bound

A satellite pass directly over an antenna site will be within view of that antenna (horizon-to-horizon) for about 15.5 minutes when the satellite is at 833 km and 16 minutes when it is at 870 km. The user of APT or HRPT can therefore expect to receive data from a circular area 6200 km in diameter centered at the location of the antenna. If one assumes that the spacecraft must be 5° above the horizon for useful data to be acquired the contact time and area is reduced to about 13.0 minutes (833 km satellite altitude), 13.7 minutes (870 km) and 5200 km.

Because the number of orbits per day is not an integer number, the sub-orbital tracks do not repeat from day-to-day although the local solar time for passing any latitude is essentially unchanged. For this reason the orbital equator crossings will occur at varying longitudes during the life-time of the satellites.

NOAA/NESS operates two Command and Data Acquisition (CDA) stations, one in Virginia and one in Alaska, to receive the environmental data from the satellite. However during three sequential orbits of the Earth (four, some days), the satellite remains out of contact with one of these sites. To eliminate delay in receipt of high priority temperature profile data during this period, a data receipt-only station receives data in Lannion, France. This station acquires stored TIP data and transmits it to the central processing facility in the United States. When this station is in use, the satellite is out of contact with the ground for no more than one orbital period per day.

Data Handling System

The Tiros-N data handling subsystem consists of four primary components:

The Tiros Information Processor (TIP) - low data rate processor
The Manipulated Information Rate Processor (MIRP) - a high data rate processor
Digital Tape Recorders (DTR)
A Cross Strap Unit (XSU)

All data available for transmission to the ground through the lifetime of the mission are processed by some or all of these components, as is shown in Figure 5.

The TIROS-N Operational system data flow is shown in Fig 6
At Lasham data is received for the Meteorological Office from the HRPT and APT broadcasts and used operationally to produce and distibute satellite pictures as described in Lecture 6. TOVS data is also received (for research use only at present).

The recorded data processed by NOAA in Washington are sent to us via the Global Telecommunications System. A list of products is shown in table 4. We also receive via a dedicated line from Washington SSU instrument data and a selection of processed TOVS instrument outputs from which we produce daily Global stratospheric analyses from 100 mb up to .1 mb.

2.2 Meteosat, The European Geostationary Satellite

This satellite was launched into a position at 0 E, 0 N in November 1977 as a member of a global set of geostationary satellites used to acquire data during the FGGE (First GARP Global Experiment). After operating successfully for two years its imaging and dissemination functions failed. A replacement satellite is to be launched on the European launcher, Ariane, but the launch has been delayed by problems with the rocket motors to June 1981 at the earliest. An operational programme of satellites is being planned to follow on through the 1980s.

The satellite is oriented in a north-south axis and spins about this axis at 100 rpm. It is equipped with a "high resolution radiometer" which allows continuous imaging of the earth in three spectral bands:

a) Visble 0.4-1.1 μm (2 simultaneous channels)
b) Infrared 10.5-12.5 μm
c) Water vapour 5.7-7.1 μm

The IFOV is 0.065 m rad for the visible channels and 0.14 m rad for infrared and water vapour resulting in 2.5 and 5 km spatial resolutions respectively at the sub-satellite point. Scanning across the earth is accomplished by satellite rotation at 100 rpm and S-N by a stepping mirror. A full disc image is obtained every 30 minutes and consists of 5000 lines in the visible and 2500 in the infrared and water vapour.

From its orbital height of $\sim$36000 km the radiometer sees the earth for only $\sim$1/20 of a revolution. A memory on board allows one line of image to be stored and transmitted to the ground in the remaining 19/20 of a revolution. This reduces the data rate required from 2.7 M bit/sec to 166 k bit/s.

The Meteosat "system" shown in fig 7 includes not only the satellite but the central ground station at Darmstadt in Germany. Here raw image data is received from the satellite and processed into corrected digital imagery of the whole disc or a European sub-sector of it and rebroadcast using the Meteosat satellite as a telecommunications link. A series of analogue (WEFAX) formats covering the whole disc image in a number of sectors are also re broadcast. Data processing at Darmstadt also produces inputs for the GTS (eg winds derived from image sequences) and processed charts for broadcast via the WEFAX service.

Some selected images from the US GOES East Geostationary satellite located at $\sim$75 W are also processed at Lannion in France and re broadcast as both digital and WEFAX images.

A 24 hr schedule of transmission is maintained to both digital (PDUS) and analogue WEFAX (SDUS) stations giving $\frac{1}{2}$ hourly coverage of the European area and less frequent full disc coverage.

When the Meteosat image service is recommenced it is planned that the Meteorological Office should receive the WEFAX data at Lasham for distribution on the SATFAX network and the Digital data at Malvern for use in connection with the composited radar data produced by the Short Period Forecasting Research Project.

Meteosat also acts as a telecommunications satellite to relay messages from a variety of Data Collection Platforms. These can be
a) self timed
b) interrogated from the central ground station
c) 'alert' ie transmit automatically when a certain measured parameter exceeds a preset threshold.

Data received at the Central Ground Station are forwarded via the GTS to users.

3 Summary of Passive Radiometer Perfomances and Discussion of Effects of performance

The measurements of radiance provided by satellite radiometers can be converted to effective brightness temperatures using the Planck equation so long as we have an adequate knowledge of the sensitivity of the instrument as a function of wave number (obtained from ground measurements). Changes in absolute radiance calibration can be determined by in-space calibration but any changes in spectral sensitivity will remain undetected. In addition the calculation of atmospheric transmittance as a function of wavenumber is very difficult, a difficulty which is aggravated when variable constituents such as water vapour contribute. These difficulties at present provide the main limitations on the accuracy with which meteorological parameters such as sea surface temperatures and atmospheric thickness can be derived.

In principal increasing the number, decreasing the spectral band width and increasing the available S/N of satellite sounders and imagers would improve the final meteorological product. This would require much bigger, heavier and more complicated instruments. In table 5 the performances of present satellite radiometers are compared with the 'ultimate' detector performance. This indicates that large improvements in performance of similar sized instruments are not to be expected unless detectors cooled to very low temperatures can be used.

The temperature sounding instruments on the TIROS-N series have already begun to utilise small fields of view in the Infra-red (allowing the opportunity to exploit gaps in cloud cover for sounding) and to use microwave wavelengths so that cloud effects are minimised. Further improvements in these areas can be expected.

The US have now demonstrated the feasibility of temperature sounding from geostationary altitude and this should allow improvements in the frequency of measurement which will be particularly valuable for mesoscale forecasting.

However continued work is required to extend knowledge of spectral transmission of the atmosphere and in techniques of using radiances in conjunction with conventional measurements even to exploit fully the radiometric performance of the current satellite instruments.

On the practical side it is of great importance both that series of satellite instruments should be continuously intercompared and attempts made to derive changes in instrument spectral performance. The techniques of comparing conventional and satellite data should also be improved.

References

More details of the instruments discussed in this lecture will be found in some ot the references given with lecture 1 of the series.

Details of the performance of the Meteorological Office Stratospheric Sounding Unit and the products derived will be found in:

'Operational Temperature Sounding of the Stratosphere' D E Miller et al Phil Trans R Soc A 296 pp 65-71, 1980

and

'The Stratospheric Sounding Unit' Performance and Products, D R Pick and J L Brownscombe, Met O 19 Branch Memorandum No 52

Table 1.--HIRS/2 instrument specifications

Channel	Central Wave No. cm^{-1}	Half Power Bandwidth cm^{-1}	Wavelength μm	Specified NEΔN mw/m^2-sr cm^{-1}
1	668.5 ±1.3	$^{+1}_{3.0-0.5}$	14.96	0.80*
2	680.0 ±1.8	$^{+4}_{10.0-1}$	14.71	0.27
3	690.0 ±1.8	$^{+6}_{12.0-0}$	14.49	0.27
4	703.0 ±1.8	$^{+4}_{16.0-2}$	14.22	0.22
5	716.0 ±1.8	$^{+4}_{16.0-2}$	13.97	0.22
6	733.0 ±1.8	$^{+4}_{16.0-2}$	13.64	0.22
7	749.0 ±1.8	$^{+4}_{16.0-2}$	13.35	0.22
8	900.0 ±2.7	35.0±5	11.11	0.11
9	1030.0 ±4	25.0±3	9.71	0.16
10	1225.0 ±4	$^{+10}_{60.0-3}$	8.16	0.16
11	1365.0 ±5	40.0±5	7.32	0.22
12	1488.0 ±4.7	$^{+15}_{80.0-4}$	6.72	0.11
13	2190.0 ±4.4	23.0±3	4.56	0.002
14	2210.0 ±4.4	23.0±3	4.52	0.002
15	2240.0 ±4.4	23.0±3	4.46	0.002
16	2270.0 ±4.7	23.0±3	4.41	0.002
17	2360.0 ±4.7	23.0±3	4.24	0.002
18	2515.0 ±5	35.0±5	3.98	0.002
19	2660.0 ±9.5	100.0±15	3.76	0.001
20	14,500.0 ±20	1000.0 ±15	0.69	0.1% Albedo

*1.70 most likely achievable

TIROS-N Operational Vertical Sounder (TOVS) Characteristics

Table 2

Characteristic	Stratospheric Subsystem (SSU)	Tropospheric Subsystem (HIRS/2)	Microwave Subsystem (MSU)
Resolution at Subpoint	147 km	17 km	109 km
Field of View	10°	1.4°	7.5°
General Spectral Regions Used	15 μm CO_2	15 μm CO_2 11 μm Window 9.7 μm 0_3 6.7 μm H_20 4.3 μm CO_2 3.7 μm Window 0.7 μm Visible	50–57 GHz 0_2
Number of Spectral Channels	3	20	4

Table 3

TIROS-N AVHRR Channel Characteristics

Channel*	Resolution at Subpoint	Wavelength (μm)	Primary Use
1	1 km	0.55 — 0.90 (0·58 - 0·68, NOAA6 onwards)	Daytime Cloud and Surface Mapping
2	1 km	0.725 — 1.10	Surface Water Delineation
3	1 km	3.55 — 3.93	SST, Nighttime Cloud Mapping
4	1 km	10.5 — 11.5 10·3 → 11·3 on 5 channel	SST, Day/Night Cloud Mapping
5	1 km	11.5 — 12.5	SST

Table 4

GTS Products From TIROS-N

Products	Accuracy Goals	WMO Code	Frequency
1. Thickness (M) Between Standard Pressure Levels	Equivalent to ±2.0°K	FM86-VI Ext. SATEM	14 Daily
2. Precipitable Water (MM) Between Standard Pressure Levels	±30%	FM86-VI Ext. SATEM	14 Daily
3. Tropopause Temp. (DEG.) and Pressure (MB)	±2.5°K ±50 MB	FM86-VI Ext. SATEM	14 Daily
4. Cloud Cover From Area of Soundings and Pressure at Average Cloud Height	±20%	FM86-VI Ext. SATEM	14 Daily
5. Clear Radiances (in Terms of Brightness Temperature, °K)	±2%	FM87-VII Ext. SARAD	14 Daily

Table 5, Comparison of the performance of the METEOSAT, TIROS-N, AVHRR and HIRS 2 10 um infra-red channels

	METEOSAT	TIROS N AVHRR	HIRS 2
Wavelength μm	10.5-12.5	10.5-11.5	11.11
Spectral band width (cm^{-1})	152	83	35
IFOV mrad km	0.14 5	1.3 1.1	27 17.4
Entrance aperture diameter mm	400	200	150
Detector diameter mm	0.070	0.173	2.16
Detector temperature-K	91	105	105
Specified NE ΔT-K (1)	0.4	0.12	0.06
Calculated NE ΔT for 'Perfect' detector and Optics K (2)	0.06	0.003	0.0002
(1)/(2)	6.7	40	300*

*Detector probably optimised for 15 μm not 10 μm

TIROS-N Spacecraft

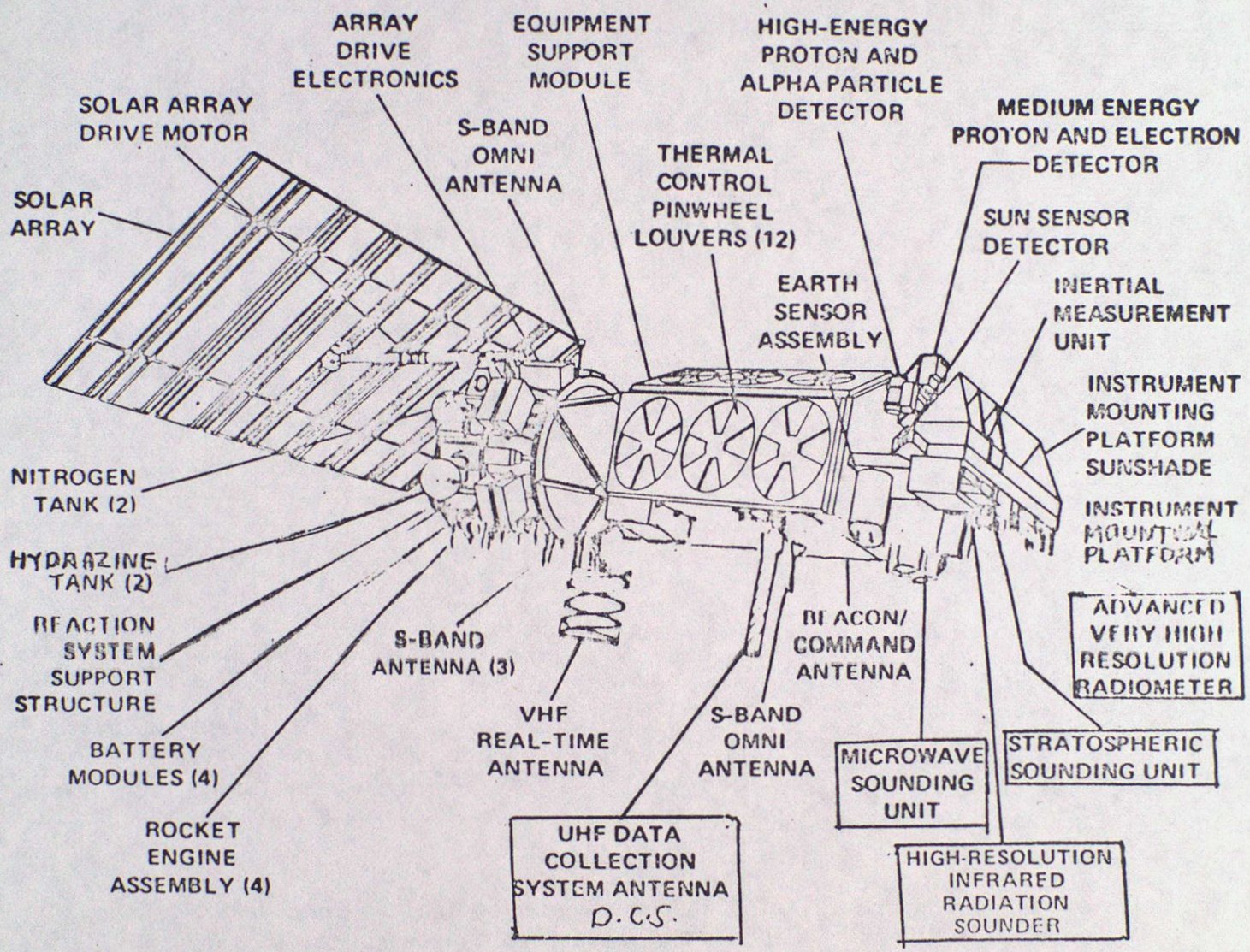

Fig 2

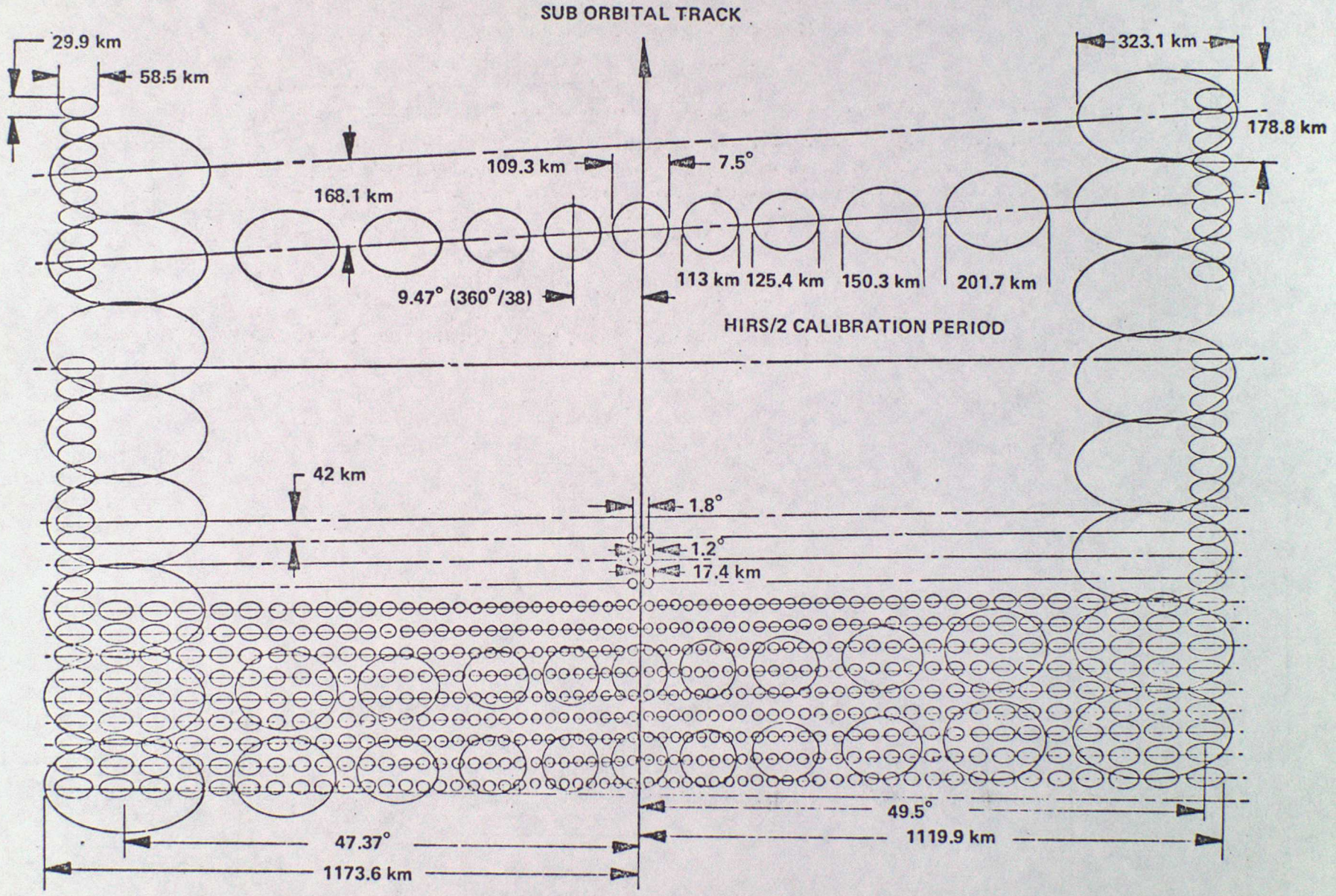

Figure 3.--TIROS Operational Vertical Sounder HIRS/2 and MSU scan patterns projected on earth

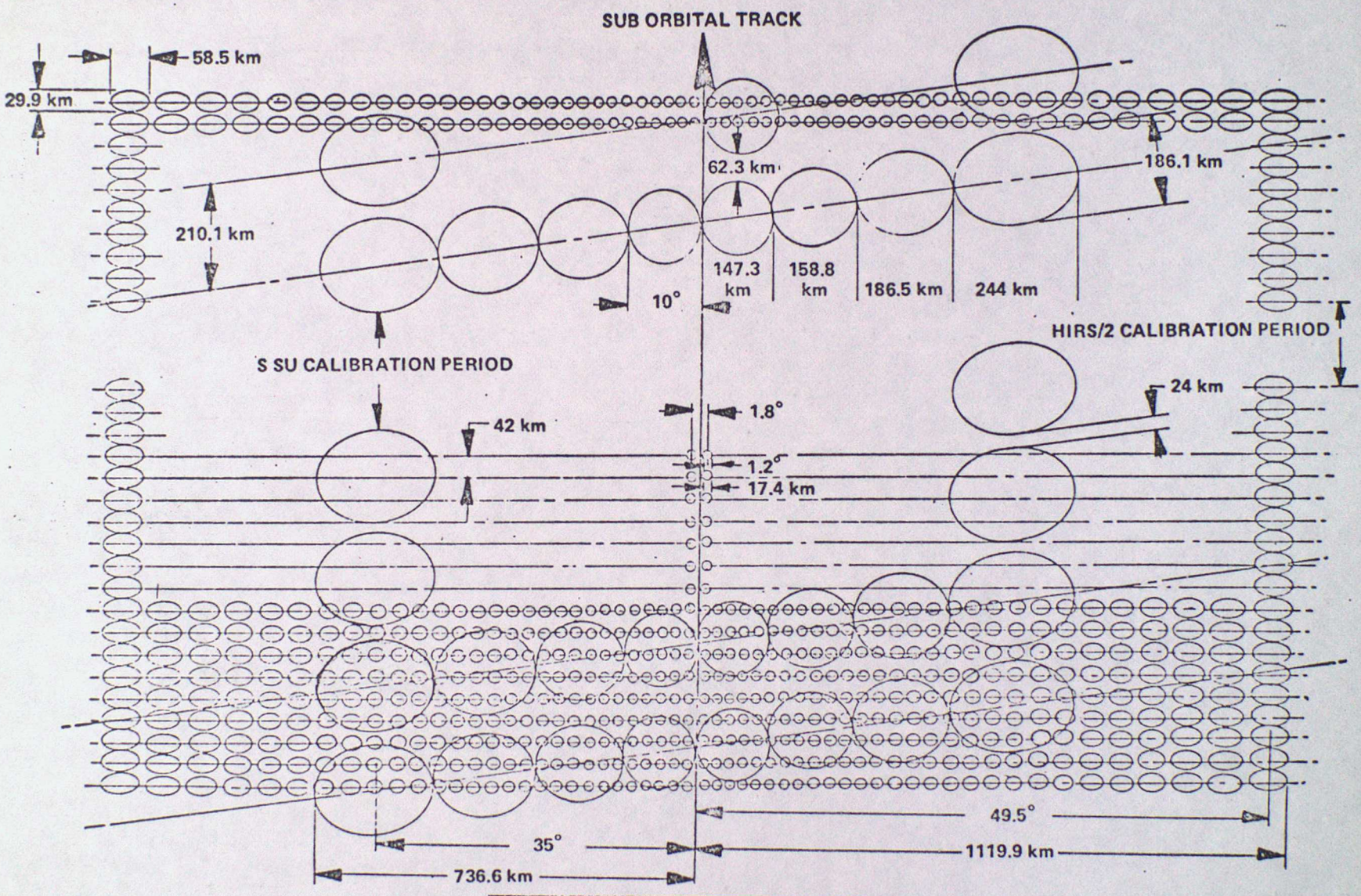

Figure 4 --TIROS Operational Vertical Sounder HIRS/2 and Stratospheric Sounding Unit scan patterns projected on earth

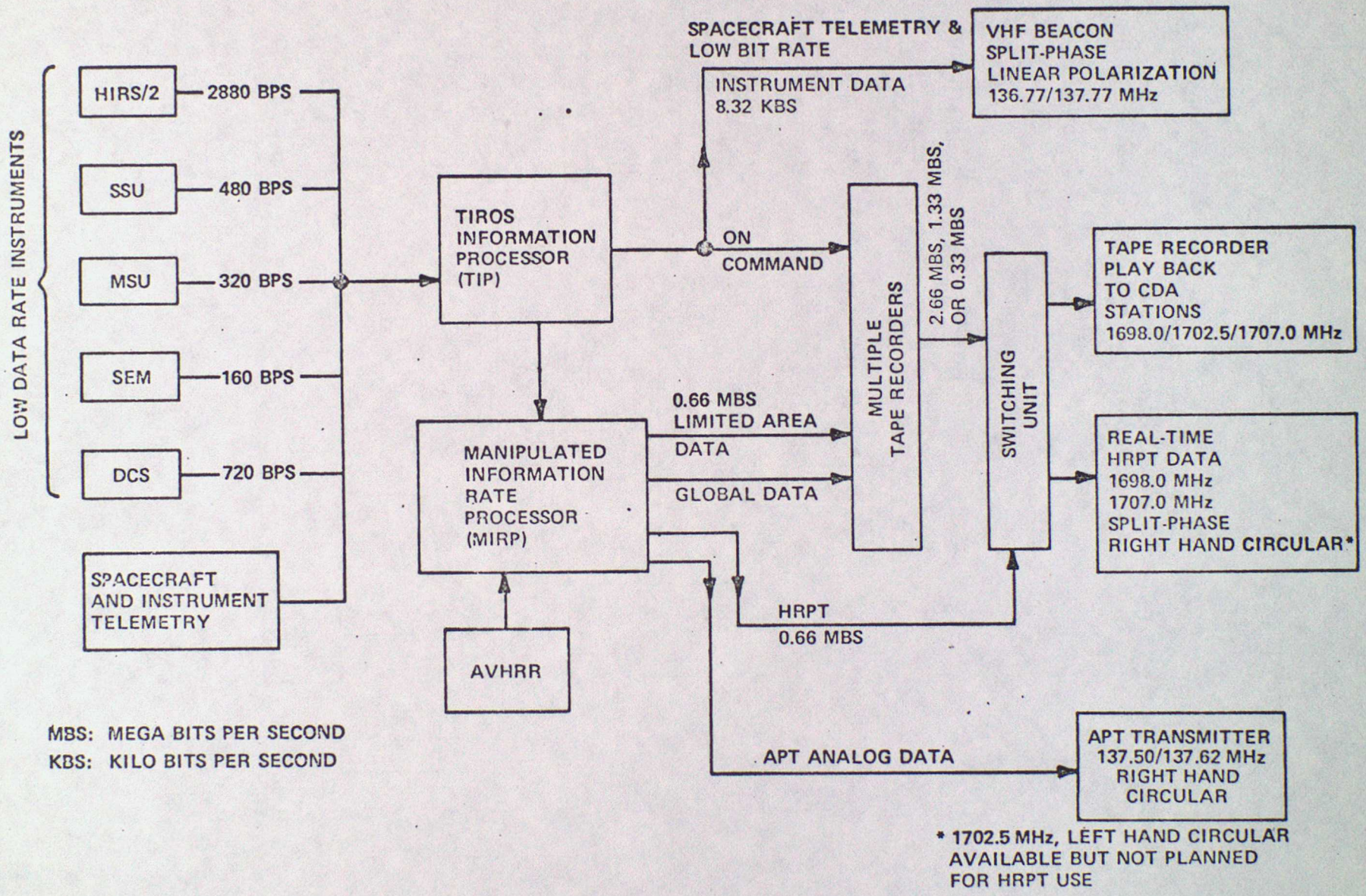

Figure 5--TIROS-N data flow diagram

Fig 6 **TIROS-N Operational System Data Flow**

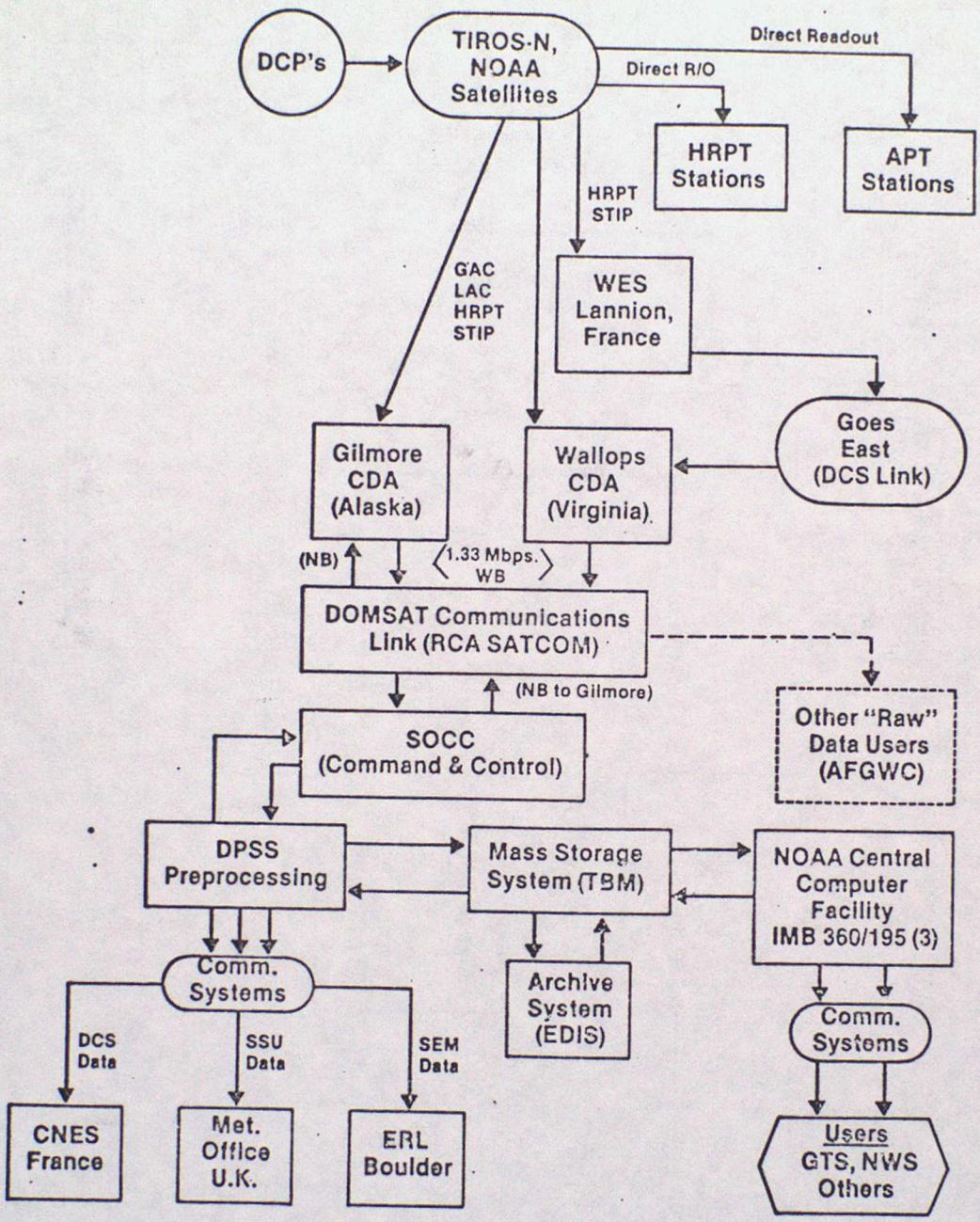

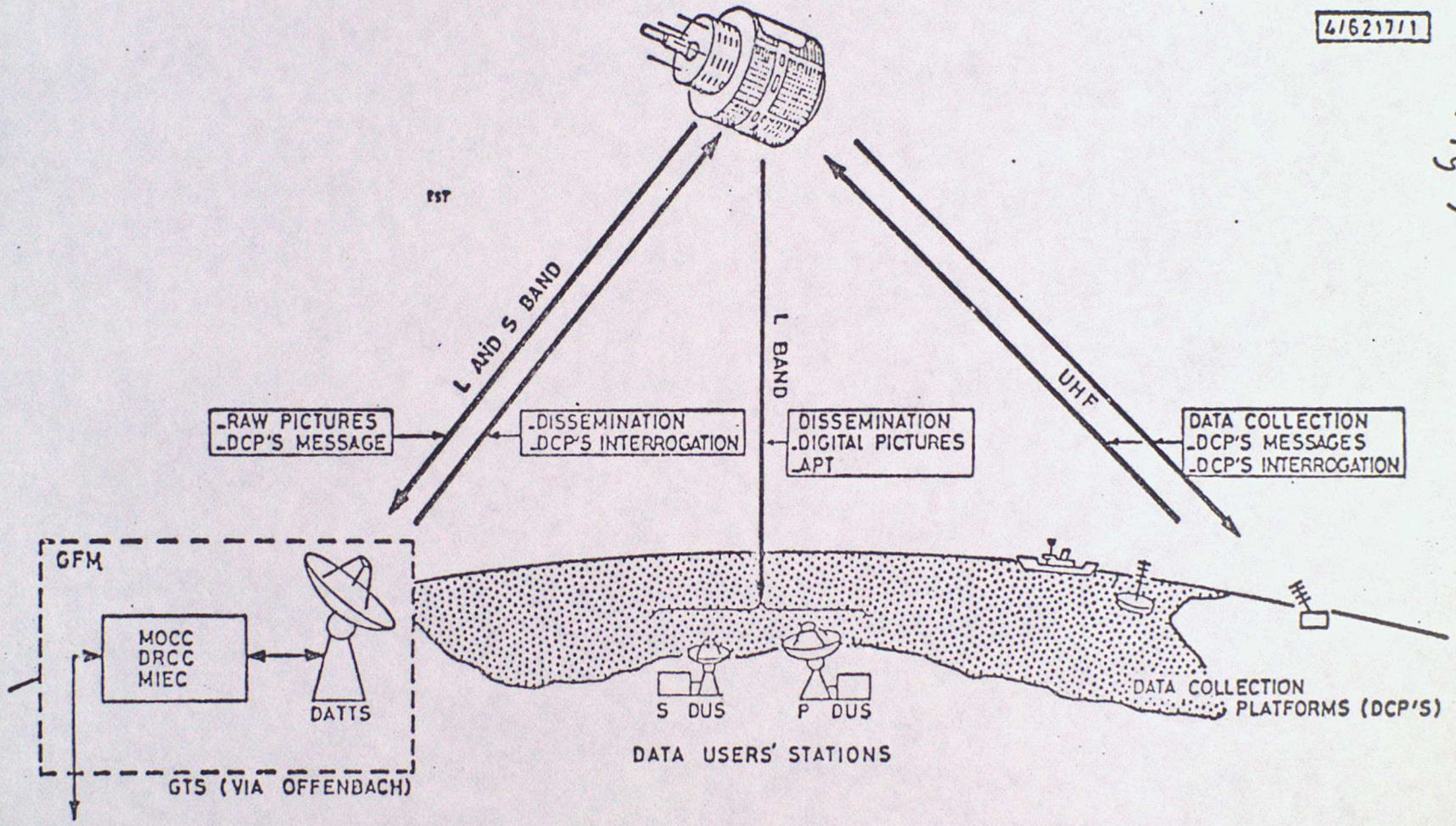
41621771
L AND S BAND
L BAND
UHF
-RAW PICTURES
-DCP'S MESSAGE
-DISSEMINATION
-DCP'S INTERROGATION
DISSEMINATION
-DIGITAL PICTURES
-APT
DATA COLLECTION
-DCP'S MESSAGES
-DCP'S INTERROGATION
GFM
MOCC
DRCC
MIEC
DATTS
GTS (VIA OFFENBACH)
S DUS
P DUS
DATA USERS' STATIONS
DATA COLLECTION
PLATFORMS (DCP'S)

Fig 7

III Radiative transfer theory applied to satellite measurements of radiation.

by J. R. Eyre

1. Introduction

This lecture develops the theory of radiative transfer as required for the interpretation of radiation measurements made by satellite instruments. The equations derived enable the calculation of the radiation intensity reaching the satellite if the state of the atmosphere and the absorption characteristics of its constituents are known. This provides a base for lectures 4 and 5 when we shall consider inverse problems, i.e. estimation of the atmospheric state given measurements of radiation.

Although the treatment is fairly general, approximations are necessary and these have been made in such a way as to bias the treatment towards problems involving infra-red radiation. The effects of the approximations must be considered before applying the results to longer or shorter wavelengths. The most important simplification is the omission of scattering by clouds and aerosols. Clouds are treated as emitting/absorbing surfaces only and radiative transfer inside clouds is not considered. In this way we need only consider radiation fluxes along the satellite viewing direction. For many infra-red problems these approximations are very good.

In common with much published work in this field, standard terminology has not been strictly applied. This reflects the inability of the available terms to cover all the variables which arise. Non-standard terms (e.g. "transmission") tend to be used liberally and to be given precise definition in context. This is the approach I have used here.

2. Absorption, transmission and emission of monochromatic radiation

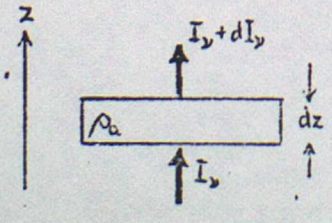

ρ_a = density of absorber

I_ν = intensity of radiation at wavenumber ν

Units
$kg\ m^{-3}$
$W m^{-2} sr^{-1} (cm^{-1})^{-1}$

The absorption of a beam of monochromatic radiation by an elemental path of absorbing gas is given by Lambert's law:

$$dI_\nu = - I_\nu k_\nu \rho_a dz, \qquad 2.1$$

and this effectively defines the monochromatic absorption coefficient, k_ν. Integrating over a path from z_0 to z_1, we obtain,

$$\int_{(I_\nu)_0}^{(I_\nu)_1} - dI_\nu / I_\nu = \int_{z_0}^{z_1} k_\nu \rho_a dz .$$

$$\therefore \quad (I_\nu)_1 = (I_\nu)_0 \exp \left\{ - \int_{z_0}^{z_1} k_\nu \rho_a dz \right\} . \qquad 2.2$$

Consequently the monochromatic transmission of the path is given by

$$\tau_\nu (z_0, z_1) = \frac{(I_\nu)_1}{(I_\nu)_0} = \exp \left\{ - \int_{z_0}^{z_1} k_\nu \rho_a dz \right\} . \qquad 2.3$$

For a homogeneous path this simply reduces to $\tau_\nu = \exp \{ -k_\nu \rho_a (z_1 - z_0) \}$, but we will generally be considering vertical or slant paths through the atmosphere and, since k_ν and ρ_a are both functions of pressure and temperature, they will also be functions of the distance along the path, z.

Besides absorbing radiation, the element of gas considered above will emit radiation with an intensity dependent on its temperature. Consider the element enclosed in a black box with walls at the same temperature, T, as the gas. The intensity emitted by the box and incident on the gas in any direction is $B_\nu (T)$, the Planck function, and so the absorption by the element in the z-direction is $B_\nu (T) k_\nu \rho_a dz$ (c.f. 2.1). We know from the 2nd law of thermodynamics that the gas must neither tend to warm nor cool. Therefore the net change of radiation passing through the gas in any direction must be zero, and so the intensity emitted in the z-direction must be $B_\nu (T) k_\nu \rho_a dz$. In other words, the coefficients of absorption and emission are both equal to k_ν. This is one of Kirchoff's laws and is strictly true only for thermodynamic equilibrium. Fortunately, in most of the neutral atmosphere local thermodynamic equilibrium (LTE) is a good approximation.

3. The radiative transfer equation

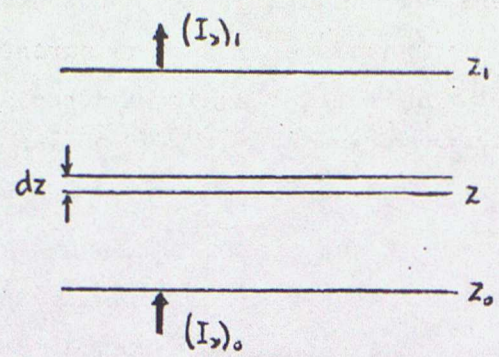

The intensity at z_1 is composed of two parts: a transmitted component, which depends on the intensity incident at z_0 and the transmission from z_0 to z_1, and an emitted component, which includes the radiation reaching z_1 from all elements, dz, between z_0 and z_1. This leads to the equation,

$$(I_\nu)_1 = (I_\nu)_0 \, \tau_\nu(z_0, z_1) + \int_{z_0}^{z_1} \left[B_\nu\{T(z)\} \, k_\nu(z) \, \rho_a(z) \, dz \right] \tau_\nu(z, z_1) . \qquad 3.1$$

By differentiating the expression for $\tau(z, z_1)$ (see 2.3) we obtain

$$\frac{d\tau_\nu(z, z_1)}{dz} = k_\nu \rho_a \, \tau_\nu(z, z_1) . \qquad 3.2$$

$$\therefore \quad (I_\nu)_1 = (I_\nu)_0 \, \tau_\nu(z_0, z_1) + \int_{\tau_\nu(z_0, z_1)}^{1} B_\nu\{T(z)\} \, d\tau_\nu(z, z_1) . \qquad 3.3$$

This is the monochromatic radiative transfer equation.

4. Satellite measurements of radiation

Equation 3.3 can be applied to monochromatic radiation emitted from the top of the atmosphere along a vertical or slant path and incident at a satellite instrument. Changing the notation so that $\tau_\nu(z)$ is the transmission from a height z to space, the radiance at the satellite is equal to the intensity at the top of atmosphere:

$$R_\nu = (I_\nu)_0 \, \tau_\nu(z_0) + \int_{\tau_\nu(z_0)}^{1} B_\nu\{T(z)\} \, d\tau_\nu(z) \qquad 4.1$$

Note that $\tau_\nu(z)$ will also be a function of θ, the zenith angle of the path.

The first term in this equation represents the contribution from the underlying surface - cloud top, land or sea - at height z_0. $(I_\nu)_0$ may include emitted, reflected and transmitted components. It depends

in general on the temperature and emissivity of the surface and, if it is not black, on the reflecting properties of the surface and the downward radiation incident on it and, for cloud, on the radiation transmitted through it. If the surface is black, then $(I_\nu)_s$ can be replaced by $B_\nu\{T_s\}$ where T_s is the surface temperature. In the infra-red this is often an adequate approximation of the sea surface and water clouds but is less good for some land surfaces and ice clouds. In the microwave region, reflection at the surface must usually be considered.

The second term in 4.1 is the contribution from atmospheric emission and can be more readily appreciated when re-written:

$$\int_{\tau_\nu(z_0)}^{1} B_\nu\{T(z)\}\, d\tau_\nu(z) = \int_{z_0}^{\infty} B_\nu\{T(z)\}\, \frac{d\tau_\nu(z)}{dz}\, dz = \int_{z_0}^{\infty} B_\nu\{T(z)\}\, K_\nu(z)\, dz \,. \qquad 4.2$$

$K_\nu(z)$ is known as a weighting function - it weights the Planck function profile corresponding to the atmospheric temperature profile. $K_\nu(z)$ is the differential of the atmospheric transmission profile; this is illustrated in figure 1 for two wavelengths, one of relatively strong and the other of relatively weak absorption. The height of the peak of the weighting function depends on the strength of the absorption and so, by using channels at different wavelengths with different absorption coefficients, radiation emanating from different layers of atmosphere can be measured. When the first term in 4.1 is negligible compared to the second,

$$R_\nu = \int_{z_0}^{\infty} B_\nu\{T(z)\}\, K_\nu(z)\, dz \,, \qquad 4.3$$

and so the radiance measured is a weighted average of the Planck function over the height region for which the weighting function has significant contribution. It is therefore related to the mean temperature of the layer. Because the weighting functions have a finite width, small scale vertical structure in the profiles of temperature (or composition) will have little effect on the radiances. For this reason we may expect variables related to the properties of a layer (e.g. thickness) to be more readily retrievable than those characterizing a level (e.g. tropopause temperature).

Equation 4.2 may be expressed using vertical co-ordinates other than height. For gases of constant mixing ratio, such as CO_2, a more convenient co-ordinate is log (pressure), since it yields weighting functions which are

nearly (but not exactly) independent of the temperature profile. This independence will be seen to be a desirable feature when we invert the radiative transfer equation to retrieve the temperature profile from the radiances.

5. Integration over frequency

So far we have only considered a monochromatic case. This is equivalent to assuming that k_ν is approximately constant over the pass-band of the radiometer. In the troposphere a typical infra-red spectral absorption line has a half-width (i.e. frequency interval over which the absorption coefficient changes from maximum to half-maximum) $\sim 0.1\ cm^{-1}$. Consequently a radiometer would need a pass-band considerably narrower than this for the monochromatic approximation to apply. Engineering limitations necessitate radiometer spectral pass-bands $\sim 10-100\ cm^{-1}$ for temperature-sounding infra-red channels. This is very much greater than the half-width of a single line and most channels encompass a spectral region with a complicated absorption spectrum caused by hundreds of lines. Therefore the radiative transfer equation needed for real instruments also contains an integration over wavenumber:

$$R := \frac{\int_0^\infty R_\nu f_\nu \, d\nu}{\int_0^\infty f_\nu \, d\nu} = \frac{\int_0^\infty \left\{ (I_\nu)_0 \, \tau_\nu(z_0) + \int_{\tau_\nu(z_0)}^1 B_\nu \{T(z)\} \, d\tau_\nu(z) \right\} f_\nu \, d\nu}{\int_0^\infty f_\nu \, d\nu} \quad 5.1$$

f_ν defines the "spectral response" of the instrument - it weights the incoming radiation at different wavelengths according to the relative sensitivity of the radiometer to such radiation. Typical relative responses are shown in figure 2 together with a molecular absorption spectrum for comparison. R, the radiance integrated over wavenumber, is usually normalised to the same units as B_ν by dividing by the integrated spectral response, $\int_0^\infty f_\nu \, d\nu$.

Equation 5.1 defines the FORWARD PROBLEM, i.e. given a knowledge of the atmospheric state and the concentrations and absorption characteristics of its absorbing species, we can calculate the intensity emitted from the top of the atmosphere as a function of wavenumber, and then, given the spectral response of the satellite instrument, we can calculate the radiance measured.

6. Absorption by single spectral lines

A single spectral line represents the transitions between two particular molecular energy states. The difference in energy between the two states determines the energy (and, therefore, the wavenumber) of the photon emitted/absorbed.

The monochromatic absorption coefficient for a single line depends on its strength and its shape. The strength is the integrated absorption coefficient of the line,

$$S = \int_0^\infty k_\nu \, d\nu \qquad 6.1$$

and depends on the probability of occurrence of a transition between the energy states. The shape depends on the physical processes broadening the line. In the atmosphere two processes are important: the range of velocities of the absorbing molecules (relative to the observer) cause Doppler broadening and the collisions with other molecules (which perturb the quantum mechanical wave functions) cause pressure or Lorentz broadening. Simple theory leads to the following expressions for absorption coefficient in each case:

$$\text{Doppler} : \quad k_\nu = \frac{S}{\sqrt{\pi}\,\alpha_D} \exp\left\{ \frac{-(\nu-\nu_0)^2}{\alpha_D^2} \right\}, \qquad 6.2$$

$$\text{Lorentz} : \quad k_\nu = \frac{S}{\pi} \frac{\alpha_L}{\alpha_L^2 + (\nu-\nu_0)^2} . \qquad 6.3$$

ν_0 is the line centre wavenumber, and α_L and α_D are the so-called "half-widths" for Lorentz and Doppler broadening respectively. These shapes are illustrated in figure 3.

$$\alpha_D = \nu_0 \left\{ \frac{2 k_B T}{m c^2} \right\}^{1/2} \qquad 6.4$$

where k_B = Boltzmann's constant, T = temperature, m = molecular mass, c = speed of light. S and α_L are more difficult to evaluate theoretically. However, for several atmospheric gases, much theoretical and experimental work has been done to determine them and tabulations of ν_0, S and α_L for the lines of many bands are available (see, for example, McClatchey et al., 1973).

In the infra-red, pressure broadening is usually dominant in the troposphere. However, since α_L is proportional to pressure, higher in the atmosphere α_L and α_D are often comparable and a line shape which is a convolution of the Lorentz and Doppler shapes must be used.

7. Some useful approximations

Equation 5.1 is difficult to evaluate in practice because it involves integrations of complicated functions over both the atmospheric path and wavenumber. Several approximations are usually required when calculating radiance numerically and those given here are among the more useful. They have been found to be adequately accurate for many calculations of atmospheric infra-red radiance.

a) The Curtis-Godson approximation

Each calculation of atmospheric transmission involves an integration over an inhomogeneous path. This can be approximated by a homogeneous path containing the same absorber amount,

$$u = \int du = \int \rho_a(z)\, dz \,, \qquad 7.1$$

and with pressure and temperature equal to the absorber-weighted means of the inhomogeneous path:

$$\bar{p} = \frac{\int p\, du}{u} \,, \quad \bar{T} = \frac{\int T\, du}{u} \,. \qquad 7.2$$

The main application of the Curtis-Godson approximation is in the calculation of mean transmissions over a spectral interval, Δz , i.e. over a line or a band, for which the monochromatic approximation does not apply. Band models can be derived to give the mean transmission,

$$\bar{\tau}_{\Delta\nu} = \frac{\int_{\Delta\nu} \tau_\nu\, d\nu}{\Delta\nu} \qquad 7.3$$

as a function of u, p and T for a homogeneous path (see below). The Curtis-Godson approximation then allows $\bar{\tau}_{\Delta\nu}$ to be calculated for an inhomogenous path characterised by u, $\bar{p}$ and $\bar{T}$. It is exact in certain special cases, namely for the mean transmission across a spectral line in the limits of both weak and strong absorption for an isothermal path where pressure broadening is the dominant line broadening mechanism. In other cases, including monochromatic calculations, the approximation is usually adequate and the error depends on the degree of inhomogeneity.

b) Path splitting

For monochromatic calculations the above approximation is improved by treating the path as a series of J more nearly homogeneous sections

and applying the Curtis-Godson approximation to each. Then, if $(\tau_\nu)_j$ is the transmission of the jth section, the combined transmission is given by

$$\tau_\nu = \prod_{j=1}^{J} (\tau_\nu)_j \quad . \qquad 7.4$$

Note that, in general, 7.4 cannot be extended to mean transmissions:

$$\bar{\tau} \neq \prod_{j=1}^{J} \bar{\tau}_j \qquad 7.5$$

This applies to series paths of the same absorbing gas. However 7.4 is applicable to the combined mean transmission of spectra which are not highly correlated. Therefore one can calculate transmissions of different gases separately and approximate their combined transmissions with 7.4.

c) Line-by-line integrations

The integration over wavenumber is most accurately performed using a "line-by-line" technique. This involves a series of monochromatic calculations at sufficiently high density in wavenumber space that the transmission function between the chosen points can be accurately interpolated and hence integrated numerically. The density required depends on the line widths and the accuracy to which the result is needed. The contributions from all significant lines are calculated at each wavenumber and so the effects of overlapping lines are automatically included. For complicated spectra this method is very demanding on computer time and requires an accurate knowledge of the spectral line parameters - their position, strength and shape.

d) Band models

Until recently line-by-line integrations have been impracticable because of the computing power required. Also, transmissions of the accuracy required (or justified by the errors in the spectral data) may often be calculated more quickly using band model techniques. These approximate the mean transmission (as defined by 7.3) over an interval of, say, 20 cm^{-1} containing many lines. For a theoretical discussion of band models and the calculation of mean transmissions see Goody (1964) or Rodgers (1976).

Having calculated mean transmissions over intervals of width $\Delta\nu$ across the spectral response of the radiometer, we can now compute the total radiance as the sum of the contributions from all intervals:

$$R \simeq \sum_i R_i f_i \Big/ \sum_i f_i \qquad 7.6$$

where f_i is the mean relative spectral response for the ith interval and

$$R_i = \frac{\int_{\Delta\nu} (I)_o \tau_b(z_o)\, d\nu + \int_{\Delta\nu} \int_{\tau_\nu(z_o)}^{1} B_\nu(z)\, d\tau_\nu(z)\, d\nu}{\int_{\Delta\nu} d\nu}$$

$$\simeq \overline{(I_o)}_i\ \bar{\tau}_i(z_o) + \int_{\bar{\tau}_i(z_o)}^{1} \bar{B}_i(z)\, d\bar{\tau}_i(z) \qquad 7.7$$

Here, mean values have been used for $(I_\nu)_o$ and $B_\nu(z)$ for each interval, Δz . This is usually a good approximation for intervals $\gtrsim 20\ cm^{-1}$ since $(I_\nu)_o$ and $B_\nu(z)$ are slowly varying functions of ν .

The integration over the atmospheric path is usually replaced by a summation over discrete layers of atmosphere. If $\bar{B}_{ni}$ is the mean Planck function for the ith spectral interval and the layer between levels $z=z_n$ and $z = z_{n+1}$, then

$$R_i \simeq \overline{(I_o)}_i\ \bar{\tau}_i(z_o) + \sum_n \bar{B}_{ni} \left\{ \bar{\tau}_i(z_{n+1}) - \bar{\tau}_i(z_n) \right\}, \qquad 7.8$$

where the summation is over all layers between z_o and space. Given a model of $\bar{\tau}_i(z)$ for each interval in terms of the absorber parameters calculated using the Curtis-Godson approximation, 7.8 and hence 7.6 can now be evaluated numerically.

References

Goody R.M. Atmospheric radiation I : theoretical basis. Oxford University Press (1964).

McClatchey R.A., Benedict W.S., Clough S.A., Burch D.E., Calfee R.F., Fox K., Rothman L.S., Garing J.S.
AFCRL Report TR-73-0096, Environ.Res.Pap.434(1973).
AFCRL atmospheric absorption line parameters compilation.

References (contd.)

Rodgers C.D. NCAR Tech.Note NCAR/TN 116+1A, March 1976.
Approximate methods of calculating transmissions by bands of spectral lines.

Houghton J.T. Cambridge University Press, 1977.
The physics of atmospheres.

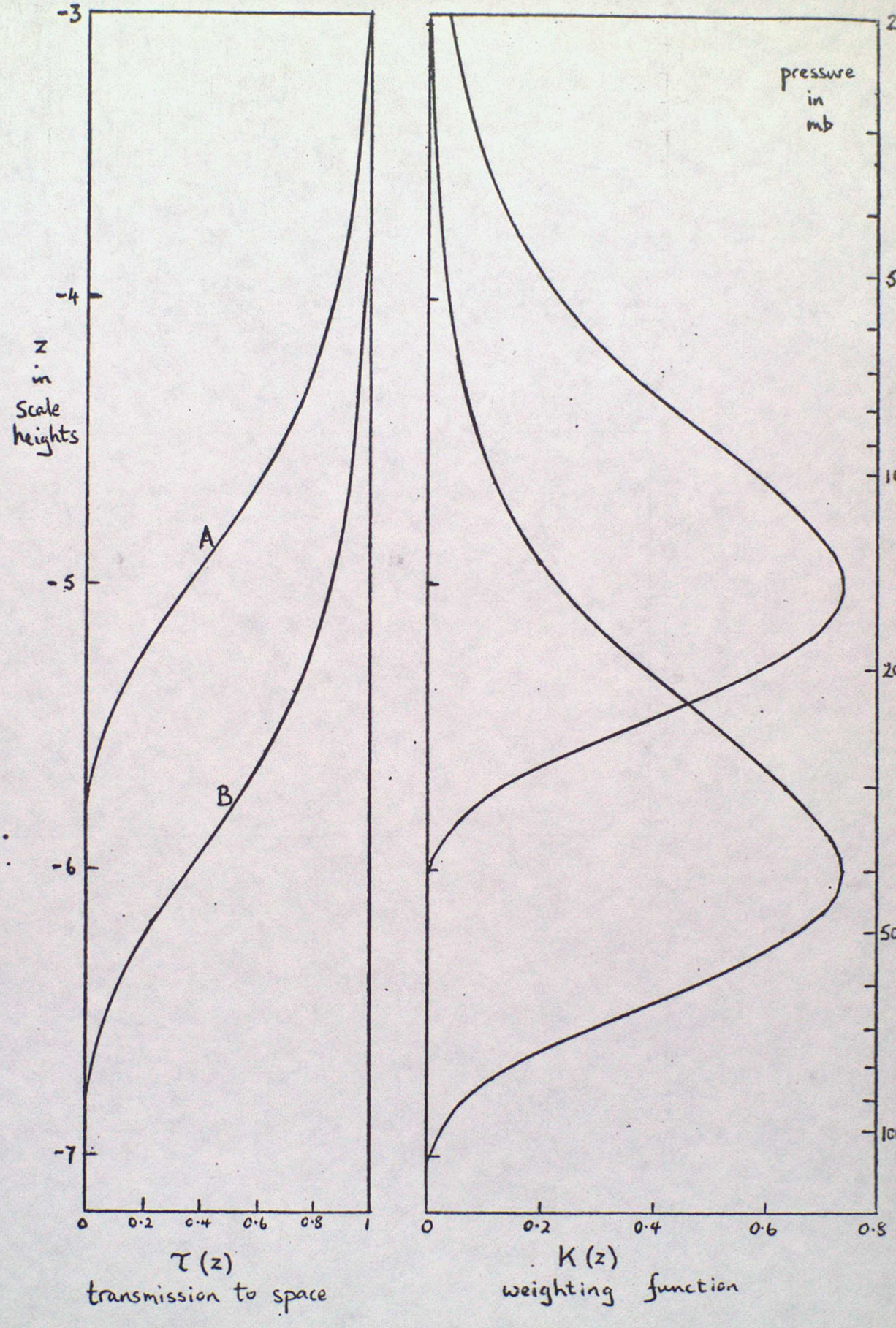

Figure 1 2 idealised transmission profiles and weighting functions at wavelengths with different absorption coefficients.

z is in scale heights, i.e. $z = -\ln(\text{pressure in mb})$

A : for wavelength of relatively strong absorption

B : for wavelength of relatively weak absorption

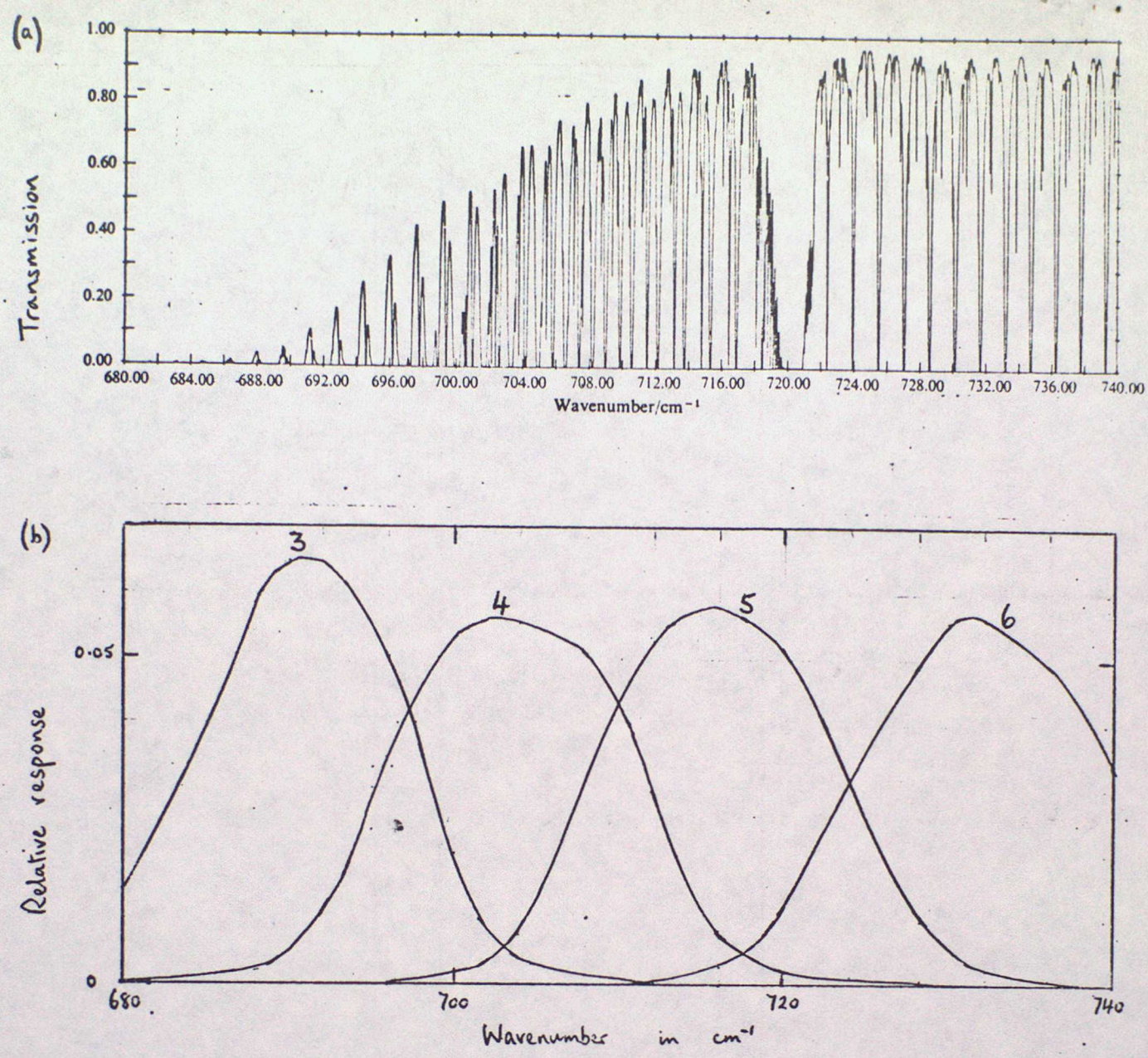

Figure 2

(a) Illustrating the fine structure of part of the 15μm CO_2 absorption band. Transmission of a 10 km horizontal path at 12km altitude. [Taken from Houghton (1977), p. 34.]

(b) The relative spectral responses of channels 3, 4, 5 and 6 of the HIRS instrument on the TIROS-N series. [c.f. Lecture 4, table 1 and figure 1].

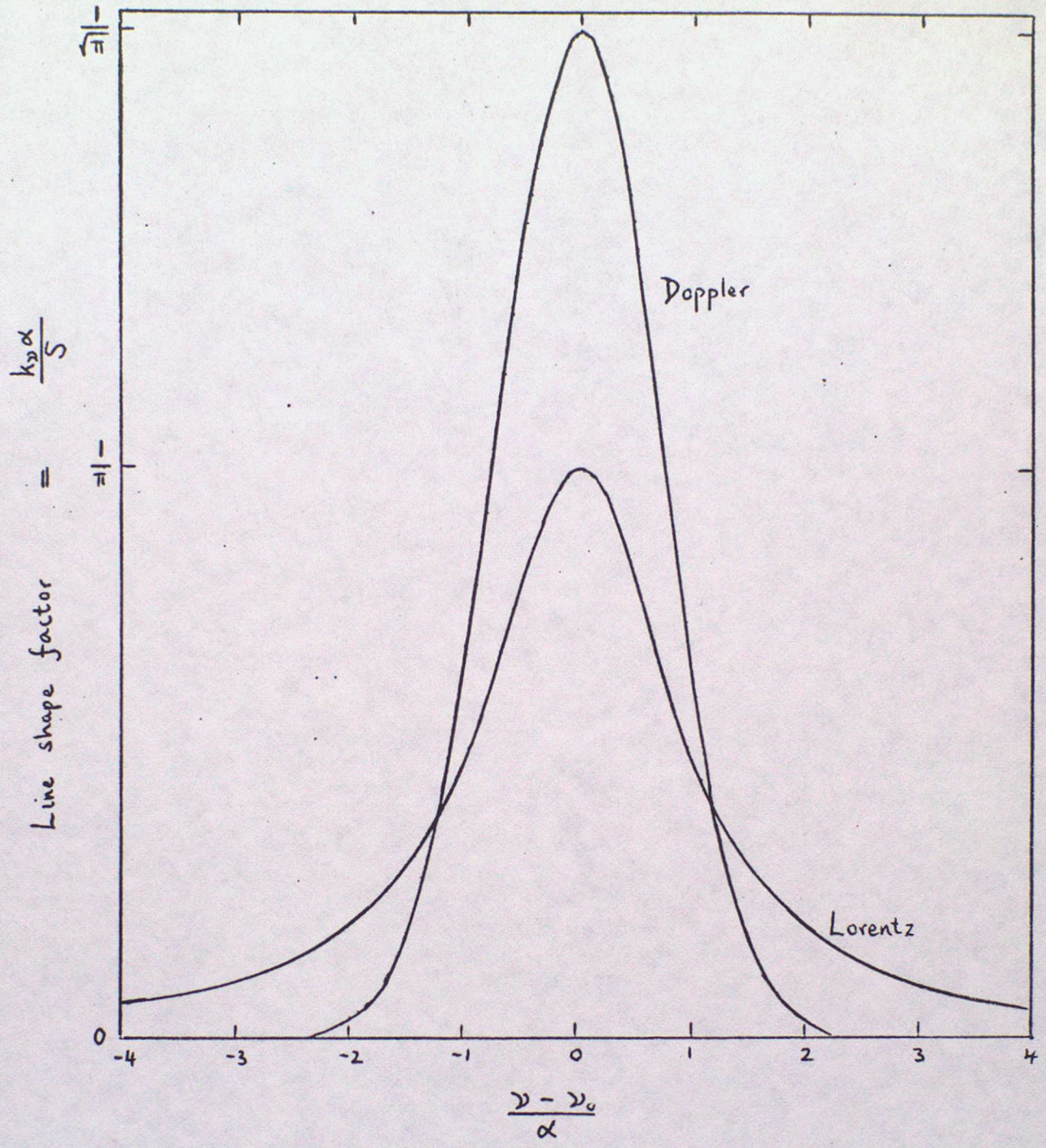

Figure 3

Illustrating the line shapes caused by Doppler and Lorentz broadening. α is the appropriate "half-width" for the broadening mechanism.

ADVANCED LECTURES - SATELLITE METEOROLOGY

IV Temperature Sounding

by J. R. Eyre

1. Introduction

We have seen in lecture 3 that the intensity of radiation emitted at the top of the atmosphere varies with wavelength and is a function of the temperature and composition structure. The wavelengths used by atmospheric sounding instruments are such that most of the radiation measured has been emitted by the atmosphere itself. Measurements of emission from gases of known concentration such as carbon dioxide and oxygen can be used to retrieve atmospheric temperature. On the other hand, if the temperature structure is known, information on the variable concentration profiles of constituents such as water vapour can be deduced from measurements at the wavelengths of their absorption bands (lecture 5). The channels used by the present sounding instruments on the TIROS-N series are given in table 1 and their approximate weighting functions are shown in figure 1.

The theory presented in lecture 3 allows us to calculate the emitted radiance given the state of the atmosphere. In temperature sounding, however, we are faced with the INVERSE PROBLEM - given the measured radiances, we have to estimate the temperature structure. The problem is usually divided into 2 stages:

(a) allow for the effects on the radiances of cloud cover,

(b) using cloud-free or "cloud-cleared" radiances, deduce the temperature profile.

Initially let us assume that we are dealing only with (b) and consider the treatment of cloud later.

2. Temperature profile retrieval from cloud-free radiances

Using the theory developed in lecture 3 we can write down an expression for the radiance measured by the ith channel of a satellite-borne radiometer.

$$R_i = (I_o)_{\nu_i} \, \overline{\tau}_i(z_o) + \int_{z_o}^{\infty} B_{\nu_i}(z) \, K_i(z) \, dz \qquad 2.1$$

Here we have assumed that the spectral range of the channel is sufficiently narrow for us to use quantities which have been averaged over wavenumber: $(I_o)_{\nu_i}$ and $B_{\nu_i}(z)$ are evaluated at some mean wavenumber ν_i, and $\overline{\tau}_i(z_o)$ and $K_i(z)$ are the appropriate mean transmittance and weighting function for the channel. The approximations involved usually produce negligible error.

For numerical solution of the problem it is more convenient to replace the integral equations by vectors and matrices:

$$R_i = \underline{K_i} \cdot \underline{B} \qquad 2.2$$

Here we have expressed the temperature profile (in the form of the Planck function profile) at a finite number of levels and the weighting function of the ith channel similarly such that $\underline{B}$ and $\underline{K_i}$ are vectors of length J = number of levels. We have also expressed the surface term as the first elements of the vectors. J must be sufficiently large for accurate approximation of an integral by a vector equation. In practice ~ 30–100 temperature levels are used.

Equation 2.2 refers to only one channel. For a radiometer with I channels we can write,

$$\underline{R} = \underline{\underline{K}} \cdot \underline{B} \qquad 2.3$$

where $\underline{R}$ is a vector of length I,

$\underline{B}$ is a vector of length J,

and $\underline{\underline{K}}$ is a matrix, J x I, containing the discrete weighting functions for all the channels.

(We have assumed that all values ν_i are sufficiently close to one another that we need only use one function $\underline{B}$. In practice allowance must be made for this. For example the measured radiances can be scaled so that they all apply to a common reference wavenumber. Other approaches are also used).

An important property of 2.3 is the linear relationship between $\underline{R}$ and $\underline{B}$ which allows us to use linear theory in the inversion. This is an approximation for a number of reasons, one of which is the slight temperature dependence of the weighting functions. The linearity of the problem is usually improved by expressing the radiances and Planck functions as deviations from mean values:

$$\underline{r} = \underline{R} - \overline{\underline{R}} \quad \text{and} \quad \underline{b} = \underline{B} - \overline{\underline{B}}$$

$$\therefore \quad \underline{r} = \underline{\underline{K}} \cdot \underline{b} \qquad 2.4$$

The fundamental difficulties of the retrieval problem can now be seen: we have I measurements of radiance and we want to obtain a profile at J points. Usually J > I, and so there are an infinite number of solutions $\underline{b}$ which satisfy the measurements $\underline{r}$. Referring back to 2.1 we see that we are attempting to obtain a continuous function from a finite number of measurements. Our task is to find from the infinite number of solutions an acceptable solution and, if possible, the most probable solution. This involves constraining the solution using a priori information, which is equivalent to adding enough equations to the problem so that we have at least as many equations as unknowns. One obvious way of constraining

the solution is to reduce the number of levels at which $\underline{b}$ is specified or express $\underline{b}$ as a linear combination of a small number of pre-selected functions so that $J \leqslant I$. Neither of these simple approaches tends to work well in practice (see Rodgers, 1976). Briefly, the problem arises from the mathematics of the inversion procedure. We are seeking a predictive equation of the form,

$$\underline{b} = \underline{\underline{D}} \cdot \underline{y} \qquad 2.5$$

The matrix $\underline{\underline{D}}$ which is obtained by the methods suggested above tends to have elements which oscillate from large positive to large negative values. Consequently any small errors in $\underline{y}$ are amplified into unacceptably large errors in $\underline{b}$. Successful inversion methods must overcome this kind of instability.

3. Some inversion methods

a. Minimum variance method

Forms of constraint which have been found to give satisfactory results are based on the statistics of $\underline{b}$ and corresponding $\underline{y}$ based on climatological sets of profiles. The "minimum variance method" minimizes the variance between the true profile $\underline{b}$ and the estimated profile $\hat{\underline{b}}$ obtained using a predictive equation,

$$\hat{\underline{b}} = \underline{\underline{D}} \cdot \underline{y} \qquad 3.1$$

This procedure leads to the well-known multiple linear regression relation:

$$\underline{\underline{D}} = E\{\underline{b} \cdot \underline{y}^T\} \cdot \left[E\{\underline{y} \cdot \underline{y}^T\}\right]^{-1} \qquad 3.2$$

where $\underline{y}^T$ is the transpose of $\underline{y}$

$[\,]^{-1}$ denotes matrix inverse,

and $E\{\cdot\}$ is the expected value operator applied to an appropriate set of profiles.

This solution is discussed by Rodgers (1976) and shown to be identical to the "maximum probability" solution for a set of profiles with Gaussian statistics.

Equation 3.2 can be applied in 2 ways:

i) We may neglect all considerations of the physics involved and collect a set of radiances $\underline{r}$ colocated with a set of radiosonde profiles $\underline{b}$ and hence derive $\underline{\underline{D}}$. This is the basis of the method currently used by NOAA to generate the soundings distributed over the GTS. It was first applied in the simple form given here (Smith et al, 1970) but has now been adapted to use the eigenvectors of the temperature and radiance vectors covariance matrices rather than the vectors themselves (Smith and Woolf, 1976).

ii) We may apply the weighting functions to a representative set of profiles in the following way:

$$\underline{r} = \underline{\underline{K}} . \underline{b} + \underline{\epsilon} \qquad 3.3$$

where $\underline{\epsilon}$ represents random measurement error.
Substituting 3.3 into 3.2 we obtain,

$$E\{\underline{b} . \underline{r}^T\} = \underline{\underline{S}}_b . \underline{\underline{K}}^T$$

$$\text{and} \quad E\{\underline{r} . \underline{r}^T\} = \underline{\underline{S}}_r = \underline{\underline{K}} . \underline{\underline{S}}_b . \underline{\underline{K}}^T + \underline{\underline{S}}_\epsilon \qquad 3.4$$

where $\underline{\underline{S}}_b, \underline{\underline{S}}_r$ and $\underline{\underline{S}}_\epsilon$ are the covariance matrices of $\underline{b}$, $\underline{r}$ and $\underline{\epsilon}$ respectively. This leads to the minimum variance solution,

$$\underline{\underline{D}} = \underline{\underline{S}}_b . \underline{\underline{K}}^T . \left[\underline{\underline{K}} . \underline{\underline{S}}_b . \underline{\underline{K}}^T + \underline{\underline{S}}_\epsilon \right]^{-1} \qquad 3.5$$

These methods are computationally fast and utilize fully existing knowledge about atmospheric covariance. Also the regression equation 3.1 can be formulated in several ways, eg radiance v Planck function profile, equivalent radiative temperature v. temperature profile, equivalent radiative temperature v. thickness. A further advantage of method (i) is that it removes biases caused by weighting function errors since weighting function information is not used.

Disadvantages of these methods (and other statistical methods) are:

i) The statistics must be chosen with care; inappropriate statistics lead to poor results and different regression coefficients are required to allow for seasonal and latitudinal variation.

ii) In general profiles with shapes which were not included in the calculation of regression coefficients cannot be retrieved. This is a consequence of relying on correlations between levels rather than on the physics of the radiative transfer problem.

b. Minimum information method

Although it can be derived independently (see Smith et al, 1972), this method is an approximation to the minimum variance method. If we approximate,

$$\underline{\underline{S}}_b = \sigma_b^2 \underline{\underline{I}}_b \quad \text{and} \quad \underline{\underline{S}}_\epsilon = \sigma_\epsilon^2 \underline{\underline{I}}_\epsilon \,, \qquad 3.6$$

where $\underline{\underline{I}}$ is an identity matrix (of appropriate magnitude),

σ_ϵ^2 is the measurement error variance,

and σ_b^2 is the profile variance,

then $\underline{\underline{D}}$ is reduced to,

$$\underline{\underline{D}} = \underline{\underline{K}}^T \cdot \left[\underline{\underline{K}} \cdot \underline{\underline{K}}^T + \frac{\sigma_\epsilon^2}{\sigma_b^2} \underline{\underline{I}}_\epsilon \right]^{-1} \qquad 3.7$$

The method has been used with equation 3.1 but with $\hat{\underline{b}}$ and $\underline{y}$ now referring to deviations from a first guess profile $\underline{B}_0$ (eg from a forecast). It has also been used iteratively and readily converges to a solution (Smith et al 1972) although the theoretical validity of this approach has been questioned (Rodgers, 1976).

c. Direct Methods

Several empirical methods which do not use statistics are to be found in the literature. The iterative relaxation method introduced by Chahine (1968) and reformulated by Smith (1970) is an example. In Smith's method the radiances $\underline{R}_0$ corresponding to a first guess profile $\underline{B}_0$ are calculated. Then the profile at the j^{th} level is adjusted according to the difference between the measured radiances $\underline{R}_m$ and the calculated radiances $\underline{R}_0$ using the weighting function values at the j^{th} level as weights:

$$(b_1)_j = (B_1)_j - (B_0)_j = \frac{\sum_{i=1}^{I} K_{ij} \{ (R_m)_i - (R_0)_i \}}{\sum_{i=1}^{I} K_{ij}} \qquad 3.8$$

From $\underline{B}_1$ the equivalent radiances are computed and the process repeated. The iteration proceeds to a solution $\underline{B}_n$ at the n^{th} step for which the difference between the measured and calculated radiances meets some criterion (related to instrumental noise).

This method is fast and directly applies the physics of the problem (including any non-linearities). The constraints here are not obvious but they are effectively introduced in 3.8 through the implicit assumption that $\underline{b}$ at each step is a linear combination of the weighting functions. In common with similar direct methods a solution is obtained which may not be the most probable solution in the statistical sense.

A defect of all methods which use weighting functions is that they propagate errors in the absorption coefficients into the solution. This

problem can be approached by:

i) improving our knowledge of the molecular spectroscopy which is involved in the calculation of transmissions,

ii) making empirical corrections to the weighting functions to eliminate biases between measured radiances and those calculated using colocated radiosonde data.

4. The effects of cloud

We have dealt so far only with the cloud-free case. When sounding the troposphere the number of such cases is limited and the areas of most meteorological interest are usually the most cloudy. The presence of cloud and the errors introduced when allowing for it in the retrieval process are at present a major limitation on the accuracy of soundings.

When there is complete cover of thick cloud there is no information in the infra-red radiances about the temperature profile below the cloud top. In such cases attempts at retrieving the temperature profile below the cloud fail. However a scheme based only on the microwave radiances, which are affected only slightly by cloud, may be used (lecture 8).

If there is only partial cloud cover, with at least part of the radiometer field of view "seeing" the earth's surface, then "cloud-clearing" techniques can be used to calculate the radiances which would be observed in the absence of cloud (but with the atmosphere unchanged in all other respects). Several methods have been proposed for calculating cloud-cleared radiances. The most successful approach was first proposed by Smith (1968). It is based on the comparison of radiances in adjacent fields of view. An extension of this method (McMillin, 1978) is currently used operationally by NOAA.

The adjacent field of view methods assume that there exists a number of fields of view which differ from adjacent fields in cloud amount (fractional coverage) but not significantly in cloud top height or other parameters. Pairs of fields of view for which this approximation is valid yield good clear column radiances; other pairs must be eliminated by various empirical tests and they usually correspond to areas of cloud with mixed heights.

If fields of view labelled 1 and 2 contain cloud fractions N_1 and N_2 at the same height then the measured radiances in any channel are given by

$$R_1 = N_1 R_0 + (1 - N_1) R_c \quad \text{in 1}$$

$$\text{and} \quad R_2 = N_2 R_0 + (1 - N_2) R_c \quad \text{in 2} \; . \qquad 4.1$$

where R_o and R_c are the radiances from completely overcast and completely clear fields of view respectively. Eliminating R_o for this pair of equations gives

$$R_c = \frac{R_1 - N^* R_2}{1 - N^*} \quad ; \quad N^* = \frac{N_1}{N_2} \qquad 4.2$$

The relative cloud cover N^* can be found if the window channel clear column radiance is estimated using knowledge of the surface temperature obtained from a priori information or the microwave radiances. Rearranging 4.2 for the window channel,

$$N^* = \frac{R_1\,(\text{window}) - R_c\,(\text{window})}{R_2\,(\text{window}) - R_c\,(\text{window})} \qquad 4.3$$

R_c is then found for all other channels by substituting N^* into 4.2. This method is illustrated graphically in figure 2.

5. Accuracy of retrieval products

Temperature soundings are a recent addition to routine meteorological observations. They were proposed theoretically, only 20 years ago and since then the required technology has been developed very quickly and continues to improve. Consequently the accuracy of the product of the TIROS-N series (operational since 1978) is a considerable improvement on its predecessors and we may expect further improvements in instrumentation and data analysis techniques to enhance the quality of the product in future. Although statistics are available on the present accuracy of satellite soundings they should not be regarded as the attainable limit of the technique.

The accuracy of satellite soundings is usually expressed as an r.m.s. deviation from some other data — colocated radiosondes or objective analyses based on conventional data. Therefore this deviation is not just the error of the satellite sounding. In the case of colocated sondes it includes the sonde errors and discrepancies arising from space and time differences allowed by the colocation criteria. Comparison with objective analysis will remove some of these errors but will introduce a dependence on the type of analysis scheme used.

Table 2 presents some statistics of r.m.s. deviations for the mean temperature of various layers using data from the sounding instruments on NIMBUS-6 (very similar to those on the TIROS-N series). The radiosonde data were colocated with remote soundings within 222 km and 6 hours. Also shown is the estimated theoretical limit of this sounding system, obtained

by calculating radiances from a set of profiles, adding realistic noise and then retrieving temperature profiles from the radiances using the minimum information method. It can be shown (Hayden, 1979) that a large part of the difference is caused by radiosonde/colocation errors. Much of the rest is caused by the cloud contamination problem. Phillips et al (1979) quote r.m.s. differences from radiosondes of 2.0K or better (1.5K in the tropics) as typical of the TIROS-N system based on comparisons in early 1979. They stress that the retrieval scheme was then undergoing refinement in the light of errors found.

The theoretical limit on the accuracy for any remote sounder is imposed by instrumental factors (noise and calibration accuracy) and by the width of weighting functions. The former can be reduced by instrumental improvements. The latter is a fundamental limitation of remote sounding, since vertical structure on a scale much smaller than the width of the weighting functions cannot be resolved. For this reason features such as the tropopause and low level inversions are not well retrieved but parameters of a broad layer such as its mean temperature or thickness (as required by numerical models) are obtained more accurately. This is illustrated in figure 3 with a typical comparison between a retrieved profile and a radiosonde profile.

The usefulness of satellite soundings in numerical forecasting obviously depends on their accuracy compared to other data and to the accuracy of the background field of the analysis. However there are other considerations. Firstly, the time taken to receive, process and transmit the data to the user may restrict the amount of data which is included in the analysis. Secondly, the asynoptic nature of the data suggests that the conventional methods of assimilation may not be appropriate. Thirdly, the ability of the analysis to accept the information contained in the data must be considered. The potential spatial resolution of the data is high compared to the radiosonde network and analysis schemes optimized on radiosonde data may smooth out the real information in the satellite soundings. Also, since it is probable that errors in adjacent retrieved thicknesses will show high correlation, it may be better to seek some way of incorporating in the analysis the horizontal gradient information contained in the radiance data. In general, the overall quality of satellite data may be comparable with radiosonde data but the two systems have very different characteristics. If no allowance is made for this fact in the analysis scheme, then the numerical model will fail to extract full benefit from the new data.

References

Chahine M T 1968 J. Opt. Soc. Am., 58, 1634.
Determination of the temperature profile of an atmosphere from its outgoing radiance.

Hayden C M 1979 WMO Technical Note No 166
Quantitative meteorological data from satellites. Chapter 1: Remote soundings of temperature and moisture.

McMillin L M 1978 Mon. Weather Rev., 106, 1590-1597
An improved method for obtaining clear column radiances from cloud-contaminated radiances.

Phillips N A, McMillin L M, Wark D Q, Gruber A 1979
Bull. Am. Met. Soc., 60, 1188-1197.
An evaluation of early operational temperature soundings from TIROS-N.

Rodgers C D 1976 Rev. Geophys. Sp. Phys., 14, 609-624.
Retrieval of atmospheric temperature and composition from remote measurements of thermal radiation.

Smith W L 1968 Mon. Weather Rev., 96, 387-396.
An improved method for calculating tropospheric temperature and moisture from satellite radiometer measurements.

Smith W L 1970 Appl. Opt., 9, 1993-1999.
Iterative solution of the radiative transfer equation for the temperature and absorbing gas profile of an atmosphere.

Smith W L, Woolf H M, Jacob W J 1970 Mon. Weather Rev., 98, 582-603.
A regression method for obtaining real time temperatures and geopotential height profiles from satellite spectrometer measurements and its application to NIMBUS-3 SIRS observations.

Smith W L, Woolf H M, Fleming H E 1972 J. Appl. Meteor., 11, 113-122.
Retrieval of atmospheric temperature profiles from satellite measurements for dynamical forecasting.

Smith W L, Woolf H M 1976 J. Atmos. Sci., 33, 1127-1140.
The use of eigenvectors of statistical covariance matrices for interpreting satellite sounding radiometer observations.

Smith W L, Woolf H M, Hayden C M, Wark D Q, McMillin L M 1979
Bull. Am. Met. Soc., 60, 1177-1187.
The TIROS-N operational vertical sounder.

HIRS Channel number	Channel central wavenumber	Central wavelength (μm)	Principal absorbing constituents	Level of peak energy contribution	Purpose of the radiance observation
1	668	15.00	CO_2	30 mb	*Temperature sounding.* The 15-μm band channels provide better sensitivity to the temperature of relatively cold regions of the atmosphere than can be achieved with the 4.3-μm band channels. Radiances in Channels 5, 6, and 7 are also used to calculate the heights and amounts of cloud within the HIRS field of view.
2	679	14.70	CO_2	60 mb	
3	691	14.50	CO_2	100 mb	
4	704	14.20	CO_2	400 mb	
5	716	14.00	CO_2	600 mb	
6	732	13.70	CO_2/H_2O	800 mb	
7	748	13.40	CO_2/H_2O	900 mb	
8	898	11.10	Window	Surface	*Surface temperature* and cloud detection.
9	1 028	9.70	O_3	25 mb	*Total ozone* concentration.
10	1 217	8.30	H_2O	900 mb	*Water vapor sounding.* Provides water vapor corrections for CO_2 and window channels. The 6.7-μm channel is also used to detect thin cirrus cloud.
11	1 364	7.30	H_2O	700 mb	
12	1 484	6.70	H_2O	500 mb	
13	2 190	4.57	N_2O	1 000 mb	*Temperature sounding.* The 4.3-μm band channels provide better sensitivity to the temperature of relatively warm regions of the atmosphere than can be achieved with the 15-μm band channels. Also, the short-wavelength radiances are less sensitive to clouds than those for the 15-μm region.
14	2 213	4.52	N_2O	950 mb	
15	2 240	4.46	CO_2/N_2O	700 mb	
16	2 276	4.40	CO_2/N_2O	400 mb	
17	2 361	4.24	CO_2	5 mb	
18	2 512	4.00	Window	Surface	*Surface temperature.* Much less sensitive to clouds and H_2O than the 11-μm window. Used with 11-μm channel to detect cloud contamination and derive surface temperature under partly cloudy sky conditions. Simultaneous 3.7- and 4.0-μm data enable reflected solar contribution to be eliminated from observations.
19	2 671	3.70	Window	Surface	
20	14 367	0.70	Window	Cloud	*Cloud detection.* Used during the day with 4.0- and 11-μm window channels to define clear fields of view.

MSU	Frequency (GHz)	Principal absorbing constituents	Level of peak energy contribution	Purpose of the radiance observation
1	50.31	Window	Surface	*Surface emissivity* and *cloud attenuation* determination.
2	53.73	O_2	700 mb	*Temperature sounding.* The microwave channels probe through clouds and can be used to alleviate the influence of clouds on the 4.3- and 15-μm sounding channels.
3	54.96	O_2	300 mb	
4	57.95	O_2	90 mb	

SSU	Wavelength (μm)	Principal absorbing constituents	Level of peak energy contribution	Purpose of the radiance observation
1	15.0	CO_2	15.0 mb	*Temperature sounding.* Using CO_2 gas cells and pressure modulation, the SSU observes thermal emissions from the stratosphere.
2	15.0	CO_2	4.0 mb	
3	15.0	CO_2	1.5 mb	

Table 1.

Characteristics of TIROS Operational Vertical Sounder (TOVS) channels

from Smith et al., 1979

To pressure level (mb): \ From pressure level (mb):	1000	850	700	500	400	300	250	200	150
100	1·2 ·4	1·3 ·4	1·3 ·5	1·4 ·5	1·5 ·6	1·8 ·7	2·0 ·9	2·4 1·4	2·8 1·7
150	1·1 ·3	1·2 ·3	1·3 ·3	1·5 ·4	1·7 ·6	2·2 ·7	2·4 ·9	2·6 1·3	
200	1·1 ·3	1·2 ·3	1·3 ·4	1·5 ·6	1·9 ·9	2·3 1·7	2·6 1·1		
250	1·1 ·3	1·1 ·3	1·2 ·4	1·5 ·7	1·7 1·1	2·4 1·6			
300	1·2 ·2	1·3 ·2	1·3 ·3	1·5 ·6	1·8 1·0				
400	1·6 ·3	1·6 ·3	1·6 ·5	1·6 ·6					
500	1·9 ·3	1·8 ·3	1·8 ·6						
700	2·5 ·4	2·3 ·5							
850	2·8 ·6								

Table 2

Statistics for retrieved layer mean temperatures from Nimbus-6 data

Upper value : r.m.s. deviation in deg. K of remotely sounded layer mean temperature from colocated radiosonde value.

Lower value : corresponding theoretical limit of r.m.s. error in the remote sounding

Taken from Hayden, 1979.

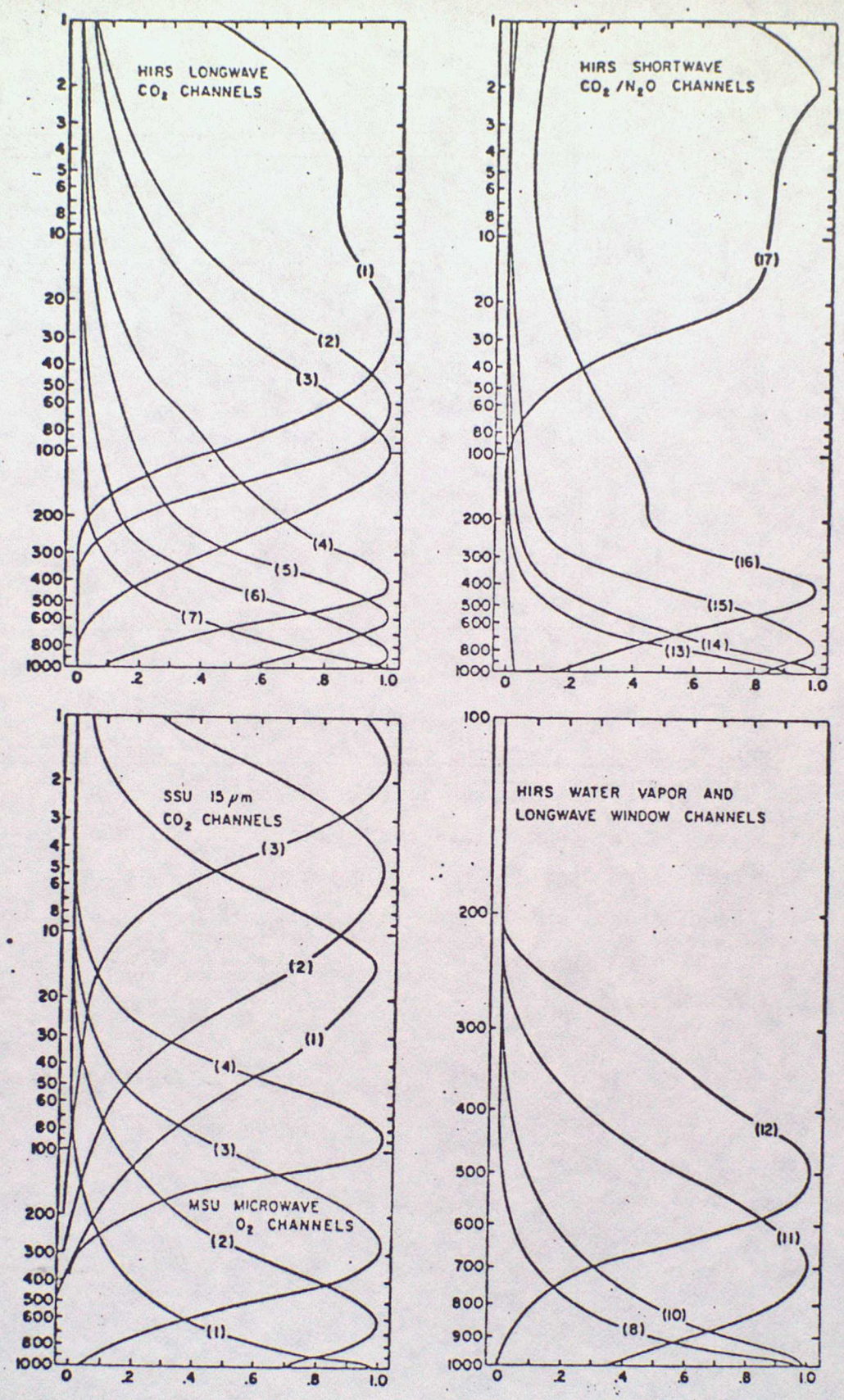

Figure 1

TOVS weighting functions

from Smith et al., 1979

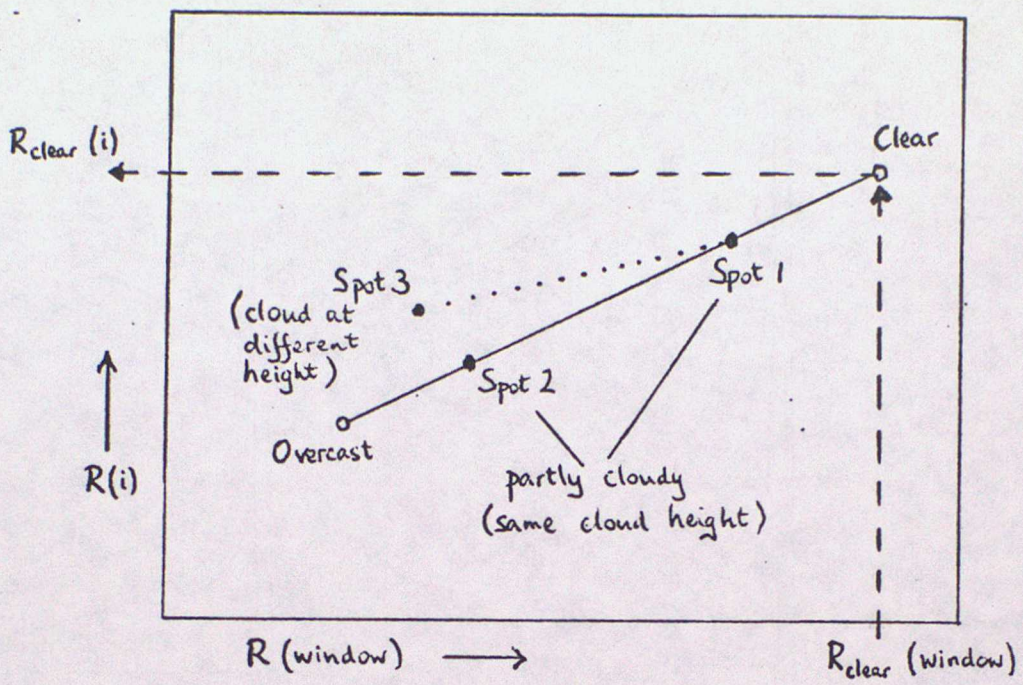

Figure 2 Illustrating the calculation of clear-column radiance

If adjacent fields of view contain different fractional cloud covers at the same height then points representing the radiances in any two channels (eg Spot 1 and Spot 2) lie on a straight line as shown in the diagram. If the clear-column radiance in one channel (eg a window channel) is known a priori, then the clear-column radiances in the ith channel can be read off as shown.

Errors arise if the clouds in the 2 fields of view are at different heights (eg Spot 1 and Spot 3) because the wrong gradient is assumed (dotted line in the diagram).

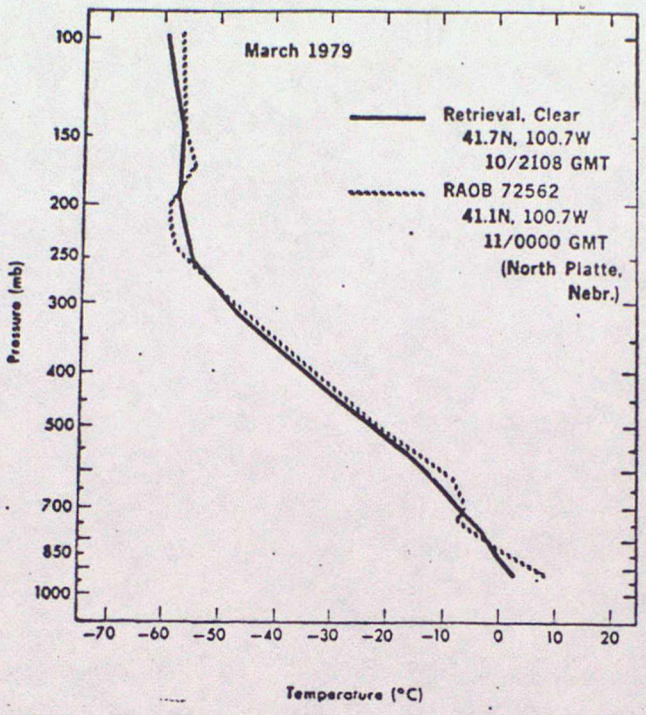

Figure 3

Comparison of a TIROS-N continental clear column retrieval and a nearby radiosonde.

from Phillips et al., 1979.

KW

ADVANCED LECTURES - SATELLITE METEOROLOGY

V HUMIDITY, SEA SURFACE TEMPERATURE AND ANALYSIS OF CLOUD

by J R Eyre

1. Retrieval of humidity from infra-red radiances

The radiative transfer equation can be formulated (see lecture 3) to express the radiance at wavenumber ν incident at a satellite-borne radiometer:

$$R_\nu = (I_\nu)_0 \, \tau_\nu(z_0) + \int_{z_0}^{\infty} B_\nu(z) \, \frac{d\tau_\nu(z)}{dz} \, dz \,, \qquad 1.1$$

where $B_\nu(z)$ is the Planck function corresponding to the temperature at height z,

$\tau_\nu(z)$ is the transmission along the viewing direction through the atmosphere from height z to space,

z_0 is the height of the underlying surface (land, sea or cloud-top),

and $(I_\nu)_0$ is the radiance emanating from the underlying surface.

We have seen in lecture 4 that, by making measurements at several wavelengths in absorption bands of gases of known concentration (such as CO_2 and O_2) for which $\tau_\nu(z)$ is known, we can invert the radiative transfer equation to find $B_\nu(z)$ and hence the temperature profile. If the temperature profile is known, then radiance measurements in an absorption band of a gas of unknown concentration profile can be used to estimate that profile.

Of particular interest is the profile of tropospheric water vapour. As in the case of temperature sounding, the measured radiances originate from rather broad layers of atmosphere. This is illustrated for the water vapour sounding channels of the HIRS instrument on the TIROS-N series in figure 1. The weighting functions shown are for a typical atmosphere but their peaks move up and down significantly with changing humidity profile. Increasing the humidity, decreases the transmission to space, raises the weighting function peak (usually to a colder part of the atmosphere), and so tends to decrease the radiance.

The retrieval of humidity mixing ratio is more difficult than that of temperature, because the radiances are related non-linearly to the humidity profile (or simple functions of it). The linear techniques described in lecture 4 are not, therefore, as accurate. It is found easier to retrieve the total precipitable water, $u(p)$, above a pressure level, p, rather than the mass mixing ratio, $c(p)$. The two quantities are related

through

$$u(p) = \frac{1}{g}\int_0^p c(p')\,dp' \quad \text{or} \quad c(p) = g\,\frac{du(p)}{dp} \,. \qquad 1.2$$

Mixing ratio can therefore be estimated from a retrieved profile of $u(p)$ but not as accurately because it is a derivative quantity.

The present operational product received in SATEM messages is the precipitable water in three layers (1000 - 700 mb, 700 - 500 mb and 500 - 300 mb) and is obtained by a statistical regression method (Smith and Woolf, 1976). For a discussion of other techniques see Hayden (1979), Shen and Smith (1973) and Weinreb (1973). Compared to temperature retrieval, little effort has been devoted to the humidity retrieval problem.

Again, the assessment of accuracy is difficult. Current techniques are thought to give results for precipitable water accurate to ~ 20-30%. Comparison with radiosondes can be misleading since radiosondes measure local profiles which are often unrepresentative of the area over which the satellite product is an average. This problem is more acute for humidity which has more local horizontal variance than does temperature. Also, in partly cloudy conditions, the satellite product will be obtained from the cloud-cleared radiances and will be biased towards the clear areas unless some correction is made. A further consideration is the error in the temperature profile used in the humidity retrieval; generally if the assumed temperature profile is too warm, the retrieved absolute humidity will be too high.

Meteosat also has a water vapour sounding channel centred at 6.3 μm which is sensitive mainly to radiation emitted by water vapour in the middle and upper troposphere. Qualitatively the images show areas of high and low relative humidity (conventionally shown on the images as light and dark respectively). The data can also be used quantitatively. One channel alone cannot be used to retrieve a vertical profile, but the mean relative humidity of the upper troposphere can be estimated. This is the approach used at ESA-Darmstadt to evaluate their "upper tropospheric humidity product" (see Meteosat System Guide, 1980). An example of this product is shown in figure 2. Alternatively, the radiance can be used in conjunction with an estimate of the temperature and humidity profile in an iterative scheme to adjust the humidity profile until the corresponding calculated radiance agrees with the measured radiance (for example, see Eyre 1980).

2. Image analysis

The underlying surface - land, sea or cloud-top - contributes to the radiation measured by the satellite. For the retrieval of temperature and

composition we are interested in wavelengths at which the atmospheric emission is dominant, although window channel information is usually required in addition. This is used to estimate the surface contribution at all wavelengths and thus allows the component of radiation corresponding to atmospheric emission to be identified. These window channels are also useful for measuring the radiative temperature of the underlying surfaces. Such information can be derived as an integral part of the full retrieval scheme for atmospheric temperature and humidity using radiometers primarily intended for atmospheric sounding. However, surface and cloud information is more successfully obtained using high-resolution imaging radiometers. The Advanced Very High Resolution Radiometer (AVHRR) on the TIROS-N series has two window channels for measuring reflected sunlight (one visible, one near infra-red) and also thermal infra-red channels (at $\sim 3.7\mu m$ and at $\sim 11\mu m$). Its ground resolution is ~ 1 km at the sub-satellite point (s.s.p.). Meteosat has channels in the visible and $11\mu m$ windows with resolutions ~ 2.5 km and ~ 5 km respectively at the s.s.p. The high resolution of purpose-built imagers (relative to sounders) is important for determining surface temperature and analysing cloud, since the smaller field of view gives a higher probability of the scene being homogeneous. Methods for measuring surface temperature rely on at least some fields of view being completely uncontaminated by cloud.

The basis of both cloud analysis and surface temperature measurement is the conversion of each radiance to a radiative temperature and then to the thermal equilibrium temperature of the scene. The problems encountered in this conversion are discussed in sections 3 and 4. The first stage in the analysis however can be considered as one of identification; for the subsequent analysis of radiative temperature to be useful we must first establish whether the scene is land, sea, cloud or mixed. This is usually done by histogram analysis. An area of the image containing many picture elements (pixels) is analysed, and consequently the retrieved values refer to this area and have a resolution lower than that of the image. The size of the area chosen depends on the application. As an example, the system used at ESA-Darmstadt for extracting meteorological parameters from Meteosat images divides each image into "segments" of 32 x 32 IR pixels (~ 150 km squares near the s.s.p.).

1-dimensional histograms can be made using thermal infra-red channel data only. Such histograms often have clearly defined modes which can be associated with different physical surfaces; land or sea can be identified, as can cloud at different heights. Figure 3 gives examples from part of a Meteosat image near the coast of Africa. 3a contains land, sea and a

very small amount of low cloud. The sea surface usually shows a more sharply defined peak than the land corresponding to a smaller range of temperature. 3b contains sea with a small amount of cloud. The range of the "colder" pixels (lower values) corresponds to a range of cloud top heights and/or varying fractional cloud cover in the individual pixels. 3c contains more cloud; in fact the number of contaminated pixels is now such that the value corresponding to the uncontaminated sea surface cannot be established with certainty. Consequently in areas such as 3b a sea surface temperature (SST) retrieval will be made but not in 3c. Operationally the shape of each histogram is tested numerically to establish whether the quality of the sea surface peak is adequate for good SST retrieval.

In the daytime visible information can be added to improve the scene identification. A 2-dimensional histogram from visible and infra-red radiance values allows much greater discrimination between different types of surface and cloud. An example is given in figure 4. The Meteosat segment processing system uses this approach where possible. The peaks in the histogram are analysed and identified using a look-up table containing information about the segment (which has a fixed geographical location) as a function of time of year and time of day. The information is in the form of expected radiances values for each surface (including cloud) which could be found. This tabulation was originally based on conventional climatological data but has been updated to take account of the observed "climatology of radiances".

3. Sea-surface temperature

The estimation of surface temperature from the measured radiative temperature requires knowledge of two other parameters: the surface emissivity and the absorption/emission by the atmosphere. The emissivity of the sea surface is $\simeq 0.99$ and varies only slightly with surface state and viewing angle. The emissivities of land surfaces (earth and vegetation) are generally lower and more variable ($\sim 0.90 - 0.98$ at 11μm) and make the determination of land surface temperature less accurate.

The estimation of "atmospheric correction" (the difference between the measured radiative temperature and that which would have being measured had there been no atmosphere) is a major problem in the retrieval of accurate SSTs. In the spectral window regions used the most important absorber is water vapour (in its monomer and dimer forms). The size of the correction

therefore varies according to the amount of water vapour in the atmospheric column between the satellite and the surface, particularly in the lower layers where the absolute humidity is highest. At 11μm the correction varies from a few tenths of a degree in very cold, dry atmospheres to values around 5K (but exceptionally up to 10K) in the tropics. The corrections are smaller in the 3.7μm window but the problems associated with reflected sunlight are such that this wavelength band is less reliable in the daytime. (At 11μm solar reflection is only a problem in a small area of the image close to the specular reflection point).

In principle calculation of atmospheric correction is straightforward. The radiative transfer equation is integrated from the surface to space to determine the amount of radiation absorbed and emitted by the atmosphere. However this requires a knowledge of the temperature and humidity profiles. They can be obtained from climatology or from a forecast model (eg Meteosat SSTs - see Meteosat System Guide, 1980) or preferably from a simultaneous retrieval using a sounding instrument (eg NOAA's Global Operational SST Computation or GOSSTCOMP system - see Brower et al, 1976). However, even with accurate profile information, such as that obtained from a series of aircraft measurements, the uncertainties in the measured profiles still lead to a major part of the error in the retrieved SST. Also, the absorption coefficients in the window regions present problems. The absorption is mainly caused by the far wings of water vapour bands centred at "distant" wavelengths or by complex water vapour dimer spectra. Neither effect is fully understood.

Examples of GOSSTCOMP products are shown in figure 5. The resolution of these products is often limited in practice by the volume of data to be processed. However the raw data have high resolution which can provide high resolution products for specialised needs (eg figure 6).

Until now all operational SST systems have been based on one-channel techniques with a separate scheme for calculating atmospheric correction from some estimate of the atmospheric state. In future this approach is likely to be replaced by a technique using two or more window channels for which the atmospheric absorption is different. In this way the atmospheric correction can be calculated quite accurately without reference to the details of the atmospheric state. The AVHRR on the next NOAA (TIROS-N series) satellite will have 5 channels instead of 4: the single 11μm window channel will be replaced by 2 channels (10.3 - 11.3μm and 11.5 - 12.5μm). These and the 3.7μm channel will provide 3 independent thermal infra-red

window channels.

Estimation of the accuracy of satellite-measured SSTs is difficult. When comparing against ship measurements it must be remembered that:

(i) ship observations have their own errors,

(ii) ship observations are point measurements whereas satellite SSTs are area averages, and

(iii) ships measure the bulk temperature from a depth in a mixed layer ~ 3-9m (using a bucket or intake method), whereas satellite SSTs refer to the uppermost fraction of a millimetre (the skin). This occasionally gives difference of up to 3 deg.K but usually the errors in SSTs from other source are larger than the bulk-skin difference.

At present, under the best conditions, the absolute temperature difference (ie biases not removed) between ship and satellite SSTs is 1-2K r.m.s. (McClain, 1979). The major errors in the satellite measurements which contribute to this difference are:

(i) absolute calibration errors,

(ii) errors caused by residual cloud contamination, and

(iii) atmospheric correction errors. At low latitudes, errors in the assumed atmospheric profiles make it difficult to reduce the r.m.s. errors in the atmospheric corrections below 1K. This may seem unreasonably large since the total correction is only ~ 5K. However calculations show that at these latitudes only ~ 50% of the 11μm radiation reaching the satellite has been emitted by the surface, the rest being atmospheric emission. The atmospheric correction is only ~ 5K because the layers emitting most radiation are the moist, lower layers which are close in temperature to the surface. Since the measured radiances are heavily influenced by the profile in the lower layers, apparent gradients in the retrieved SST field can be caused by temperature and humidity variations in the lower layers.

Using multi-channel techniques it should be possible to reduce the atmospheric correction errors below 0.5K, but these methods still have to be proved operationally.

Finally, it should be noted that the accuracy of the retrieved product can be improved by assuming that SST changes slowly. This provides a method of quality control: retrievals are assimilated into a background field produced from previous data thus allowing unreasonable differences between observation and background to be detected.

4. Cloud analysis

The image analysis techniques described in section 2 allow the infra-red radiances to be associated with clouds at different heights. As with the SST retrieval, the radiance associated with each identifiable group of pixels can be converted to a brightness temperature and interpreted as a cloud top temperature. Corrections are made for atmospheric emission/absorption above the cloud. This is much less of a problem than for SST, firstly because the cloud top is usually above the moist, lower layers and so the correction is small, and secondly because we are not usually interested in such high accuracy in temperature as we are for SST. A more important problem in cloud analysis is that of emissivity. High layer clouds in particularly are often semi-transparent in which case the measured radiance is partly cloud emission and partly radiation transmitted through the cloud. This can lead to an overestimate of the cloud temperature and an underestimate of its height.

The Meteosat operational system at Darmstadt will provide cloud analysis on the same segment grid ($\sim$ 150 km square at the s.s.p.) as for SST and upper tropospheric humidity. The 3 most significant layers of cloud will be reported in terms of fractional coverage and cloud top temperature. (This product was not operationally available from Meteosat 1).

Satellites with their extensive coverage provide excellent platforms for analysis of cloud. One obvious limitation of such a system is imposed by viewing from above. Cloud base cannot be measured and lower cloud is often observed by a veil of high cloud. The fractional cloud covers estimated, therefore, are as seen from above. This is not ideal for many purposes but is appropriate for the computation of outgoing long-wave radiation and reflection of solar radiation. Such data are likely to be useful in climate studies.

References

Brower R L, Gohrband H S, Pichel W G, Signore T L, Walton C C 1976
NOAA Tech. Mem., NESS 78.
Satellite derived sea-surface temperatures from NOAA spacecraft.

Eyre J R 1980 Met O 19 Branch Mem. 58
Direct use of Meteosat water vapour channel radiances to improve the humidity analysis in a forecast model.

Hayden C M 1979 WMO Technical Note No 166
Quantitative meteorological data from satellites. Chapter 1: Remote soundings of temperature and moisture.

McClain E P 1979 WMO Technical Note No 166
Quantitative meteorological data from satellites. Chapter 3: Satellite derived earth surface temperatures.

Meteosat System Guide 1980 ESA publication (ESOC/MDMD)

Shen W C, Smith W L 1973 Mon. Weather Rev., 101, 29-32
Statistical estimation of precipitable water with SIRS-B water vapour radiation measurements.

Smith W L, Woolf H M 1976 J. Atm. Sci., 33, 1127-1140
The use of eigenvectors of statistical covariance matrices for interpreting satellite sounding radiometer observations.

Weinreb M P 1973 3rd Conf. on Probability and Statistics in Atmospheric Science, 231-235.
Estimation of atmospheric moisture profiles from satellite measurements by a combination of linear and non-linear methods.

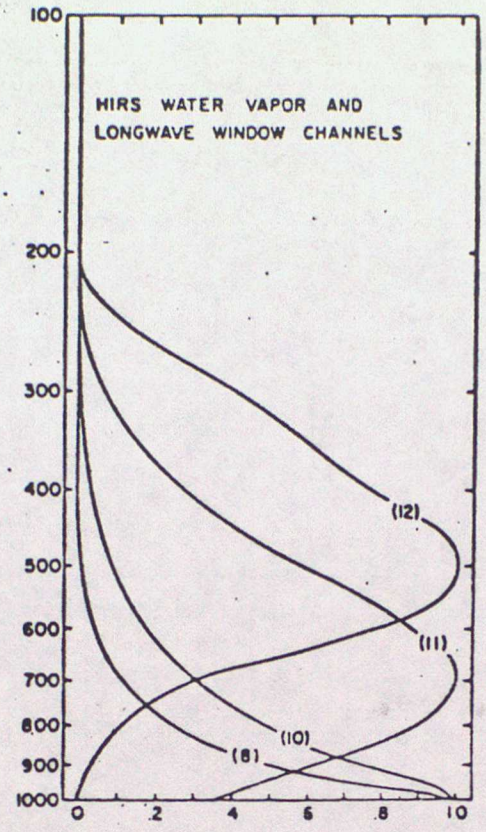

Figure 1

Weighting functions of TOVS channels for sounding water vapour

Channel	Wavelength (μm)	
10	8.3	} Water vapour absorption band
11	7.3	
12	6.7	
8	11.1	Window region

See lecture 4, table 1, for more details.

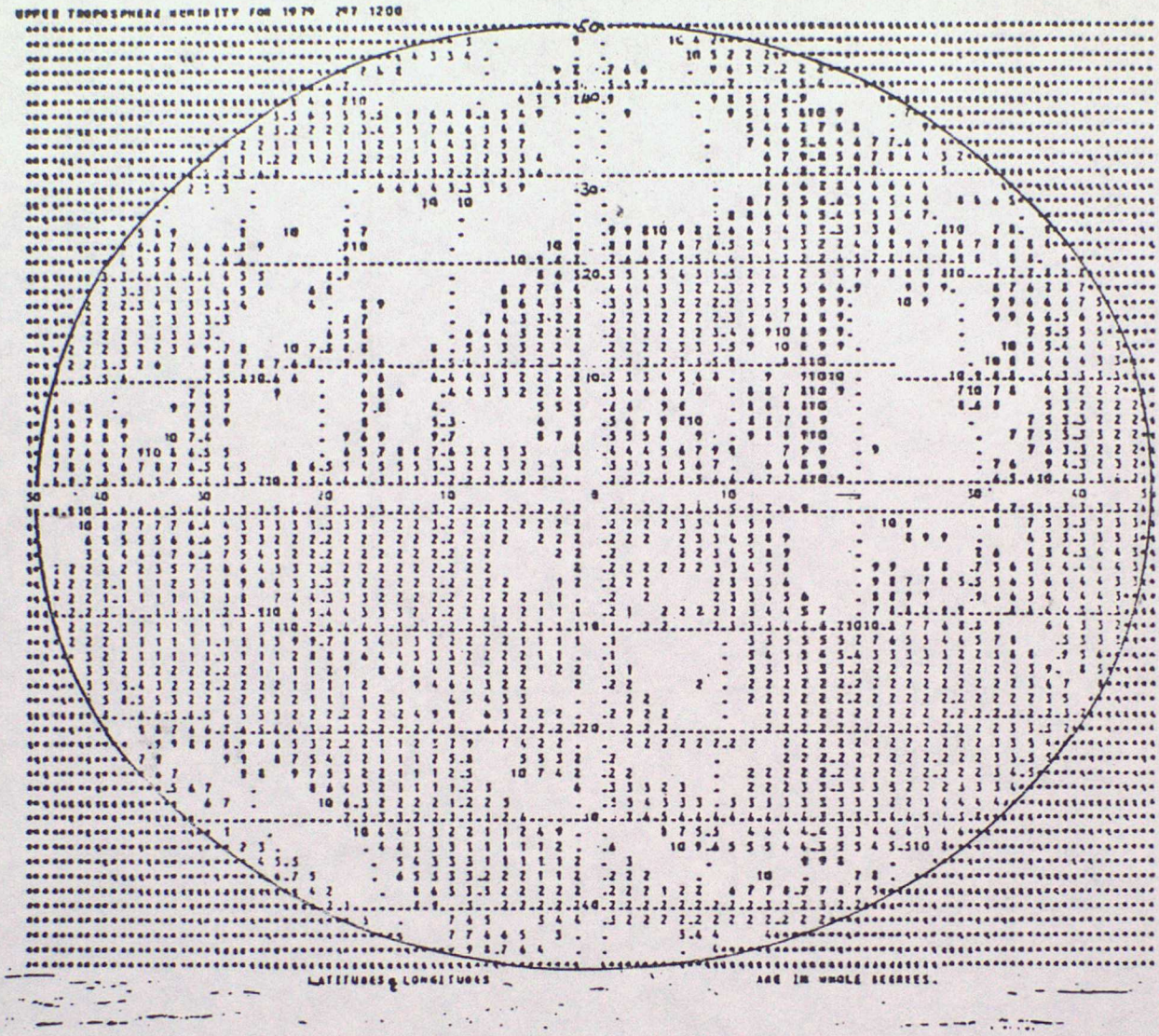

Figure 2

An example of ESA's Meteosat "upper tropospheric humidity" product.

The 50° great circle arc of the processing area is shown.

Numbers are average layer humidity in tens of percent.

An omitted results indicates either

i) a cloud affected result, or

ii) a retrieved humidity >100% or <0% which could occur when an inappropriate temperature profile is used in the retrieval.

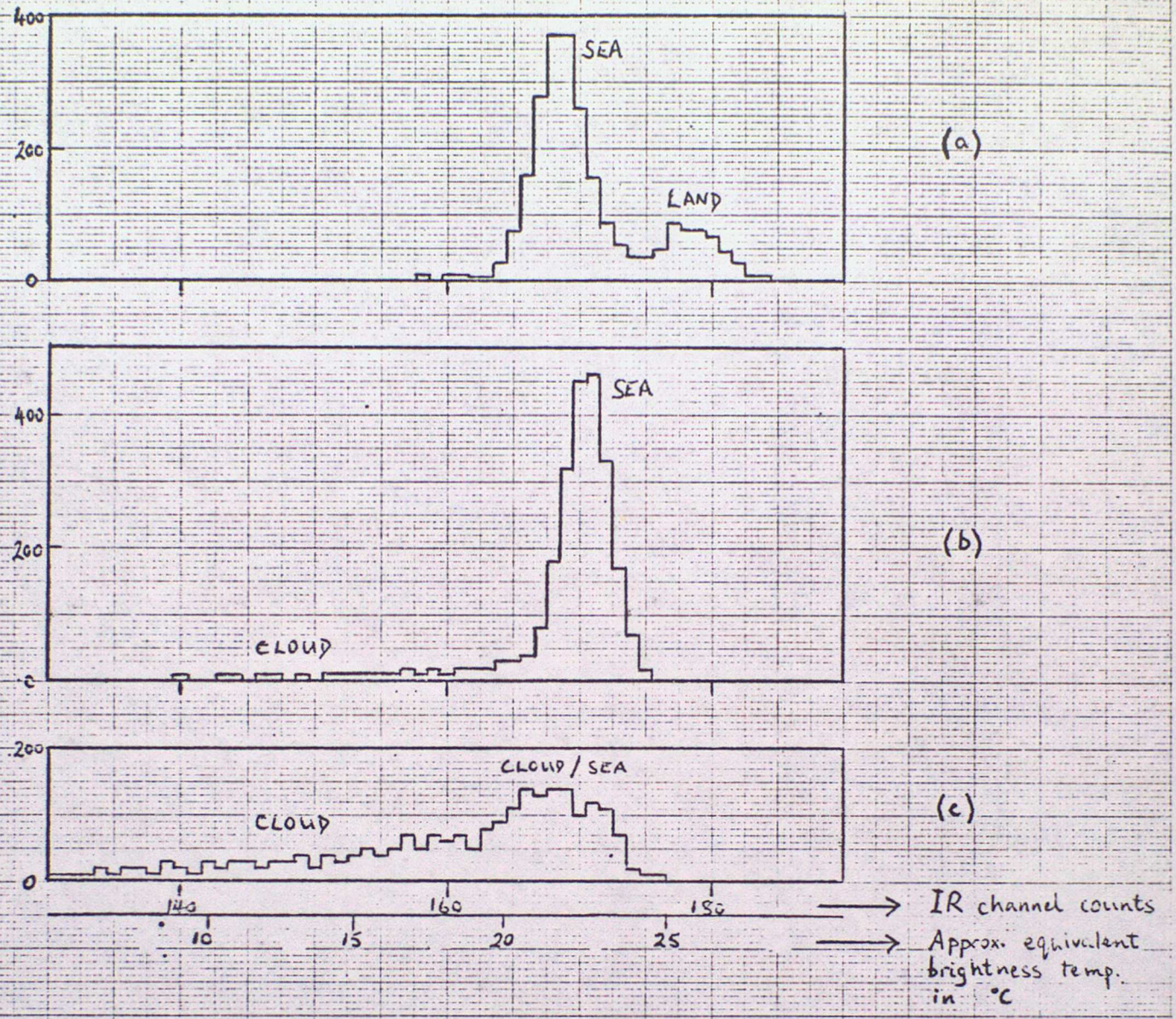

Figure 3

Histograms from squares of 50 x 50 Meteosat IR channel pixels.

3 areas near the coast of W. Africa in December, 1978.

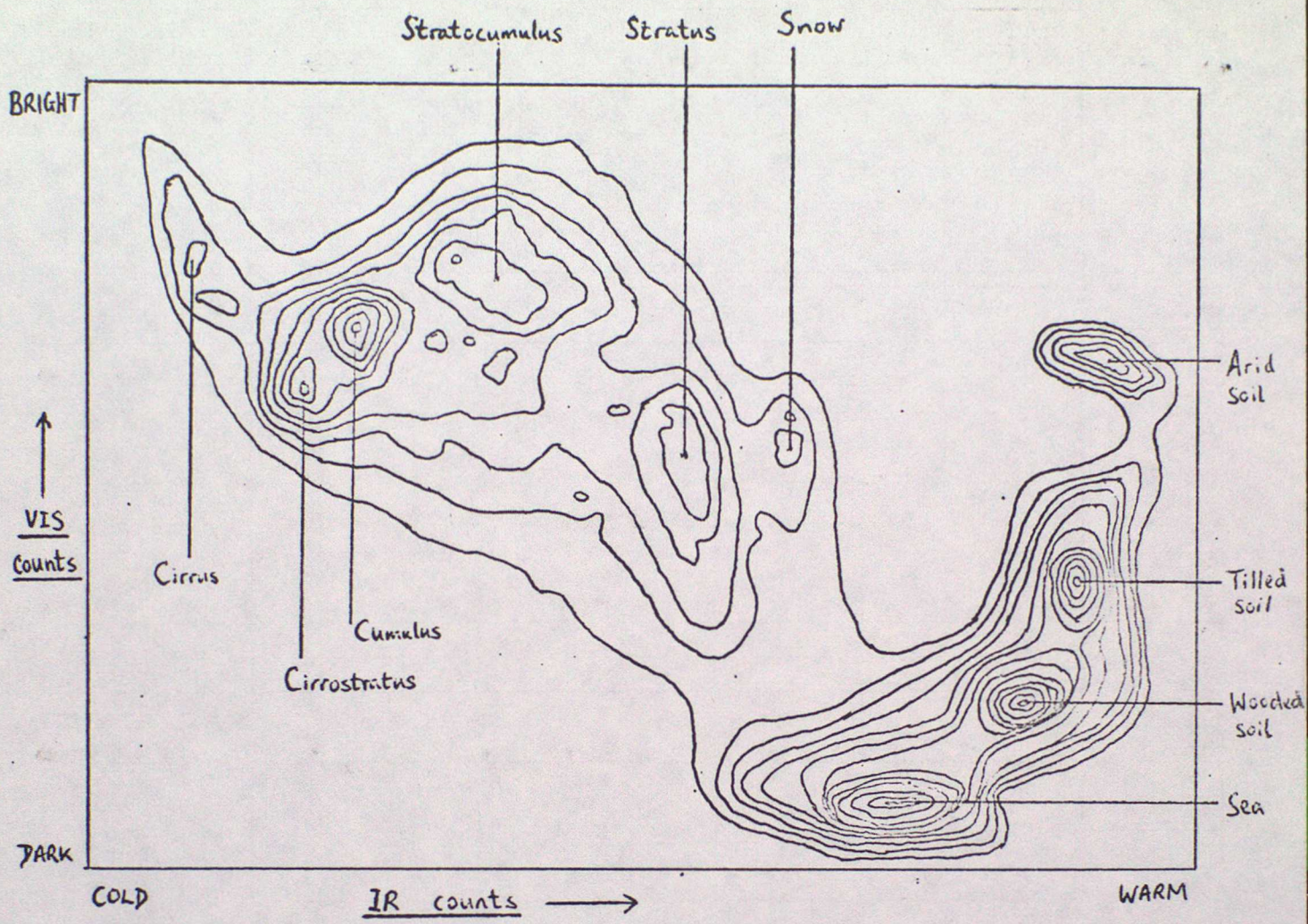

Figure 4

Peaks representing different surfaces in a 2-dimensional histogram formed from Meteosat visible and infra-red radiances

Figure 5

(a) GOSSTCOMP SEA SURFACE TEMPERATURE

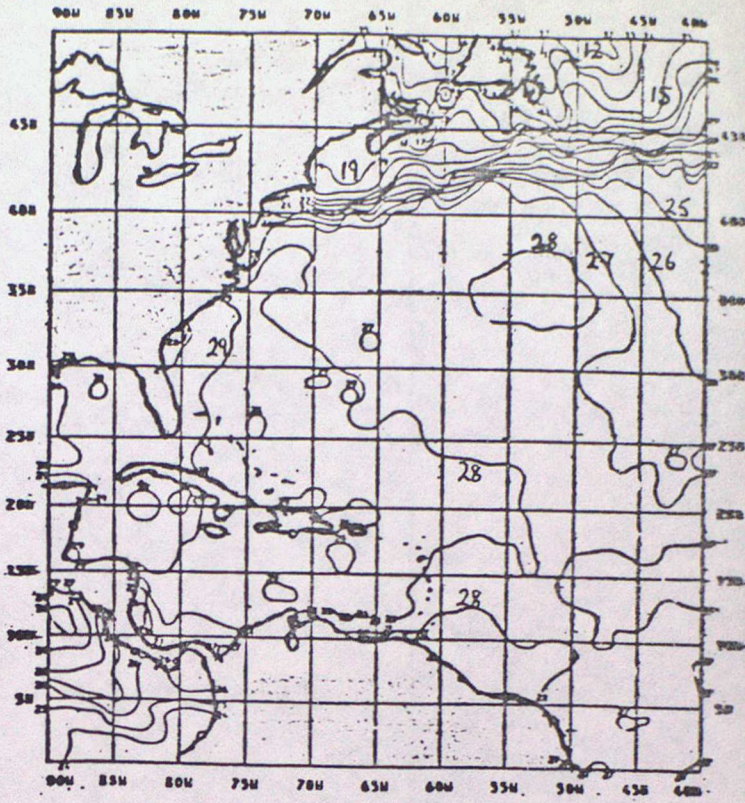

(b)

(c)

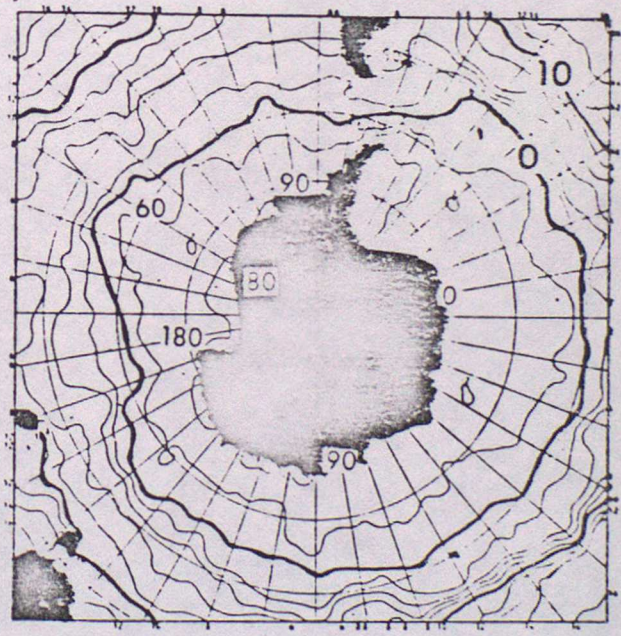

Examples of GOSSTCOMP products

(a) Western North Atlantic — 17 August 1976

(b) Polar stereographic plots — 24 August 1976

Temperatures in °C.

Taken from McClain (1979).

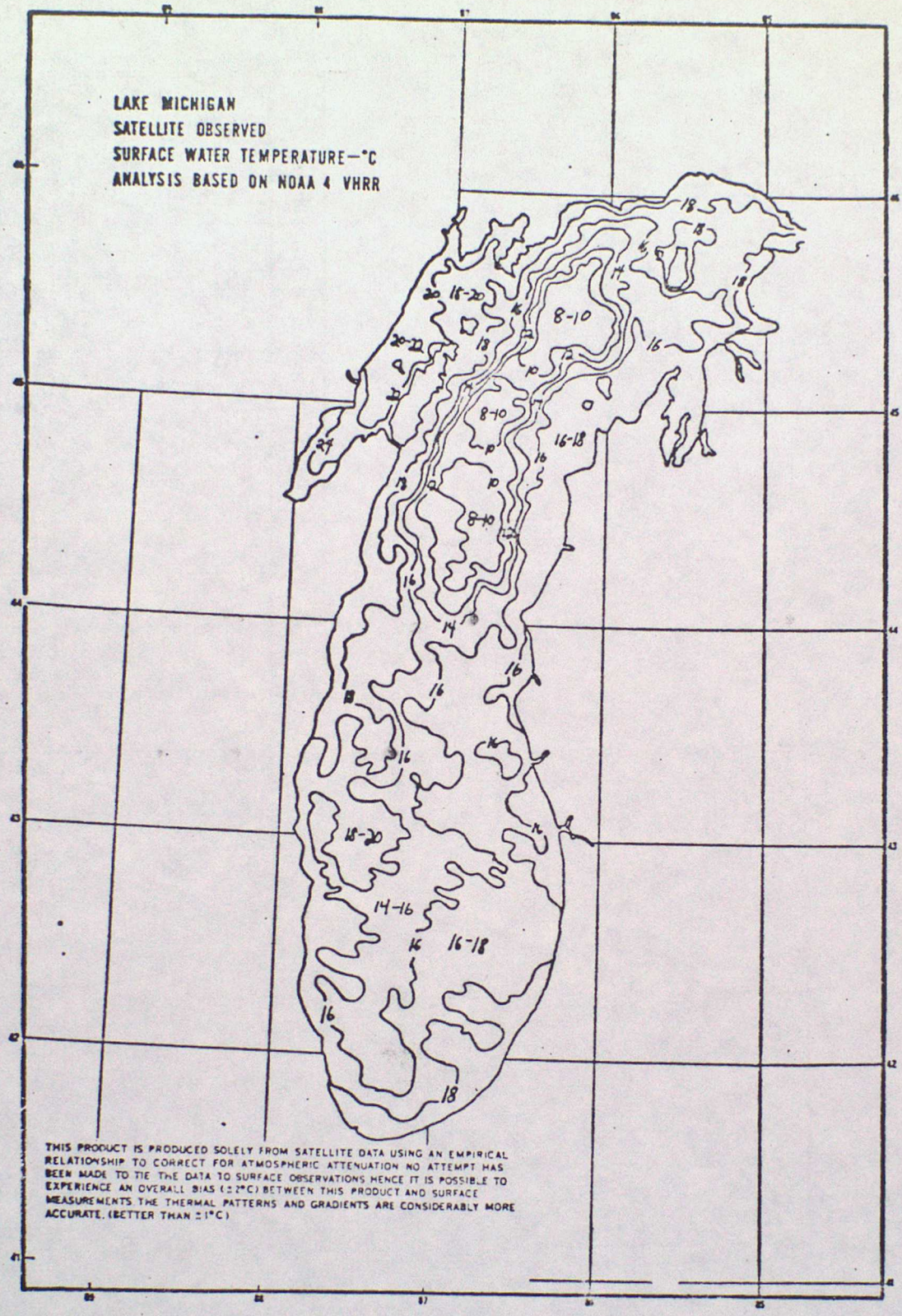

Figure 6

An example of a high resolution SST product.

Lake Michigan from NOAA 4 VHRR data, 6 June 1976 at 1530 GMT

JC

SATELLITE METEOROLOGY - LECTURE 6 - IMAGES

1. Fundamentals

Most present-day imaging systems consist basically of a radiometer with a very small field of view and an arrangement by which it can scan a much larger area. As it scans, the radiometer in effect views tiny elements of the total scene in rapid succession. It measures the radiance from each and images are constructed by displaying these radiance values as shades of grey in their correct relative positions. The tiny picture elements are known as pixels and their size determines the limiting spatial resolution of the imaging system. This is generally between about 1 km and 10 km.

There are 2 preferred parts of the spectrum for imagery; visible wavelengths between about 0.4 μm and 0.7 μm and the infra-red 'window' around 11 μm. Of other channels used the water-vapour channel on Meteosat, at 6.3 μm, is of particular interest. Their characteristics will be considered briefly in turn.

a. Visible (VIS) images

The VIS channels measure reflected radiation in the visible part of the spectrum, and the features which appear brightest in the image are those which reflect sunlight most strongly. They are not necessarily clouds. Snow cover, desert surfaces and smooth sea surfaces can all at times appear just as bright as clouds. The observed brightness depends on illumination (sun angle), viewing geometry (angular position in relation to the satellite and to the sun) and reflectivity or albedo. Conover (1965) listed some average albedos measured from satellite pictures. For clouds they ranged from 29% for fair weather cumulus over land up to 92% for large and deep cumulonimbus. Terrestrial surfaces included sand in New Mexico (60%), snow a few days old (59%) and the Pacific Ocean (7%). Cloud reflectivity depends on cloud thickness, particle size distribution and composition and the character of the upper cloud surface. When using VIS pictures it is helpful to remember that, in general, increased brightness is associated with thicker clouds, especially in cyclonic cloud systems. Under similar conditions of illumination, water clouds appear brighter than ice clouds of the same thickness. The shadows and highlights that are present in VIS imagery are often particularly valuable in revealing the structure and texture of cloud systems.

b. Infra-red (IR) images

IR images are derived from radiation emitted by cloud and temestrial surfaces and provide essentially a representation of the temperature distribution. This is because at the wavelengths used, emissivities are mostly close to unity (ie the surfaces can be considered to radiate as black bodies) and atmospheric attenuation is small. In some quantitative uses of IR imagery, however, account has to be taken of both these parameters and their variations. Emissivity can be significantly less than unity for the cirrus clouds, while atmospheric attenuation becomes increasingly important as water vapour content increases. This attenuation causes a radiating surface viewed by a satellite-borne radiometer to appear colder than it actually is. In order to have some similarity in the appearance of clouds of IR and VIS images the convention is to arrange the grey-scale of the former so that warm surfaces (high radiance values) appear dark, and cold surfaces (low radiance values) appear light.

Extensive use is made of both VIS and IR imagery, one complementing the other in many applications. Altogether, however, the IR is probably the more widely used, partly because of its relationship to temperature and partly because of its uninterrupted availability.

c. Water vapour (WV) images

These Meteosat images were derived from radiance measurements in the 5.7 μm to 7.1 μm water vapour absorption band in the infra-red. At these wavelengths radiation reaching the satellite is emitted by water vapour in the upper troposphere, roughly between 600 mb to 300 mb, and by any high clouds present. The intensity of the radiation depends on the temperatures of the layers from which it originates. With high humidities the radiation to space is from relatively high (cold) levels and with low humidities it is from lower (warmer) levels. There is thus a relationship between radiance and humidity. The grey scale on WV imagery is normally arranged so that moist areas appear bright and dry areas dark. Tops of high clouds (especially vigorous Cb) show up as very bright features.

It will be recalled that TIROS-N AVHRR has 4 channels, namely:-

1.	0.55 to 0.90 μm	VIS
2.	0.72 to 1.10 μm	VIS/Near IR
3.	3.55 to 3.93 μm	IR
4.	10.5 to 11.5 μm	IR

Channel 2 provides images very similar to those from channel 1 but with improved land/sea contrast and some significant differences in the appearance of certain ice and snow surfaces. These differences give an indication of the inception of melting. Channel 3 used in conjunction with channel 4 gives better night-time sea surface temperature determination than channel 4 alone but this is not so in day-time because it suffers severe contamination by reflected solar radiation. The fifth channel (11.5 μm to 12.5 μm) to be added to later versions of the AVHRR will allow a 2-channel determination of sea temperatures at all times.

2. Main uses of satellite imagery

Images from current operational satellites provide a wealth of information about atmospheric prosses and phenomena on scales ranging between near-global and meso-scale. Those of operationalinterest include:-

Cloud cover - type, extent/amount, height
Surface temperature - land, sea, also cloud top temperature
Winds and flow patterns
Vertical motion, stability, etc
Synoptic systems and related features - depressions, fronts etc
Snow and ice cover
Turbulence
Aerosols - haze, volcanic dust, etc
Humidity

The list is not exhaustive - it is given simply to illustrate the diversity of information that the imagery provides. It will be evident that some items listed can be obtained directly from the images while others have to be inferred. For example, the presence of sunglint (an area of strong solar reflection from the sea surface) implies an area of smooth sea, which in turn implies light surface winds. Using simultaneous images from 2 or more channels together often yields information that cannot be obtained from any

of the channels separately and resolves uncertainties in the interpretation of data from a single channel. High cloud and sea fog may look virtually identical on a VIS image but they are easily distinguished on an IR image.

An individual image can provide much information but if sequences are available movement and development can be observed as well. Many operational users have some kind of 'rapid replay' facility for sequences of geostationary images and it is their experience that especially in meso-scale work the technique frequently shows interesting and important developments which are otherwise apt to pass unnoticed.

In addition to their use and application in operational meteorology the images are widely used in other fields. These include:-

Climatology	(for cloud cover, albedo and other radiation balance parameters, sea temperatures, snow and ice limits etc)
Oceanography	(especially effects related to sea surface temp)
Land use/Vegetation cover studies	
Hydrology	(soil moisture and evaporation mapping, rainfall monitoring)

3. Image processing and enhancement

a. General

Images are essentially a large array of radiance values and when expressed in digital form they can be processed by computer to facilitate their interpretation or use in some way, either qualitatively or quantitatively. A common type of processing is that termed 'enhancement', in which the grey levels of an image are systematically adjusted so that information can be interpreted visually at a higher rate or additional information is made more apparent. High quality digital images contain far more radiometric levels than the 16 or so which the human eye can distinguish, so it is only by some kind of 'stretching' of the scale that some of the finer points of the image will be seen at all. In the same way, enhancement is often of value in partially overcoming limitations of an image display device. The enhancement can be a simple linear one, in which a small range of the original radiance values is expanded to occupy a much larger range of levels on the output display, or it can be more complex, such as modifying the histogram of radiance values to approximate to a Gaussian distribution and thus give better overall contrast. By application of an appropriate enhancement curve, the grey-scale of an IR image can be made linear with respect to the temperatures it represents.

Although a specific enhancement can be performed regularly on all images from a particular source, maximum flexibility in enhancement and other forms of processing is achieved through the use of interactive techniques on a video display system. Such techniques are being used increasingly and various sophisticated prupose-built image processors are now in commercial production. (They are, of course, built for use with many types of images and not just those with meteorological content). Facilities available on a processor such as the IDP 3000 of the RAE Remote Sensing Unit include:

Image ratioing (division of one image by another)
Intensity normalisation(division of one image by the average of all component images)
Contrast enhancement (modification of contrast to highlight specific differences in the image)
Colour enhancement (modification of colour to highlight specific differences in the image)
Level slicing (identification of image areas lying within given range of intensities)
Contouring (as level slicing but for very small ranges of intensity
Area measurement (a count of the number of pixels in a defined region)
Statistical evaluation (measurement of histograms and multivariate statistics to determine the optimum processing parameters).

b. Within the Meteorological Office

In the Office image processing is performed on a dedicated PDP 11/60 computer, known as AUTOSAT and operated by Met O 5. Although the capabilities of the AUTOSAT system do not match those of the more elaborate processors it performs a very useful operational role in both the processing and the dissemination of imagery.

The principal processing tasks performed are enhancement, re-projection and animation. Enhancement involves adjustment of the grey-scales, using one of a number of pre-determined enhancement tables stored in the system, to improve the image contrast and minimise its variation with time of day, season, different satellites etc. The output is regularly monitored by representative user stations who can request a change in the enhancement if they believe it would be advantageous. Grey-scale wedges containing 16 steps from black to white are disseminated automatically to users every day to facilitate adjustment and tuning of recorders. The re-projection task converts images to a polar-stereographic projection on a scale of approximately 1:20 M (which matches many widely-used forecast charts) and constructs a composite picture using images from consecutive passes. Time taken for the re-projection varies between about 10 and 30 minutes for a single pass, depending of the orientation of the pass. Linked to AUTOSAT is a black and white TV display located in the Central Forecast Office; it can be used to display and expand selected sectors of the images, to set up animated image sequences, to display images with different enhancements applied and to request hard-copy output of any images available for display.

AUTOSAT has been in operational use for only a few months and further development of its capabilities can be expected.

4. Display devices

However good the image data quality, the image available to the user can only be as good as the display device will permit. Communications may also impose significant constraints on the end-product but they will not be considered here.

Although the Office uses Muirhead facsimile recorders for almost all its imagery displays a great variety of display devices is available.

Advantages of electrolytic recorders like the Muirhead ones are that the images are immediately available and no chemical processing is necessary. Though not cheap, they are considerably less expensive to buy and to operate than some of the alternatives. Disadvantages are that they are very 'mechanical' by modern standards and tuning is critical. The high grade tonal paper used can reproduce up to 15 grey levels when the recorder is correctly adjusted. Alternative hard copy devices include some in which the image is produced by a modulated laser beam and which can reproduce up to 64 grey-levels.

Some requirement for hard copy is likely to remain for a long time yet but the trend is to increasing use of soft copy TV-type devices, like those mentioned in connection with the IDP 3000 and AUTOSAT. Used in conjunction with a data storage facility such a device is very versatile and in particular allows rapid replay of image sequences. If the display uses colour instead of black and white, visual interpretation and assimilation of most images is made easier and the number of radiometric levels which can be recognised visually is substantially increased.

5. Reception, dissemination and use of images in the Office

Initial reception of all imagery used operationally in the Office is at Lasham in Hampshire. The facility is run jointly by RAE and the Office. 2 lines link Lasham directly to Bracknell. Data received regularly at Lasham and relayed to Bracknell are:

- all APT imagery from TIROS-N series satellites while within approx 3000 km of Lasham (normally 3 or 4 consecutive passes of each satellite twice daily)
- AVHRR sectors which include the British Isles (1 or 2 from each satellite twice daily)
- selected transmissions from GOES-E
- selected Meteosat formats (when available)

Except for the AVHRR, all are analogue transmissions. The AVHRR, received initially as digital data, is put into an APT-type analogue format prior to transmission to Bracknell. All data received at Bracknell are input to the AUTOSAT computer which performs the processing operations already described. Output is to the CFO display and the SATFAX network. The latter is a facsimile network using high quality post office lines and serving more than 30 outstations. Latitude/longitute grids are added (on the basis of orbital parameters disseminated daily by NOAA/NESS) to the polar-orbiter imagery at outstations, although the re-projected composites have the grids incorporated.

Detailed use and application of the images varies according to the particular interests and responsibilities of each station but the majority are used as what can be broadly described as aids to synoptic analysis. Many offices serving airfields make good use of the images as briefing aids. One of their uses in CFO is in adjustment of the numerical model humidity analyses - a procedure in which heights and thicknesses of cloud are estimated from the images and converted to approximate humidity values (see Moore (1980)).

The Radar Research Laboratory at Malvern is developing techniques for use of satellite image data in conjunction with radar data for short-period forecasting, (see for example Browning (1980)). Very briefly, the satellite data are being used to extend the coverage provided by the radar observations of precipitation and to fill gaps in those observations.

Satellite imagery, unlike radar, does not indicate areas of precipitation directly. However quantitative comparison of the 2 types of data, where both are available, allows estimates of precipitation to be made from satellite data alone in adjacent areas. Furthermore, good indications of precipitation are now being obtained using VIS and IR data together. Only Meteosat can provide data with the frequency required for this specialised application. During the life of Meteosat-1 the relevant section of the Meteosat analogue imagery was digitisedat Bracknell and relayed to Malvern via a Post Office line. Facilities for direct reception of Meteosat digital data are however being installed at Malvern for use as soon as imagery is available from Meteosat-2.

6. References

Conover J H, 1965, Cloud and terrestrial albedo determinations from TIROS satellite pictures. Journal of Applied Meteorology Vol 4 No 3 pp 378-386.

Moore J G, 1980, The use of satellite pictoral data in weather forecasting. Meteorol Mag 109 pp 78-88.

Browning K A, 1980, The FRONTIERS plan: a strategy for using radar and satellite imagery for very-short-range precipitation forecasting. Meteorol Mag 108 pp 161-184.

7. For Further reading

Geneva, WMO, 1973 The use of satellite pictures in weather analysis and forecasting. Tech Note No 124.

DH

SATELLITE METEOROLOGY - 7

DETERMINATION OF WINDS FROM CLOUD DISPLACEMENTS

1. Introduction

A number of different satellite techniques for measuring winds have been tried or proposed in recent years but the only one to have been used operationally for any length of time is that in which the winds are derived from measurements of cloud displacements. The high repetition rate of images from geostationary satellites makes them well-suited to this technique and all 3 operators of geostationaries regularly compute and disseminate winds (although there have been no Meteosat winds since the imaging mission failed in November 1979).

The basis of the method is simple; identifiable cloud features are tracked from one image to the next, and on the assumption that they move with the wind their displacements over a known period of time can be converted to a wind speed and direction. Unfortunately this assumption is not always valid. For instance, development or decay of clouds may give the illusion of motion, movement of clouds may reflect the motion of synoptic systems rather than wind, orographic clouds may remain stationary while a strong wind blows through them, and so on. Steps must therefore be taken, either in initial selection of the winds to be tracked or in a subsequent quality control procedure, to exclude all meteorologically unacceptable tracers.

Another major difficulty concerns the relationship between the movement of a cloud having significant vertical extent and the wind at a particular level. The clouds are viewed from above and the measurements relate essentially to the cloud top, but the movement of the cloud may be largely determined by the wind at some lower level. Various studies have been made of this problem; one was by Hasler et al (1979) who tracked clouds over parts of the Atlantic and the Caribbean, using an aircraft which at the same time made detailed wind observations. They concluded that for oceanic trade wind cumulus, and cumulus in oceanic sub-tropical high pressure regions, the cloud motion corresponds closely to the wind at cloud base. For oceanic cumulus near fronts agreement is best with the mean wind in the cloud layer, and the same is true for high level cirrus clouds.

Despite the unsuitability, for wind determination, of clouds that are developing or dissipating, it should be noted that individual small cumulus clouds could hardly be tracked anyway because the spatial resolution of the radiometer is not good enough. This does not mean that winds cannot be determined in areas of cumulus; sequences of pictures reveal a high degree of persistence, over periods of the order of an hour, in the mesoscale patterns of trade wind cumuli, cumuli congestus, etc. It is these patterns, and not individual cloud cells, that are tracked as they are carried along with the wind.

Because of the uncertainties in interpretation of cloud displacements in terms of winds, the velocities derived from the displacements should strictly be termed cloud motion vectors (cmv's) instead of winds.

2. Methods

There are 3 basic stages:-

(i) measurement of cloud displacement
(ii) assignment of height
(iii) quality control

The details of implementation of the 3 stages differ between operators although there is a good deal of common ground. The ESA (European Space Agency) method, in which (i) and (ii) are performed automatically, will be described, and then manual methods, optical methods and the procedures of NOAA/NESS (the US Satellite Service) and JMSC (Japanese Meteorological Satellite Centre) will be discussed briefly.

2.1 The ESA automatic method

The starting point is a sequence of three consecutive full-disc infra-red images, the images being at 30 minute intervals. Steps in the process can be summarised as:

Image referencing
Segment processing and tracer selection
Wind vector determination
Height attribution
Manual (interactive) quality control
Final processing and dissemination

These will be considered in turn.

2.1.1 Image referencing

It is essential for accurate cmv determinations that there should be a high degree of precision in the relative registration of successive images. An error of only 1 IR pixel (ie approx 5 Km near the sub-satellite point) in the relative registration of 2 images one hour apart will produce an error of 1.4 ms^{-1} in the derived wind.

Image referencing is achieved by software which relates the actual image to the reference image (ie the image that would be obtained if the spacecraft was in its nominal position and orbit with no irregularities in its motion). It computes the 'deformation' of each actual image, using a model of the spacecraft dynamical characteristics and recent measurements of orbital parameters. Additional checks involve automatic detection of the earth's horizon, and interactive processing in which the apparent and reference positions of certain well-defined landmarks are compared.

2.1.2 Segment processing and tracer selection

The segment processing task was described in an earlier lecture (no 5) in this series. It will be recalled that the end product is a table associating each cluster of observed radiance values with a physical source of radiation, (sea surface, cloud etc). This is for each of the 3000 or so segments (32x32 pixels) within 50° great circle arc of the sub-satellite point. The tables are checked by the wind programme for suitable cloud tracers; processing of data in a segment ends if there is no cloud at all, if there is total and uniform cloud cover or if certain other tests related to the magnitude and

separation of histogram peaks associated with cloud fail. Note that at this stage the tracers are 'suitable' only in respect of the data quality and not necessarily meteorological considerations.

2.1.3 Wind vector determination

This is the heart of the process. Three consecutive IR images, in digital form, are used. A target segment is cut from the central image of the three (time H hours) and a matching cloud pattern is sought in the image for H+$\frac{1}{2}$ hr. This is done mathematically using a cross-correlation technique. The search area is made up of 3x3 segments centred at the same position as the target segment. If displacements of the target area within the search area are made in steps of one pixel there are 65x65 possible positions for it (see Fig 1). A correlation coefficient is computed between the 2 sets of image data for all the 65x65 positions and maximum values, best thought of as peaks in a correlation surface, indicate where the best match exists.

The number of spurious matches is substantially reduced by repeating the search procedure using the H-$\frac{1}{2}$ image. Only those correlation peaks which are symmetrical between the 2 determinations at H+$\frac{1}{2}$ and H-$\frac{1}{2}$ are retained.

At this point it is necessary to determine which layer of cloud, in segments with more than one layer, is to be associated with the correlation peak. Reference is made to the histogram cluster analyses in the segment processing task. Radiance values in the target segment are enhanced by taking the values from one cluster (ie one cloud layer) only, setting all other radiances to random values but retaining their true mean value, and repeating the correlation procedure. This is done, in turn, for each histogram cloud cluster. The one giving the highest correlation value is the one required.

As the final step in this stage quadratic curves are fitted to the correlation surface so that the position of the peak can be determined to the nearest 1/10th pixel. The position of each peak is converted directly into a cloud motion vector and when this has been done there exists, for each cloud tracer, a pair of vectors (one from H-$\frac{1}{2}$ to H, and the other H to H+$\frac{1}{2}$) and a knowledge of the radiance values associated with the tracer. The 2 vectors are not combined until a later stage.

2.1.4 Height attribution

Values of 11 μm radiance associated with each tracer are converted to equivalent temperatures and hence, by reference to an appropriate temperature/height relationship, to the height of the cloud. NWS (Washington) forecast temperature profiles in grid form have been used by ESA in the past but there have been problems with timing - it has been necessary to use a 12-hr forecast at T+24 hours because of transmission delays etc. ECMWF forecasts are contemplated for Meteosat-2 operations. The timing problem apart, there are 2 major difficulties in this method of height assignment. Firstly it assumes that the cloud top is radiating as a black body (with emissivity of unity) and secondly the relationship between temperature and height is frequently not known to the accuracy required, especially near the tropopause. A consequence of the black-body assumption is that thin high cloud is liable to be assigned to unrealistically low levels and a correction for the semi-transparency of cirrus to radiation originating at lower levels is an integral part of the ESA processing. It utilises simultaneous water vapour channel radiances. Cirrus has a low transparency to water vapour radiance and provided there is sufficient contrast between the radiance originating from the cirrus and that from the background an estimate of the blackbody radiation of the

cirrus can be obtained.

2.1.5 Manual quality control

As indicated earlier it is possible for all the preceding steps to be performed correctly and yet for the end-product to be of no value to the meteorologist. If, for instance, the target segment includes a fairly straight cloud edge, a quite meaningless correlation can be obtained. To eliminate such cases ESA operate a manual quality control procedure in which all derived winds and heights are scrutinised by an experienced meteorologist before dissemination. Using an interactive console the calculated cmv's are displayed on a television screen, superimposed on the animated sequence of images used. The operator normally scrutinises one quadrant of the full processing area at a time, though he can use a 'zoom' facility to magnify selected portions. With a cursor and light-sensitive pen he deletes all winds which

- do not appear to correspond to the movement of any cloud
- appear to be attributed to the wrong height band
- appear to be associated with orographic cloud
- appear to be associated with development rather than true cloud movement
- are associated with the movement of a cloud system rather than individual elements within the system.

Various additional facilities on the console enable suspect winds to be examined in more detail. The operator can vary the animation speed, modify the grey levels, display radiance values of cloud tracers, display assigned pressure levels of cloud tops, etc.

2.1.6 Final processing and dissemination

The correlation peaks at H-$\frac{1}{2}$ and H+$\frac{1}{2}$ are used as end points for the determination of a final wind vector representing the mean wind over the one-hour period. Winds and their heights are then put into SATOB code for general distribution over the GTS. A typical run takes about 4 hours from start to finish and yields around 500 winds, though there are wide variations from day to day.

2.2 Manual methods

The so-called manual methods that are used operationally are really a combination of manual and automatic stages - to perform the whole operation manually would be too time-consuming. In most cases the principal distinction between manual and automatic techniques is that in the former an operator selects the tracers, designating their initial (and sometimes final) positions on an animated sequence of images. The computation of a wind vector is then done automatically.

ESA have developed a manual technique to supplement the output from their automatic method where, for example, the latter gives a low yield. It is an interactive system using the same console as the quality control. After the operator has indicated with the cursor the initial and end positions of the selected tracer, the computer system takes over and runs the correlation matching scheme already described to get a more precise wind vector than would be possible visually. Height assignment of 'manual' cmv's is possible in various ways. Where they relate to a cloud layer used in the automatic process a similar height can be used with reasonable confidence. Alternatively the characteristic radiance can be used to provide a temperature, and ultimately a height, using a water vapour channel correction for semi-transparent high

cloud if appropriate.

2.3 Optical method

This method of measuring cloud displacement is claimed to be more accurate than others but is too slow for operational use. Developed largely at LMD Paris, the apparatus (called an optical correlator) enables up to 4 consecutive images, projected independently, to be superimposed or shown in rapid sequence. After initial adjustments to align the pictures they are projected in sequence and further adjusted until a chosen target cloud appears motionless. The cmv can be calculated from the geometry of the apparatus and the image displacements. Height assignment is less precise; LMD designate the winds 'high' 'medium' or 'low' on the basis of visual interpretation.

2.4 Operational procedures of NOAA/NESS and JMSC

NOAA/NESS consider that the selection and tracking of low-level cloud tracers, usually patterns of cumulus clouds, is relatively straightforward and amenable to almost total automation. Their computer system takes 4 images at 30 min intervals, selects the best pair using various quality criteria, registers them, selects cloud targets at pre-determined locations on a $2\frac{1}{2}^{0}$ lat/long grid, and computes winds from the 30 min displacement of the targets. All winds produced are assigned to 900 mb. There is an initial quality control check by automatic comparison with an 850 mb analysis and a final manual check. For medium and high level winds NOAA/NESS use a manual method in which initial and final positions of selected tracers are extracted from a movie loop. Height assignment is similar to ESA's but without a water vapour channel correction for high cloud.

JMSC have 2 techniques. In the first, targets are manually selected and tracking is by a cross-correlation technique. This is normally restricted to clouds below about 400 mb. The second technique, used for clouds at higher levels, involves a film loop of IR images on which target clouds are selected and tracked. In all cases heights are determined via cloud top temperatures. Statistical values of emissivity are used in the temperature determination of high clouds. All winds are subject to an interactive quality control which includes a comparison with radiosonde winds. Up to 400 winds are produced twice daily.

3. Errors and validation

3.1 Sources of errors

The errors can be conveniently separated into:

(i) errors in the measurement of cloud displacement.
(ii) errors in using that measurement to infer the wind, and in assigning a height.

The first group can be evaluated fairly precisely. Image resolution, image registration and the precision with which the cloud pattern matching can be achieved are all involved. In automatic methods, where the position of a correlation peak can be specified to 0.1 pixel, the image registration is all-important. ESA claim that the relative registration error between 2 Meteosat

images an hour apart is normally less than 0.5 IR pixels, which is equivalent to a wind error of about 0.7 ms^{-1} in the centre of the image. In manual methods however the operator may not be able to mark the final position of the cloud target to better than ± 2 pixels, and the resulting contribution to the wind error is likely to exceed that due to registration error. Tracking over a longer time interval may help; there is a need to achieve the best possible balance between time interval, registration and displacement distance.

The second group comprises errors caused by one or more of the following:

- cloud tracer did not move with the wind
- motion of tracer was controlled by wind at a different level
- cloud top temperature was not determined correctly
- conversion of cloud temperature to height not correct

Hopefully quality control eliminates most cases of the first kind, leaving what are essentially all height assignment errors. Evaluation is difficult but they can be gauged from comparisons with independent measurements, discussed below.

3.2 Co-location comparisons

Most schemes that have been used to assess the quality of the satellite winds have involved comparisons with conventional wind observations. Comparisons with radiosonde winds have been made regularly by the operators of geostationary satellites, under the auspices of the group for Co-ordination of Geostationary Meteorological Satellites (CGMS). They cannot however give a completely satisfactory measure of the satellite wind accuracy because, apart from small differences in time and location which are often present, the 2 systems have different characteristics. The sonde is measuring at almost a point in the horizontal, though with some averaging in the vertical, while the satellite is measuring a mean wind over a horizontal area some 200 Km square. There are difficulties of this sort in nearly all validations - there is no value which can confidently be used as "truth".

Table 1 shows results of Meteosat/sonde co-location comparisons made at Bracknell using the following CGMS criteria for co-location:

Latitude and longitude	: Within 2° (but 3° longitude poleward of 25°N and S)
Height	: Within 50 mb (35 mb for pressures below 700 mb)
Time	: Within 3 hours

The seasonal variation apparent from the mean speed of the satellite winds reflects the fact that although Meteosat views equal areas North and South of the equator, the majority of comparisons were in the European and Mediterranean areas. A feature of particular interest is the marked bias in speed differences for high-level winds. Various explanations have been suggested, and a tendency for automatic tracking techniques to underestimate the strength of the wind has been postulated by some workers, but it is believed that much of the bias arises from incorrect height assignment. If the Meteosat winds are assigned to levels that are too high they are likely, on a majority of occasions, to be compared with sonde winds that are stronger than appropriate.

Because of the position and time differences permitted by the co-location criteria, the interpretation of some of the values in Table 1 is not clear. To provide some kind of yardstick against which they can be judged, equivalent statistics have been prepared for differences between pairs of radiosondes satisfying the same criteria. Some results are shown in Fig 2, which includes

both kinds of difference plotted against separation distance. At low and medium levels the Meteosat/sonde values are comparable with the sonde/sonde values. At high levels the agreement is less good.

Table 2 shows corresponding Meteosat, GOES and GMS statistics for May and July 1979. (Statistics for GOES-E and GOES-W have been combined into a single set of figures as the same processing methods are used). There is no clear superiority of one system over the others and in most respects there is a good measure of agreement between all three. At first glance it might appear from the vector difference values that Meteosat is superior to GOES and GMS for high level winds, but both of the latter show a much higher mean speed.

3.3 Other evaluations

3.3.1 As a further check on the compatibility of winds from different satellites CGMS have organised comparisons between winds in the 'overlap' areas of adjacent satellites, eg that part of the Atlantic included within the processing area of both Meteosat and GOES-E. Results indicate an encouraging degree of consistency.

3.3.2 Comparing satellite winds with those implicit in some kind of synoptic objective analysis avoids many of the problems of co-location comparisons and allows comparisons wherever satellite winds are reported. Furthermore, winds from an objective analysis are likely to represent the average flow across an area better than localised sonde measurements. In the course of their FGGE data assimilation work, Birch and Lyne (1979) obtained the values of RMS vector difference between satellite winds and winds from model analysed fields shown in Table 3. These particular values relate to a few days during the 2nd Special Observing Period. They cannot be compared directly with the co-location figures in Tables 1 and 2 because of different height groupings but at high levels they are roughly $\frac{2}{3}$ of the co-location values and they are generally rather lower than the others at medium and low levels too.

3.4 General assessment

The consensus that emerges from the various validation studies made is that for most purposes the quality of satellite winds is not significantly different from that of sonde winds, though difficulties with height assignment make the high level satellite winds slightly less satisfactory than those at lower levels.

4. References and further reading

Hasler A F et al 1979 In-situ aircraft verification of the quality of satellite cloud winds over oceanic regions. J Applied Met, 18, p 1481.

Birch N T and Lyne W H 1979 The use of satellite data in a data assimilation scheme during FGGE. MRCP 472.

WMO 1979 Wind derivation from geostationary satellites. Chapter 2 of Technical Note No 166.

ESA 1980 Wind vector determination. Section 5.4 of Meteosat system guide.

Hubert L F and Thomasell A 1979 Error characteristics of satellite-derived winds. NOAA Technical Report NESS 79.

Table 1

METEOSAT/SONDE CO-LOCATED WIND COMPARISON STATISTICS

(Units: Metres per second)

	Jul 78	Nov/Dec 78	Jan/Feb 79	May/Jun 79	Nov 79
HIGH LEVEL WINDS (Above 400 mb)					
No. of comparisons	104	395	1516	564	427
Mean vector difference	11.3	16.5	12.6	9.1	14.3
RMS vector difference	13.3	21.2	15.3	12.9	17.8
Mean speed of satellite winds	16.0	19.0	20.0	14.7	18.8
Algebraic mean speed difference	-5.1	-7.8	-5.0	-3.8	-8.2
MEDIUM LEVEL WINDS (699 to 400 mb)					
No. of comparisons	38	211	511	382	223
Mean vector difference	9.8	8.8	9.6	7.5	7.6
RMS vector difference	12.2	11.6	12.2	9.1	9.5
Mean speed of satellite winds	13.9	10.2	12.2	10.2	12.0
Algebraic mean speed difference	3.9	-3.8	-4.4	-2.1	-0.6
LOW LEVEL WINDS (700 mb & below)					
No. of comparisons	13	90	105	237	125
Mean vector difference	6.5	5.2	5.5	5.1	5.6
RMS vector difference	8.1	7.2	6.8	6.0	6.8
Mean speed of satellite winds	8.8	6.6	8.5	8.5	8.7
Algebraic mean speed difference	3.8	0.2	0.8	2.0	-0.8

TABLE 2

COMPARATIVE CLOUD WIND STATISTICS FOR MAY-JUNE 1979

SATELLITE/SONDE CO-LOCATIONS

	METEOSAT	GOES E/W	GMS
High Level (< 400 mb)			
No	564	469	1440
Mean Vector Diff	9.1	10.6	13.4
RMS " "	12.9	13.0	15.8
Mean Speed	14.7	24.0	27.7
Algebraic Mean Speed Diff	-3.8	2.7	2.5
Medium Level (699-400 mb)			
No	382	31	193
Mean Vector Diff	7.5	7.5	7.1
RMS " "	9.1	8.7	9.4
Mean Speed	10.2	13.0	8.8
Algebraic Mean Speed Diff	-2.1	2.5	0.9
Low Level (Up to 700 mb)			
No	237	644	442
Mean Vector Diff	5.1	4.7	4.6
RMS " "	6.0	5.6	6.0
Mean Speed	8.5	7.7	6.9
Algebraic Mean Speed Diff	2.0	-0.8	0.5

All speeds in ms^{-1}

Algebraic mean speed diff is (satellite minus sonde)

TABLE 3

RMS VECTOR WIND ERRORS DURING MAY-JUNE 1979

- FROM MRCP 472 (BIRCH & LYNE)

Layer (mb)	METEOSAT	GOES-E	GOES-W	GMS
Above 200	5.0	7.3	8.3	8.1
400 to 200	7.7	9.8	9.2	10.2
600 to 400	4.6	6.4	9.3	6.6
800 to 600	3.2	5.6	5.8	5.2
1000 to 800	2.2	3.6	3.8	3.6

Units : ms^{-1}

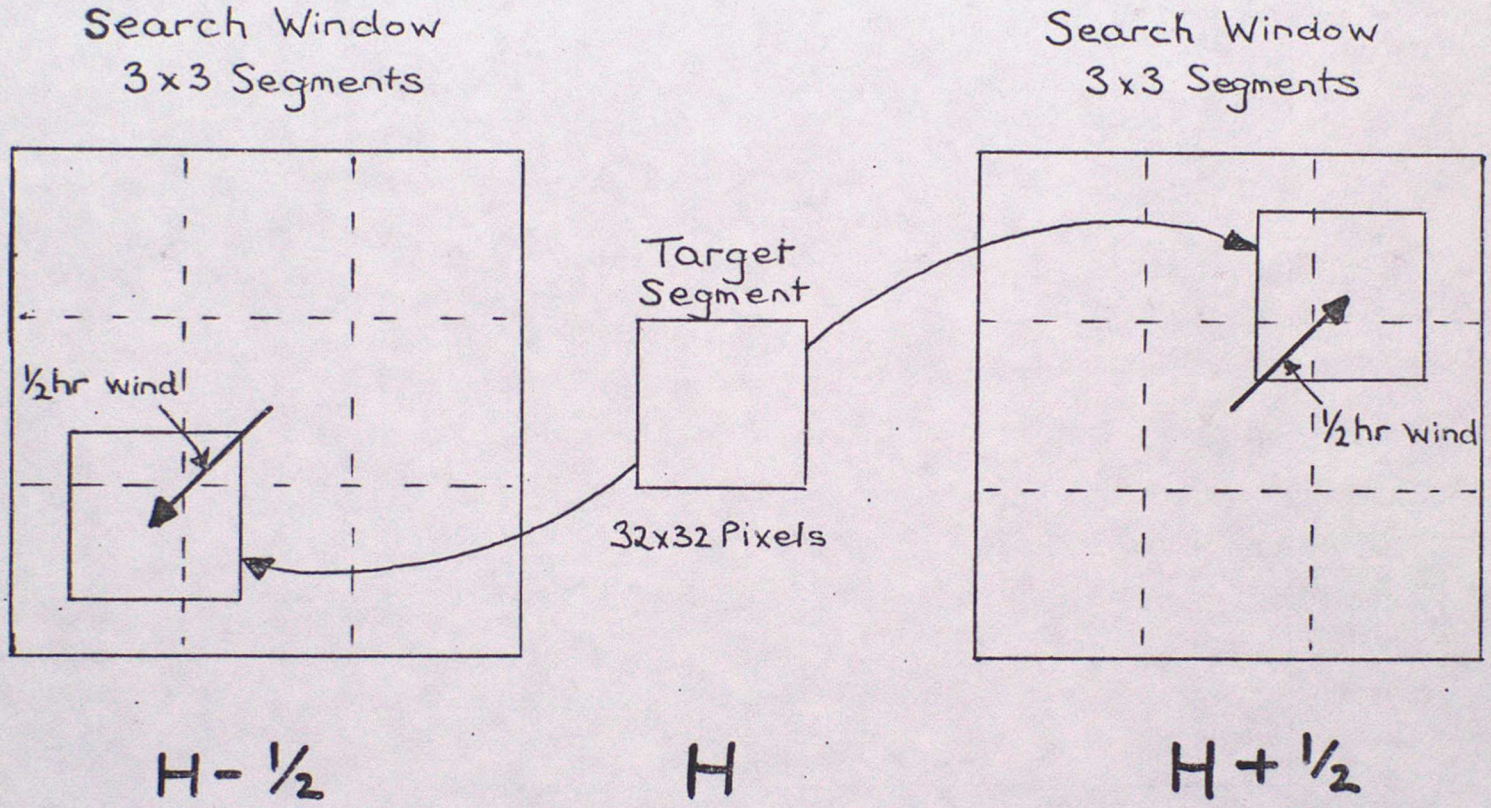

FIGURE 1 CORRELATION MATCHING
- SEARCH PROCEDURE

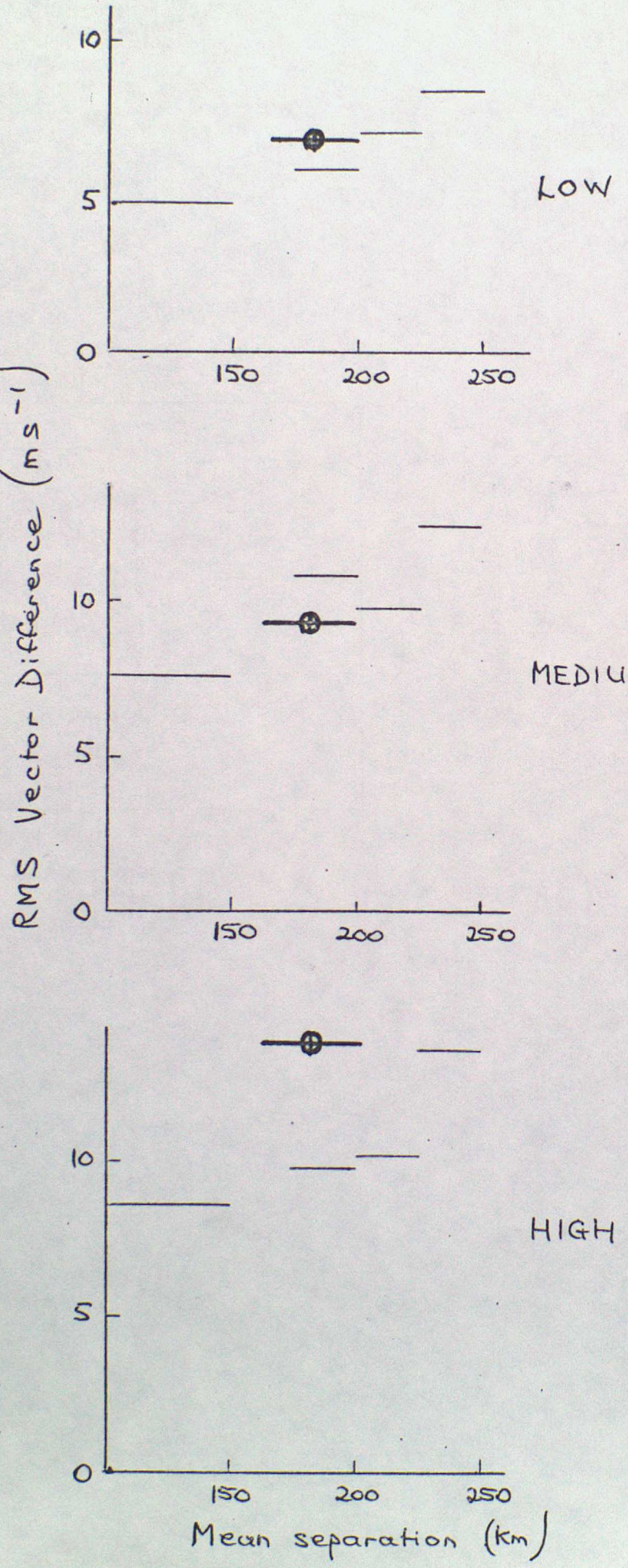

FIGURE 2

Comparison of RMS Vector Differences for co-located winds.

Key:

— sonde/sonde

⊕ satellite/sonde

8. MICROWAVE TECHNIQUES by D Offiler

8.1 Introduction

This lecture will deal with the techniques whereby meteorological (and oceanographic) parameters can be deduced from satellites using radiation in the microwave region.

By microwave, we mean that part of the electromagnetic spectrum with wavelengths between 5 mm and 10 cm or in frequency terms, 3 and 60 GH_z - although these boundaries are not rigid cut-off points. With the post-war development of radar, this part of the spectrum was divided into bands, as shown in Table 1 (left). These bands have recently been reclassified, giving more regular divisions (right).

One reason why microwaves are used extensively for purposes such as tracking radars and telecommunications, and which makes them suitable for remote sensing is that for frequencies below 50 GH_z, atmospheric attenuation is low, even in clouds. At low enough frequencies (less than 10 GH_z), attenuation by rain is also acceptably low. So for remote sensing from satellites, measurements can be made in clear or cloudy weather and even in moderate amounts of rain, to an acceptable accuracy.

Satellite microwave remote sensing of the atmosphere and surface may be split into two distinct types: passive (radiometric) and active (radar). Some recent instruments and their satellites in each category are listed in Table 2. Although these lectures are on 'Satellite Meteorology', some other applications of microwave remote sensing - eg oceanography - will be briefly mentioned. Microwave techniques can also be used, of course, for surface (and aircraft) based sensing of the atmosphere and oceans, the Malvern rain-radar programme being a good example.

8.2 Passive Microwave Remote Sensing

8.2.1 The Radiative Transfer Equation

Passive sensing of the atmosphere and surface using thermal radiation in the microwave region is similar to that for infra-red sounding (lectures 3 and 4).

From the Planck function for wavenumber, ν (cm^{-1}):

$$B_\nu = \frac{c_1 \nu^3}{e^{c_2 \nu / T} - 1}$$

and for microwaves, $\nu \sim 1$, so $\frac{c_2 \nu}{T} \ll 1$, and $B_\nu \approx \frac{c_1}{c_2} \cdot \nu^2 T$ or the blackbody radiation is proportional to the emitting temperature for a given frequency. This part of the Planck curve is known as the Rayleigh-Jeans approximation and it is common when using microwave frequencies to use the term 'brightness temperature' in place of 'radiance'. The brightness temperature of an object is the temperature that object would have, if it were a perfect blackbody, in order to give

the same radiance as that emitted at its actual temperature. Ie $\overline{T_B} = \epsilon . \overline{T}$ where ϵ is the effective emissivity.

In lecture no 3, the monochromatic radiative transfer equation was derived. The equivalent equation in terms of brightness temperature, T_B is:

$$\overline{T_B}(f,\theta) = \tau(f,0)^{\sec\theta} . \varepsilon_s . T_s + \int_0^H T(h) . W(f,\theta,h) + \tau(f,0)^{2\sec\theta} . (1-\varepsilon_s) . T_{space} \qquad (1)$$

where:

F	is frequency
θ	is the off-nadir viewing angle (for slant paths)
ε_s	is the surface emissivity
T_s	is the physical surface temperature
T(h)	is the atmospheric temperature at height h
T_{space}	is the space brightness temperature (2.7K)
$\tau(h)$	is the transmission from height h to the satellite height, H
($\tau(0)$	is the total transmission from surface to H)
W	is the atmospheric temperature weighting function, and is given by:

$$W(f,\theta,h) = \left\{1 + [1-\varepsilon_s] . \left(\frac{\tau(f,0)}{\tau(f,h)}\right)^{2\sec\theta}\right\} . \frac{\partial \tau(f,h)^{\sec\theta}}{\partial h} \qquad (2)$$

Similarly to the infra-red case the first term on the right of equation (1) is the surface contribution, the second term from the atmosphere. The third term is included to account for the 2.7K space brightness temperature reflected from the surface back up to the satellite. Similarly, the equation for the Weighting Function (2) includes downward atmospheric emissions reflected by the surface.

8.2.2 Surface emissivity

In infra red work, the 'surface' emissivity is usually taken to be close to unity for most surfaces including cloud tops and the reflection terms in equations (1) and (2) may be ignored. However, microwave emissivity varies greatly with the nature of the surface. Over land, the emissivity varies between about 0.8 and 1.0 and depends on vegetation cover, soil type, moisture content and microwave frequency. Sea surface emissivity ranges from about 0.3 to 0.7 and depends on salinity, temperature, wind speed (surface roughness and foam cover effects), viewing angle, polarisation and frequency. Thus, over the sea, the emissivity plays an important part in the determination of the Weighting Function. Figure 1 shows the variation in emissivity of a water surface with viewing angle for different windspeeds and polarisations, at a frequency of 10.7 GH_z.

8.2.3 Atmospheric absorption

At microwave frequencies, there are two major absorbing gasses: molecular oxygen and water vapour, both due to rotational states. Oxygen has two absorption bands centred at 60 and 118 GH_z and water vapour single lines at 22.2 and 180 GH_z.

Since oxygen is a well mixed gas, it can be used for temperature sounding in exactly the same way that carbon dioxide is used for infra red sounding. The water vapour line at 22 GH_z may be used to determine column amounts of precipitable vapour.

Absorption by both gases is weakly dependent on temperature but more on pressure and composition (pressure broadening). Figure 2 shows the absorption coefficient, α (km^{-1}) against frequency for various levels in a standard atmosphere. (Absorption in dB/km $= \alpha.(10 \log_{10} e)$.) Note that water vapour absorption falls rapidly with decreasing vapour content, but that oxygen absorption is still relatively high at 100 mb, where the individual lines in the 60 GH_z band are now showing as the effects of pressure broadening decrease.

Temperature weighting functions for the Microwave Sounder Unit (MSU) on Tiros N/NOAA series, calculated from equation (2) and using the same standard atmosphere, are shown in Figure 3. The effect of the surface can be seen to decrease the weighting of the lower levels of the atmosphere over land (high emissivity) and that a slant viewing path raises the height of the peaks by 1 - 2 km.

Oxygen and water vapour are not the only absorbers of microwave radiation: clouds and precipitation also absorb, depending strongly on frequency, amount of absorber and its temperature. Plots of attenuation coefficient (per unit amount of absorber) against frequency are shown in Figures 4 and 5 for cloud liquid water and rain respectively, for various temperatures. The effects of ice cloud and frozen precipitation are very much less than for their liquid counterparts, and in practical applications of remote sensing may be ignored without affecting retrieval accuracy.

8.2.4 Simulated brightness temperatures

Given an atmospheric temperature profile, surface conditions and amount of liquid cloud and precipitation, and using the sections 8.2.1 to 8.2.3 above, we can calculate a simulated brightness temperature for any (monochromatic) frequency. Figure 6 is a plot of calculated brightness temperates against frequency for different model atmospheres, showing the effects of the various absorbers with frequency. At high frequencies, (above about 55 GH_z), oxygen absorption is so great that the weighting function peaks high in the atmosphere and the brightness temperature is close to the physical temperature at that level. The 22 GH_z broadened line shows up well against the background of low surface emission from the sea. Over a land surface, higher background radiation reduces this contrast, making vapour retrievals less reliable.

8.2.5 Retrieval of Meteorological Parameters

Satellite measured brightness temperatures (or microwave radiances) are best combined with infra red radiances when retrieving parameters such as temperature or thickness,

using the techniques described in previous lectures. However, passive microwave measurements can be used alone and are especially useful when infra red retrievals are not available or are unreliable, as in totally cloudy areas. Indeed, microwave sounding can deduce parameters that infra red cannot, for example rainfall rates or sea surface wind speeds. However, spatial resolution, typically 30-100 km, is generally poorer than infra red.

The choice of frequencies for a particular instrument will depend on the application required. For atmospheric temperature sounding, the Scanning Microwave Sounder (SCAMS) on Nimbus 6 and the MSU on Tiros N/NOAA 6 have channels on the low frequency edge of the 60 GH_z band (SCAMS at 52.85, 53.85 and 55.45 GH_z, MSU at 50.30, 53.74, 54.96 and 57.05 GH_z). In addition, SCAMS has a channel at the peak of the water vapour line (22.23 GH_z) and one at 31.65 GH_z. These two latter channels used in combination are used to determine total integrated water vapour content and total cloud liquid water amount. The Scanning Multichannel Microwave Radiometer (SMMR) on Seasat and Numbus 7 have lower frequency channels (6.6, 10.7, 18.0, 21.0 and 37.0 GH_z) at both horizontal and vertical polarisations. These allow sensing of the surface, with low atmospheric attenuation, of surface temperature, surface roughness (and thence wind speed), soil moisture and ice cover and type as well as water vapour, cloud liquid water and rainfall rate.

Whatever parameter is being retrieved, it is most common to use a regression technique:

$$P = a_0 + a_1 F(T_{B_1}) + a_2 F(T_{B_2}) + \ldots$$

$$= a_0 + \sum_i a_i F(T_{B_i}) \qquad \text{where i is the ith channel}$$

The function F may be the measured brightness temperature (T_B) itself, or a non-linear form, such as $\log_{10}(T_B - 285)$. The coefficients (a's) are found initially usually from a large set of simulated brightness temperatures using a statistical set of atmospheric profiles with a rainge of surface conditions, cloud layers and perhaps rainfall, or after some time of operating, from colocated surface-based measurements. Because of the large emissivity variation between land and sea, different sets of coefficients are normally used for each case, and they may also be a function of scan angle from nadir.

8.2.5 Examples

The following examples are all from the SCAMS instrument on Nimbus 6, and show the kind of product that passive microwave instruments on their own can provide.

Figure 7 is a chart of retrieved 1000-500 mb thickness (solid lines) from three orbits 1040 GMT to 1420 GMT on 19 February 1976. For comparison, the CFO subjectively analysed field (dotted lines) is also shown. Despite extensive cloud cover and large emissivity changes between

land and sea, the general pattern is well retrieved: comparisons with radiosonde 1000-500 mb thicknesses showed a standard deviation of about 2.5 Dm over two five-day periods in August 1975 and February 1976.

Figure 8 is a plot of retrieved precipitable water vapour against that derived from nearby radiosondes over a two-week period in 1975 in the Tropical Pacific. Comparison time series for five of these sonde stations is shown in Figure 9.

The high measurement density and repeated coverage provided by satellites allow time averaged plots of various quantities - Figure 10 and 11 show mean water vapour and liquid (cloud) water contour maps over the same two weeks as above. The ITCZ show up clearly as a band of moist and cloudy air.

8.3 Active Microwave Remote Sensing

Active remote sensing is basically a radar technique. A beam of microwaves is transmitted, reflected from the surface and received back at the satellite to infer some property of the surface, such as its roughness, or just how far away it is. Active instruments may be divided into three groups of scatterometers, altimeters and synthetic aperture radars, according to their function and mode of operation. As yet none of these has flown on an operational satellite, but one of each type was flown on the experimental oceanographic satellite Seasat in 1978, and are likely to be on operational satellites in the mid - 1980's.

8.3.1 Scatterometers

Scatterometers may be used to infer surface wind vectors over the ocean by the more basic measurement of the level of microwave power backscattered from the surface. Backscattering is due to in-phase reflection from a rough surface; for incidence angles greater than about 25 degrees, backscattering occurs when the Bragg condition is met:

$$\Lambda \sin\theta_i = n\lambda/2$$

where Λ is the surface roughness wavelength, λ is the radar wavelength, θ_i the incidence angle and n=1, 2, 3.... For first order Bragg Scettering (n=1) and at microwave frequencies (wavelength $\sim$ 1 cm), Λ corresponds to small capillary waves superimposed on larger gravity waves. These capillary waves are generated by the instantaneous local wind. The level of backscatter from an object is usually expressed as the Radar Cross Section (RCS or σ) which is defined as the area intercepting that amount of power, which when scattered isotropically, produces an echo equal to that received from the object. For extended targets, such as the sea surface, the backscatter is expressed as the Normalised Radar Cross Section (NRCS or σ°) which is the RCS per unit area. In terms of other (known or measureable) radar parameters,

$$\sigma^\circ = \frac{64\pi^3 R^4}{\lambda^2 L_s G_0^2 \left(\frac{G}{G_0}\right)^2 A} \cdot \frac{P_R}{P_T} \qquad (3)$$

where R is the slant range to the target cell and A its actual area, λ is the radar wavelength, Ls are atmospheric

and system losses (attenuation), Go the peak antenna gain, G/Go the relative antenna gain in the target direction. P_T is the transmitted power and P_R the received power. Equation (3) is often referred to as the Radar Equation. (σ° is often given in decibels ie $\sigma^\circ(\text{dB}) = 10 \log_{10}\sigma^\circ$)

Experimental evidence from wind-wave tanks and static, aircraft and satellite mounted scatterometers over the ocean show that σ° increases with surface wind speed, decreases with incidence angle and is also dependent on the beam azimuth angle with respect to wind direction. It is generally lower for horizontal polarisation than vertical and the dependence of σ° on radar frequency seems to be small over the range 5 to 20 GH_z.

Figure 12 is a plot of averaged Skylab and aircraft scatterometer data of vertical polarisation σ° against relative wind direction for various windspeeds, at 30 degree incidence angle. 0° corresponds to looking upwind, 90° crosswind and 180° downwind; note that the downwind peak is slightly lower than the upwind peak. An empirical function can be fitted to these curves of the form:

$$\sigma^\circ(U,\phi,\theta_i) = a_0^p(U,\theta_i) + a_1^p(U)\cos\phi + a_2^p\cos 2\phi \qquad (4)$$

where a_0, a, and a_2 are proportional to $\log_{10}$ U, U being the wind speed, ϕ the relative wind direction and P=V or H polarisation.

If two σ° measurements are made at different azimuth angles, wind direction can be deduced as well as wind speed. This was the principle of operation of the Seasat-A Scatterometer system (SASS) - Figure 13 - which had two beams either side of the subsatellite track, one 45° forward, one 45° to the rear. A measurement of σ° is taken with the forward beam and a few seconds later a second, orthogonal measurement is taken with the rear beam of the same patch of ocean. (These SASS-type instruments do not have pencil-shaped beams as in many radars, but are fan-shaped in the vertical plane with peak power at about 40° incidence, so spreading the microwave energy across the swath. All cells across the swath are illuminated simultaneously, each cell position being distinguished by the doppler shift of the return frequency, rather than time range-gating). Unfortunately, the solution of wind speed and direction from the two σ°'s is not unique: there are in general four solutions, one direction in each quadrant each with small speed differences. Figure 14 is a plot of wind solutions for a Seasat pass over the JASIN area. The 'correct' solution must be deduced by reference to other sources of data such as the pressure field. (The next generation of Scatterometers, one American and one European, to be flown in the mid-1980's will attempt to reduce this ambiguity by using a third beam at an intemediate azimuth angle or by combining the σ° measurements from simultaneous horizontal and vertical

polarisations respectively. This will give three or four σ^o measurements per cell instead of the two for SASS).

Assuming that the 'correct' solution is taken, SASS comparisons with surface experiments in the Gulf of Alaska (GOASEX) and North Atlantic (JASIN) indicate standard deviations of about 1.5 m/s in speed and 15^o in direction, well within the design goals of $\pm$2m/s or 10% (whichever is greater) and $\pm$ 20^o.

8.3.2 Altimeters

Satellite altimeters primarily measure the time taken for a short pulse of microwave energy to travel from the instrument vertically down to the (sea) surface and back. The height of the antenna is thus ct/2 where c is the speed of light. The altimeter on Seasat was designed to measure this distance to $\pm$10 cm. By calibrating the orbital parameters of the spacecraft by laser tracking ($\pm$8 cm) above some reference Earth, the ellipsoid, the actual Earth's shape can be measured. In the short term, this reflects the variation in the surface due to tides, ocean currents etc, and over a longer time average, the Earth's geoid. Some examples of ocean surface height are given in Figure 15 (due to sub-surface topographical features) and in Figure 16 (due to ocean current circulation).

Because the surface is not generally smooth, the leading edge of the return pulse is not square, but smeared out, due to there being a height difference from the crest (early return) to trough (late return). The amount of smearing (the slope of the leading edge of the return pulse) is related to the average roughness of the surface, and is used to measure the significant wave height (SWH or $H_{1/3}$) - the average height of the highest one-third of all waves. The Seasat altimeter achieved this to an accuracy of about 0.5 m. Figure 17 is an example of return pulse shape for two different SWH's.

The altimeter can also measure the level of return, and thence wind speed (but not direction) in a similar manner to a nadir-looking scatterometer. Preliminary results indicate Seasat altimeter wind speed accuracies of about $\pm$2m/s. Figure 18 shows SWH and σ^o measurements over Hurricane Fico in the Pacific on 16 July 1978.

8.3.3 Synthetic Aperture Radar (SAR)

The SAR is basically a high resolution imaging radar. The one on Seasat had a resolution of 25 metres, and since the smaller the resolution cell size, the larger the required antenna (other things being equal), an antenna several kilometers long is required. Obviously for a satellite this is not possible, but a SAR achieves its resolution with an antenna of, say, 20 m length by using the satellite motion over seconds to generate an apparently large aperture, hence its name.

The SAR measures Bragg backscatter from capillary waves, as for the scatterometer, but by multiple looks during the aperture generation, correlates the σ^o modulation by gravity waves to detect the larger waves (> 50 m wavelength). By complex ground processing, an optical image is formed, in which can be seen land (geographical and geological) features, ocean waves and subsurface phenomena such as internal waves and sand banks. These subsurface features are detected since they modulate the surface σ^o by some as yet unexplained mechanism.

Optical Fourier transforms of SAR ocean images yield two-dimensional intensity spectra which show the dominant ocean wavelength and its direction (with an ambiguity of 180°). Comparison with the GOASEX data indicate that the Seasat SAR spectra can be used to measure these quantities to about ±15% in wavelength and ±20° in direction . This SAR did not have absolute calibration, so the wavelength energy in the spectra cannot be measured absolutely; future SARs would probably have this calibration and capability.

8.4 References

8.4.1 Passive Techniques

Grody, N.C., 1976: Remote sensing of atmospheric water content from satellites using microwave radiometry. IEEE Trans. Antennas Propagat. AP-24, 155-162.

Grody, N.C., P.P. Pellegrino, 1977: Synoptic scale studies using the Nimbus 6 microwave spectrometer. J Appl. Met. 16, 816-826.

Moyer, V, J.R. Scoggins, N-m Choy, G.S. Wilson, 1978: Atmospheric structure deduced from routine Nimbus 6 satellite data. M.W.R. 106 1340-1352.

Offiler, D, 1978: Tropospheric retrievals from a satellite passive microwave spectrometer. Met O 19 Branch Memo No 49.

Rosenkranz, P.W., D.H. Staelin, 1978: Typhoon June (1975) viewed by a scanning microwave spectrometer. J Geophys. Res 83 No C4, 1857-1868.

Staelin, D.H. et al, 1975: The scanning microwave spectometer (SCAMS) experiment. Nimbus 6 User's Guide, Goddard Space Flight Centre, 59-86.

8.4.2 Active Techniques

Grantham W.L. et al, 1977: The Seasat-A satellite scatterometer. IEEE J Ocean Eng., OE-2, No 2, 200-206

Jones, W.L., et al 1977: Aircraft Measurements of the Microwave Scattering signature of the Ocean. IEEE Trans. Antennas Propagat. AP-25, No 1, 52-61

Jones, W.L., et al, 1978: Algorithm for inferring wind stress from Seasat-A. J Spacecraft and Rockets, 15, No 6, 368-374.

Krishen, K., 1971: Correlation of Radar Backscattering Cross Sections with ocean wave height and wind velocity. J Geophys Res., 76, No 27, 6528-6539.

Long, M.W.: Radar Reflectivity of Land and Sea. Lexington Books, Mass., USA.

Zetler, B.D., G.A. Maul, 1971: Precision requirements for a spacecraft tide program. J Geophys. Res 76, No 27, 6601-6605.

General reports:

Boundary Layer Met, 13 Nos 1-4, January 1978. Special issue: IUCRM colloquium on 'Radio Oceanography'.

Science, 204 No 4400, 29 June 1979, 1405-1424 Preliminary Seasat reports.

Seasat Gulf of Alaska Workshop II Report. National Aeronautics and Space Administration, No 622-107. Jet Propulsion Laboratory, Pasadena, Calif., January 1980.

IEEE J. Ocean Eng., OE-5, No 2, April 1980. Special issue on the Seasat-1 sensors.

MICROWAVE BAND DESIGNATIONS

Post-war bands

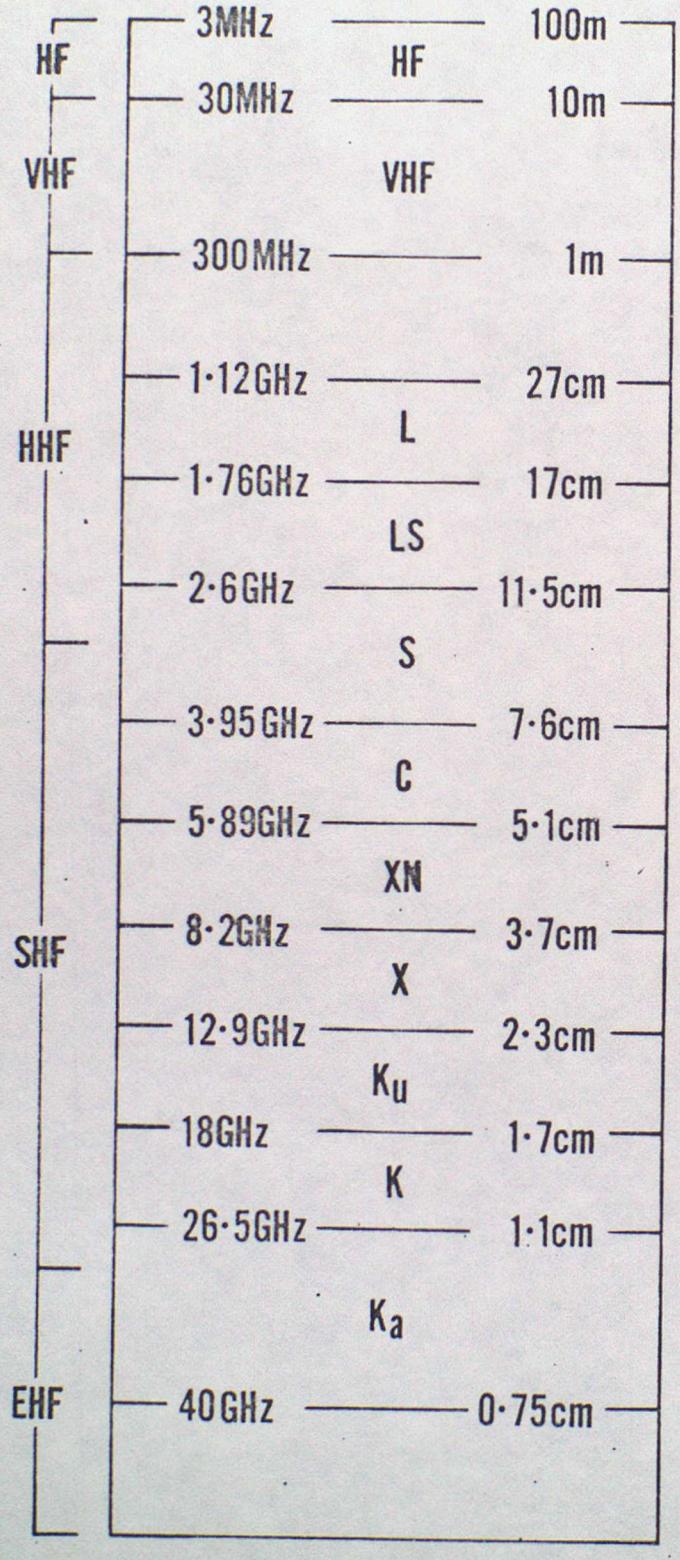

Tri-service bands

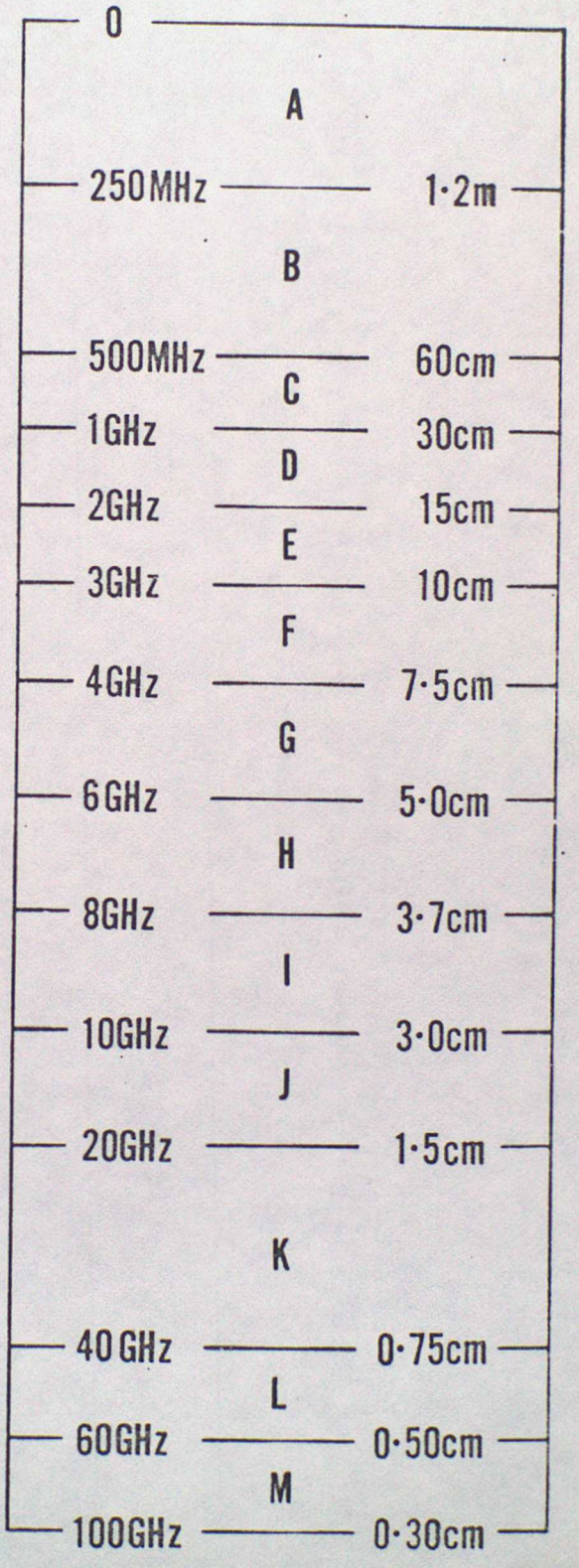

Table 1.

SOME METEOROLOGICAL/OCEANOGRAPHIC MICROWAVE INSTRUMENTS

Table 2.

Passive	Active
Scanning Microwave Sounder (SCAMS) – Nimbus 6 Scanning Multichannel Microwave Radiometer (SMMR) – Seasat and Nimbus 7 Microwave Sounding Unit (MSU) – Tiros N/NOAA series	Seasat–A Scatterometer System (SASS) – Seasat (and Skylab S–193) Radar Altimeter – Seasat and GEOS-3 Synthetic Aperture Radar (SAR) –Seasat

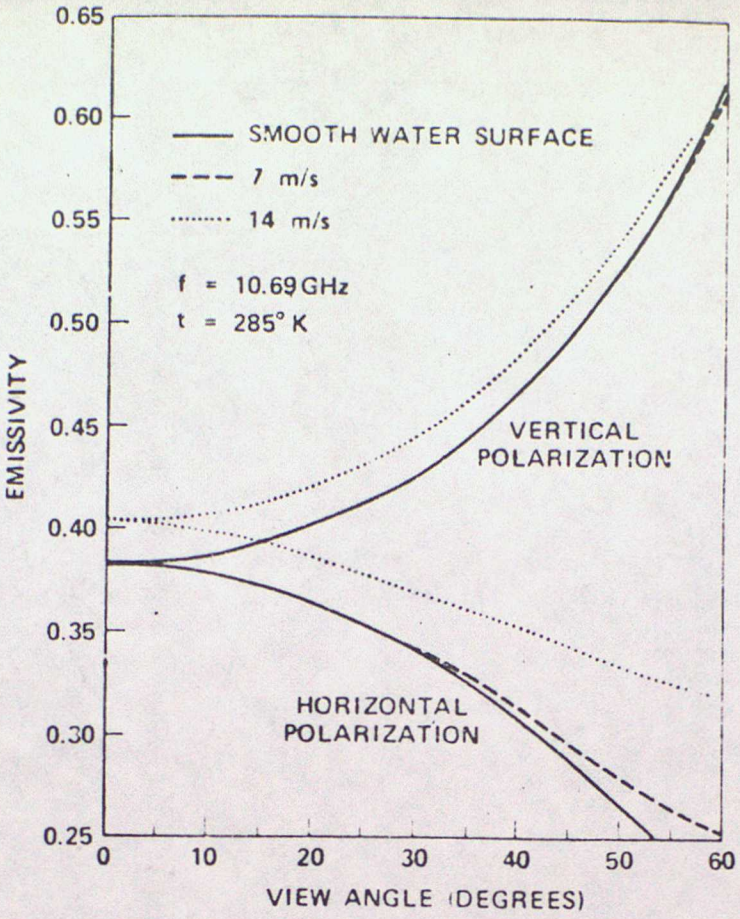

Figure 1 Emissivity as a Function of View Angle for a Smooth Water Surface and for the Ocean Surface with 7 and 14 m/s Wind Speed

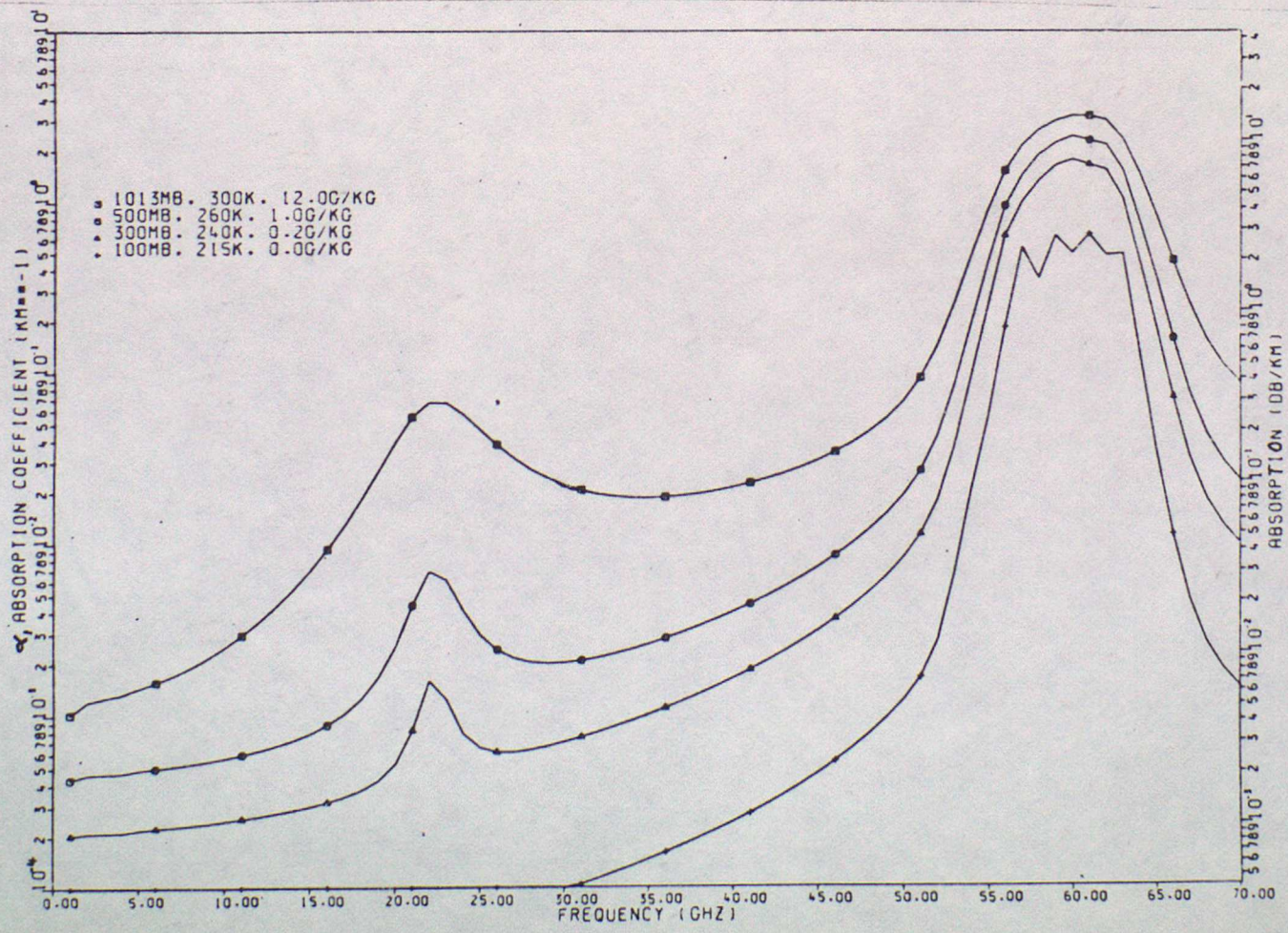

Figure 2. Variation of absorption coefficient with frequency for various pressure levels of a standard midlatitude summer atmosphere, due to water vapour and molecular oxygen.

Figure 3. M.S.U Weighting Functions

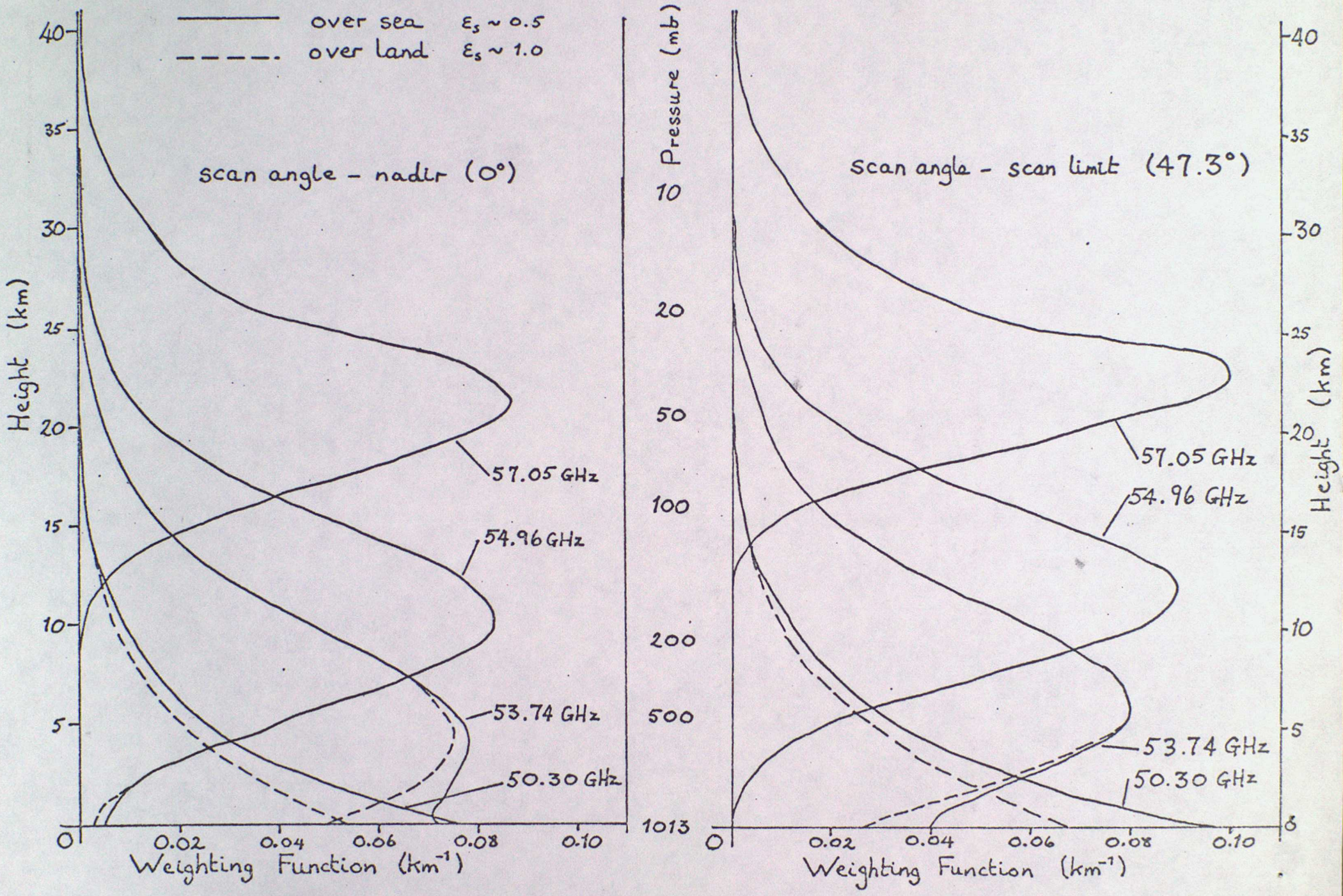

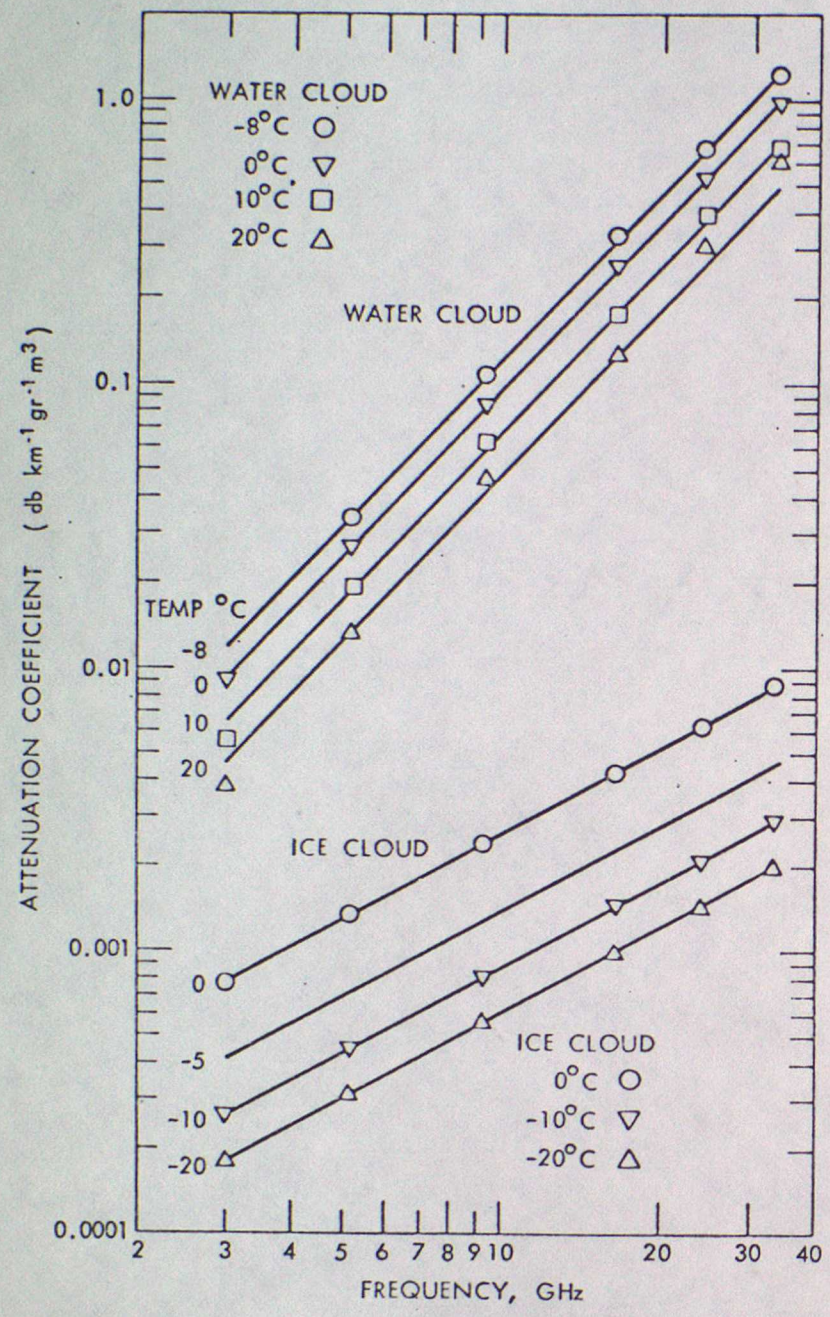

Fig. 4. Microwave attenuation coefficients for clouds. From Benoit (1968).

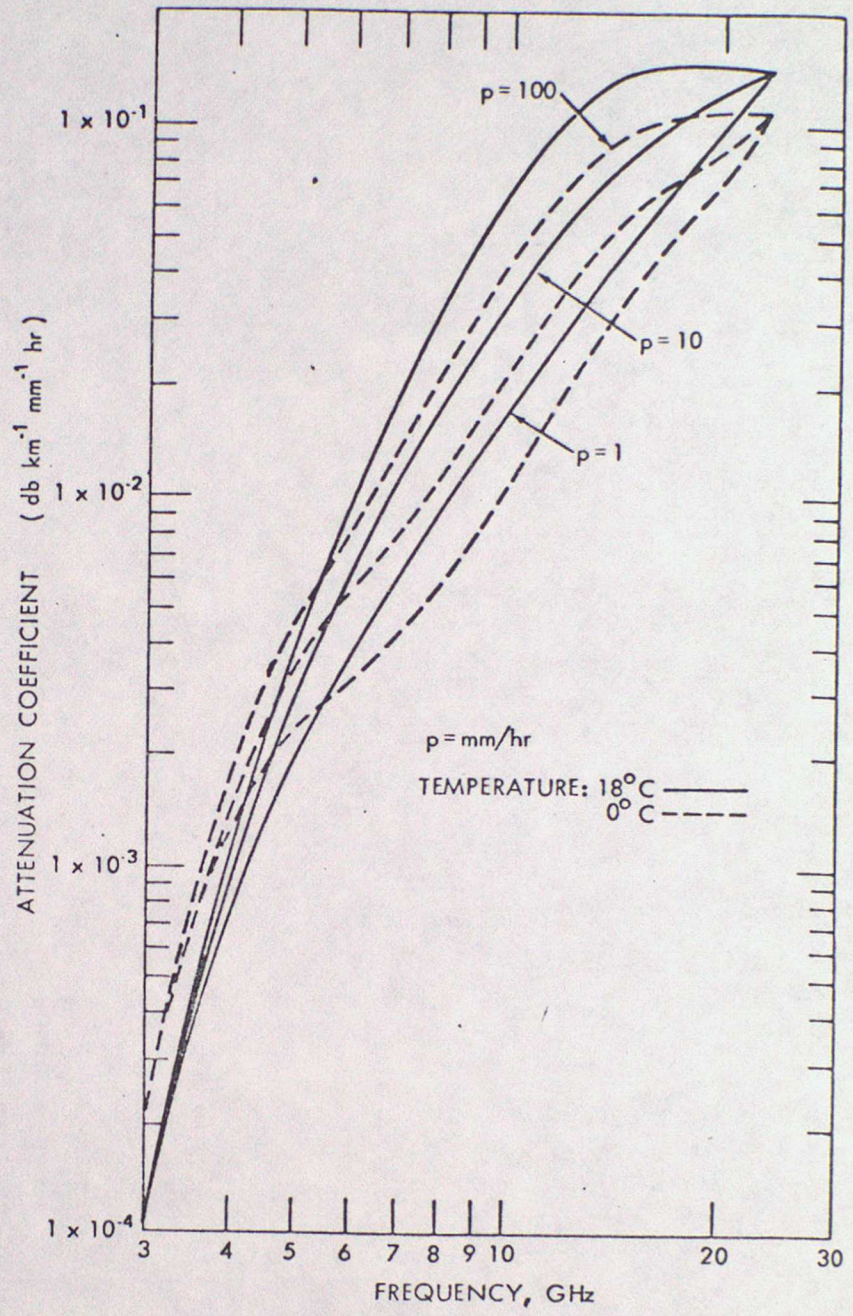

Fig. 5. Microwave attenuation coefficient in rain. From Benoit (1968).

Figure 6. Variation in calculated brightness temperatures with frequency for different atmospheres.

(a) Calm sea at 288k, no atmosphere.
(b) Curve (a) plus oxygen absorption due to a midlatitude summer standard temperature profile.
(c) Curve (b) with 2.2g/cm^2 water vapour, distributed as 10exp(-h/2.2) g/kg. (h in km)
(d) Curve (c) with a cloud layer of 0.2 mm liquid water.
(e) Curve (d) with 1 mm/hr rainfall.

The figures above the abscissa refer to the SCAMS channel numbers.

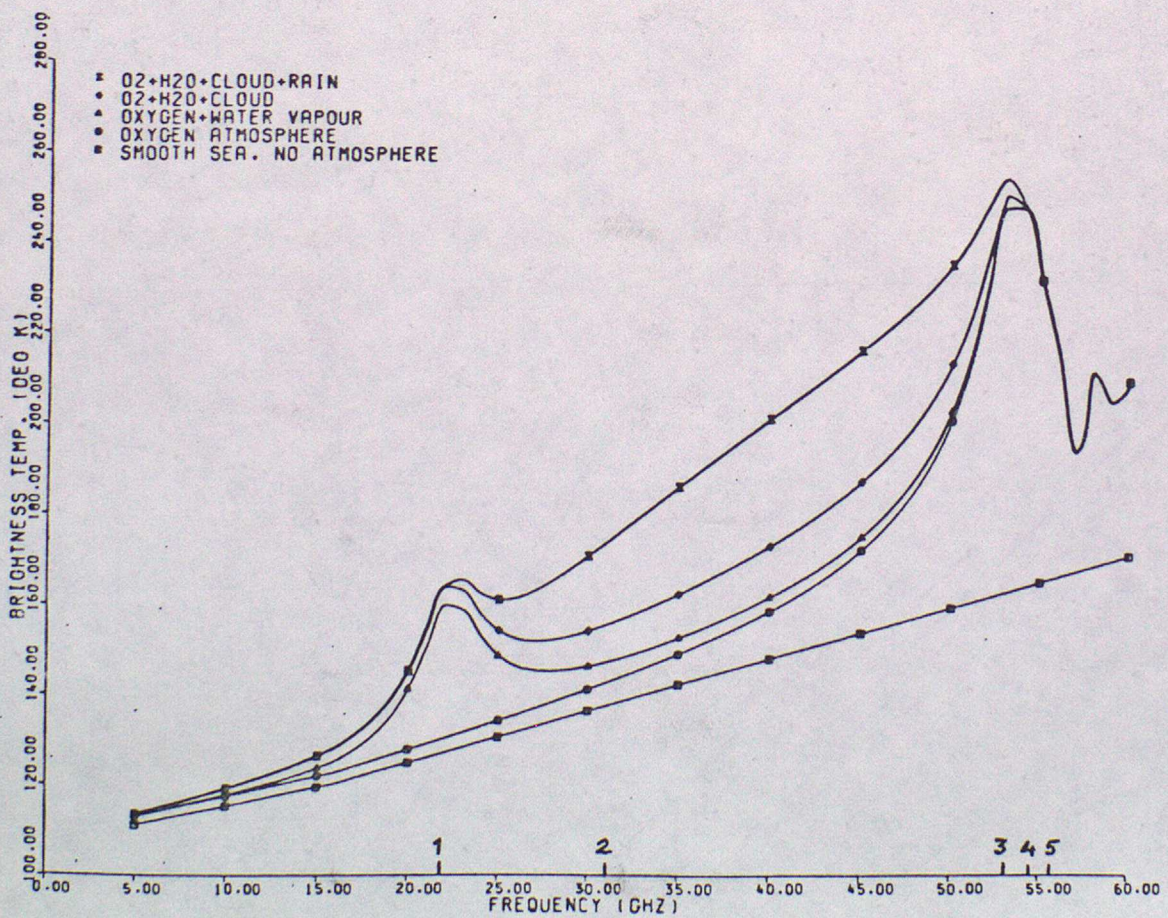

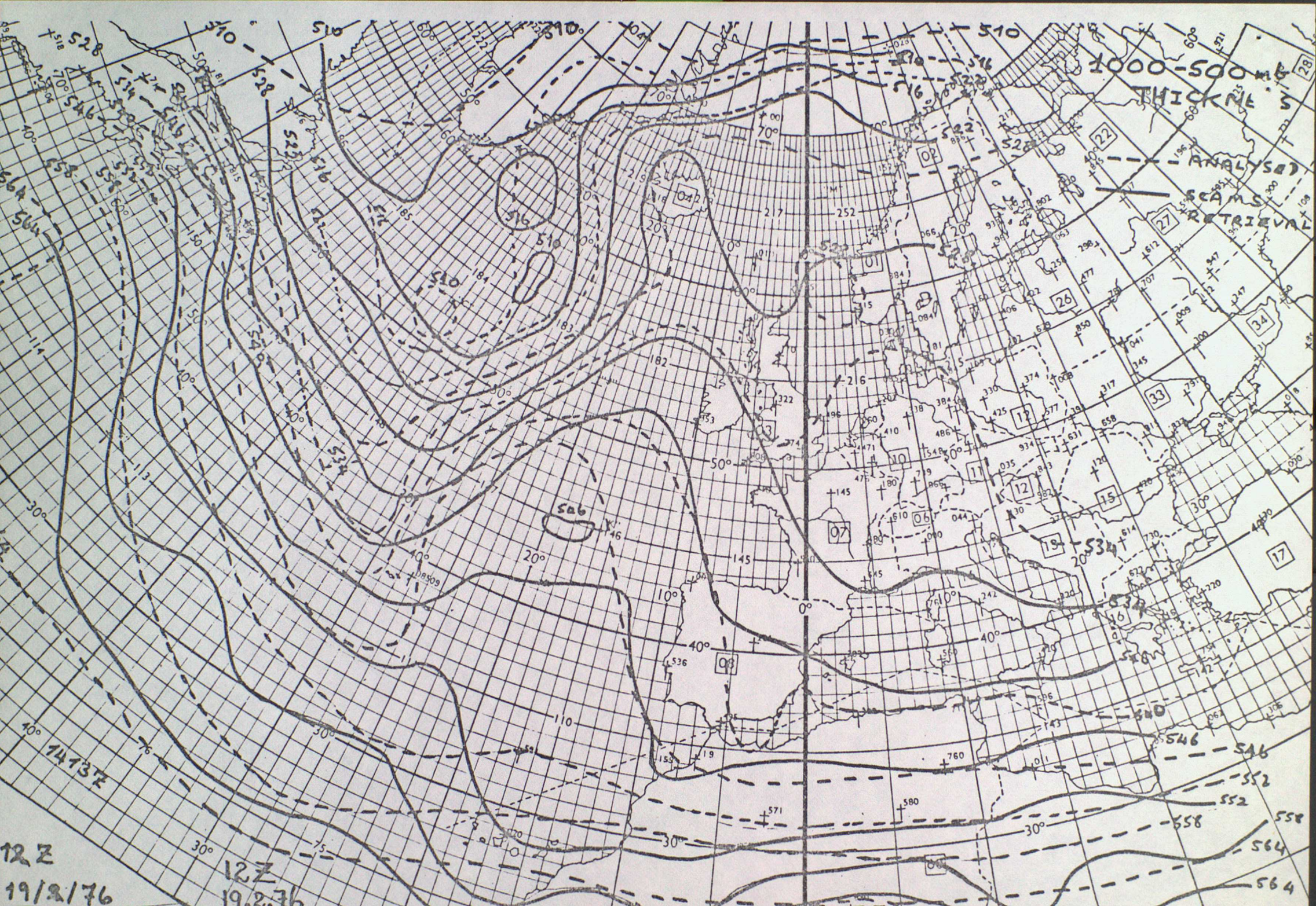
1000-500 mb
THICKNESS
ANALYSED
SCAMS
RETRIEVAL
12Z
19/2/76
12Z
19.2.76

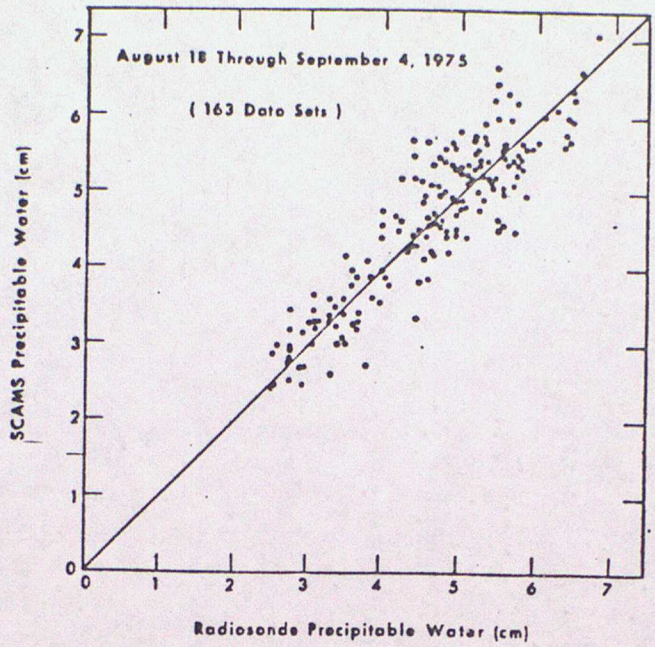

Fig 8. Comparisons of precipitable water derived from SCAMS and from nearby radiosondes (see Fig. 3) for the period 18 August–4 September 1975.

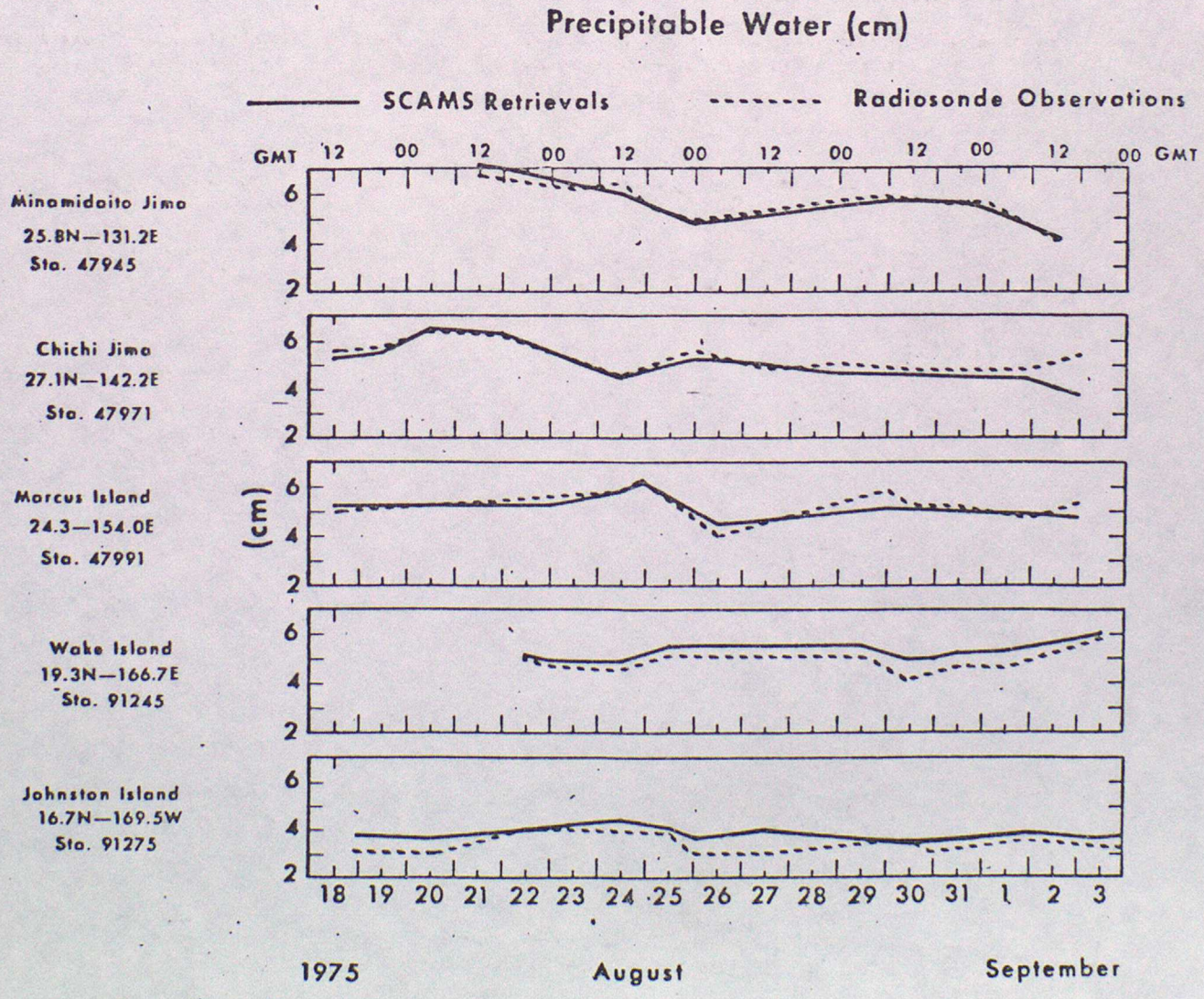

Fig. 9. Temporal variations of precipitable water obtained from SCAMS compared with that of five nearby radiosondes.

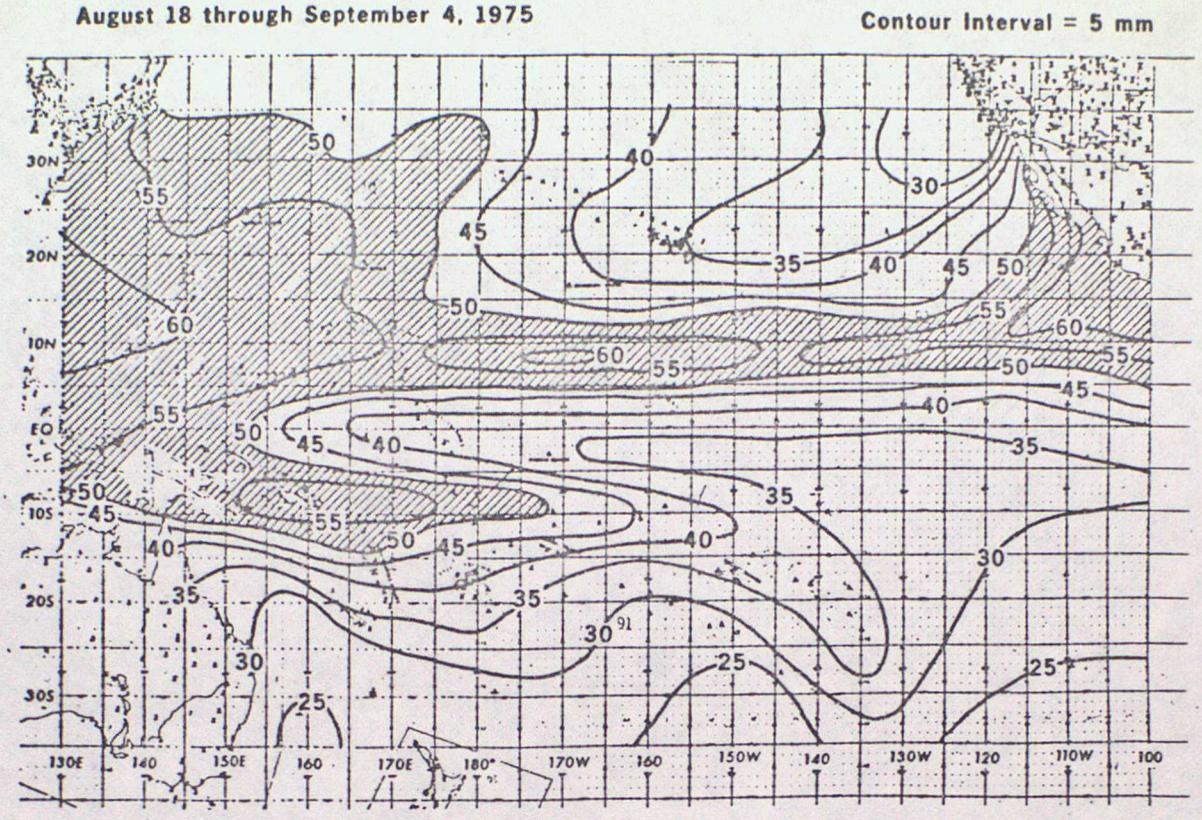

Fig 10. Mean precipitable water (mm) derived from SCAMS for the period 18 August–4 September 1975. Shaded area includes greater than 50 mm of precipitable water. Land areas are free of contours.

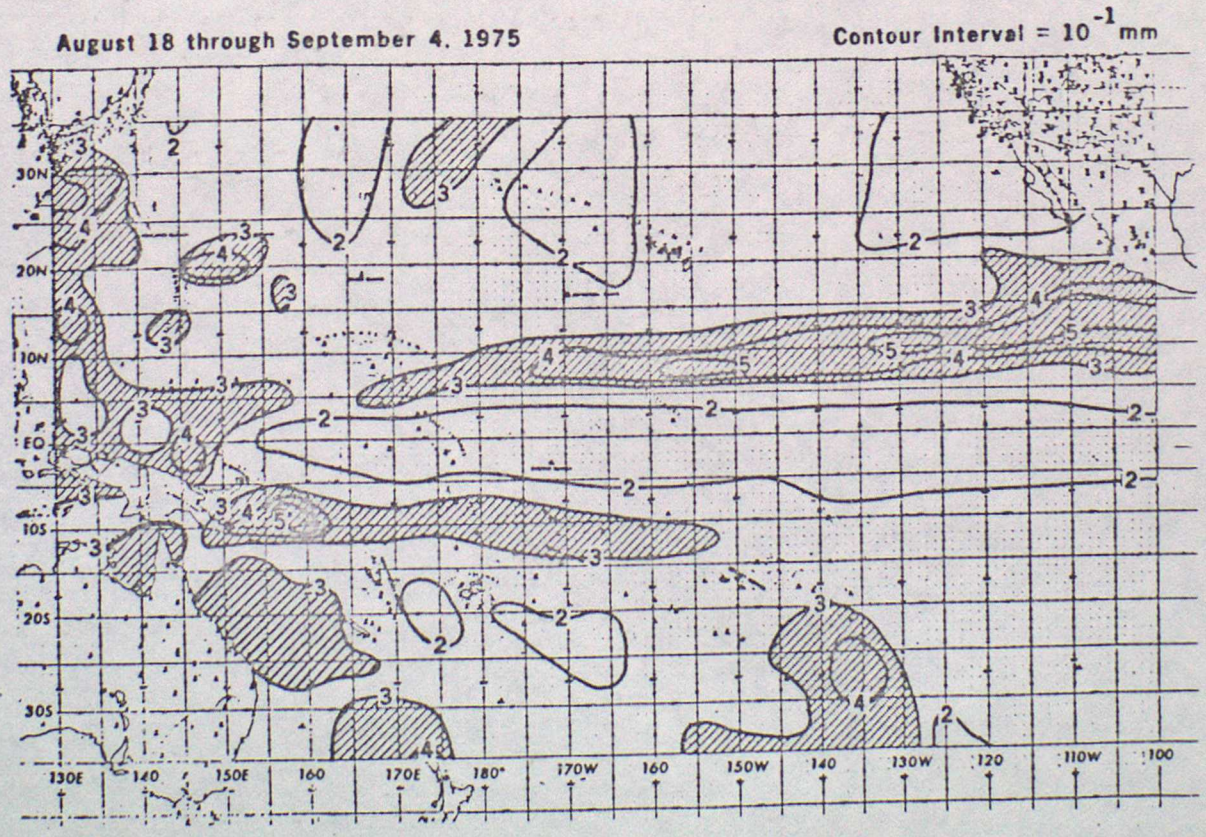

Fig 11. Mean liquid water (10^{-1} mm) derived from SCAMS for the period 18 August–4 September 1975. Shaded area includes greater than 0.3 mm of liquid water. Land areas are free of contours.

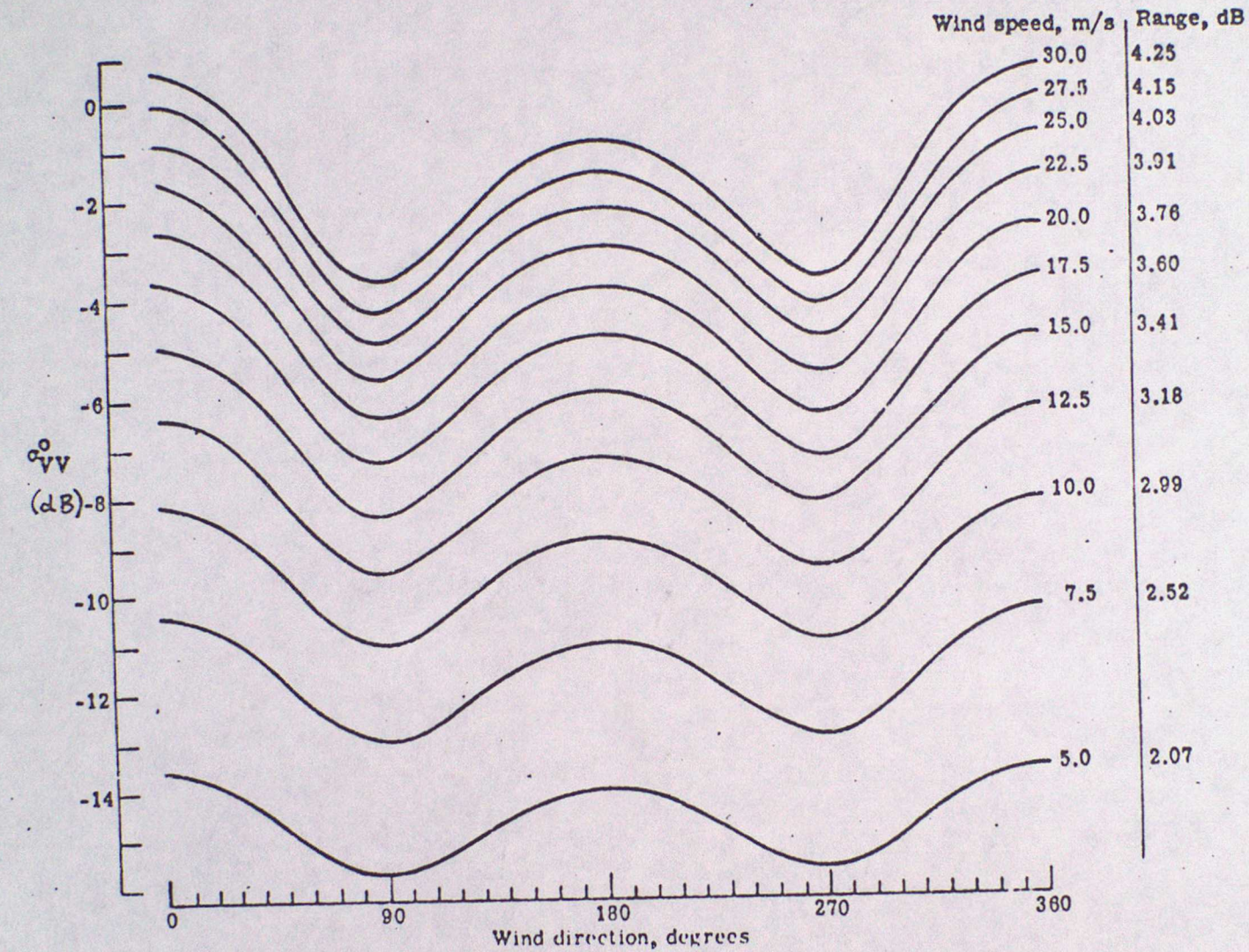

(a) σ^o_{VV} vs. wind azimuth angle.

Figure 12. Scattering coefficient dependence on wind azimuth angle at $\vartheta_i = 30^o$.

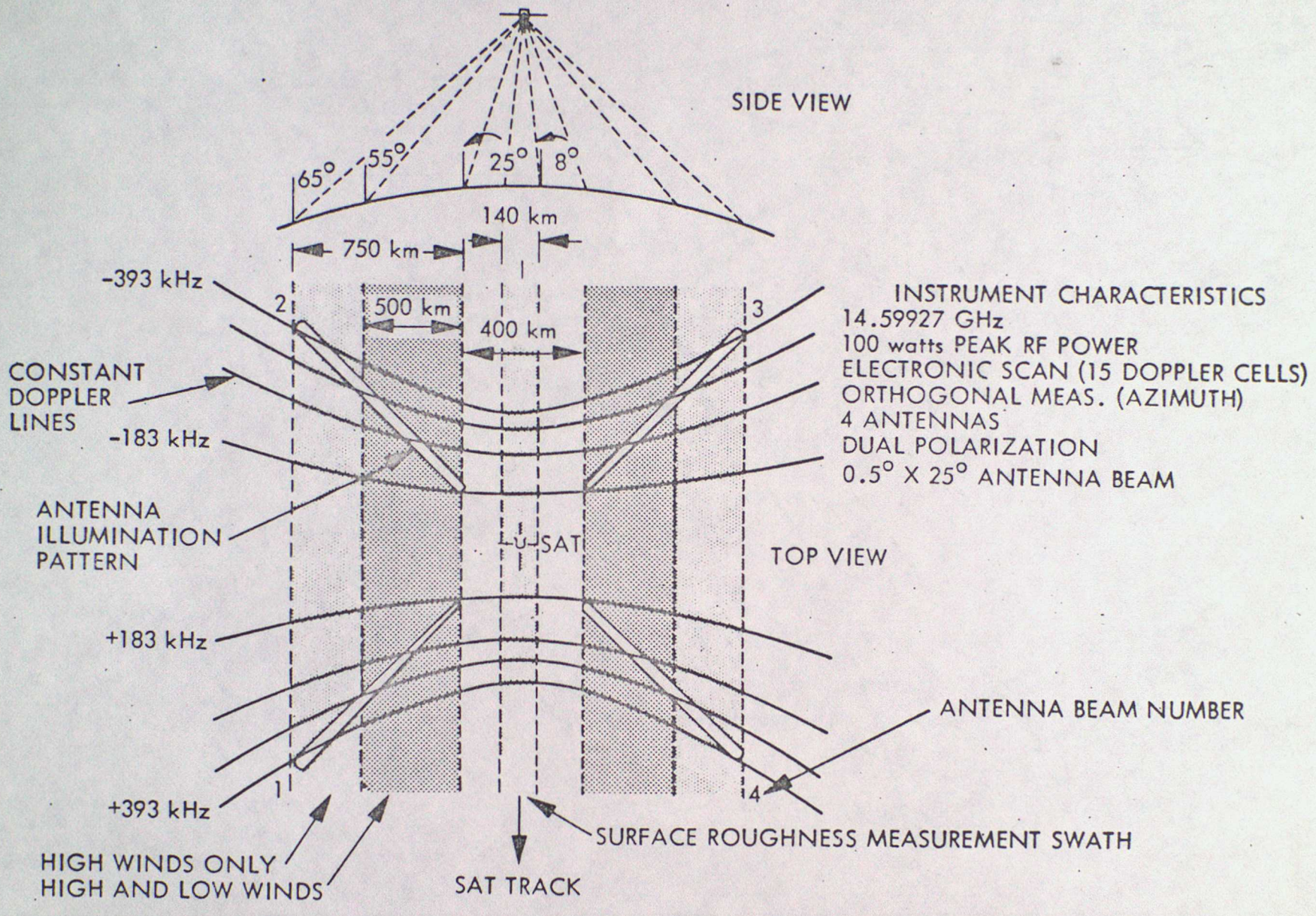

Figure 13. Scatterometer Ground Pattern and Swath

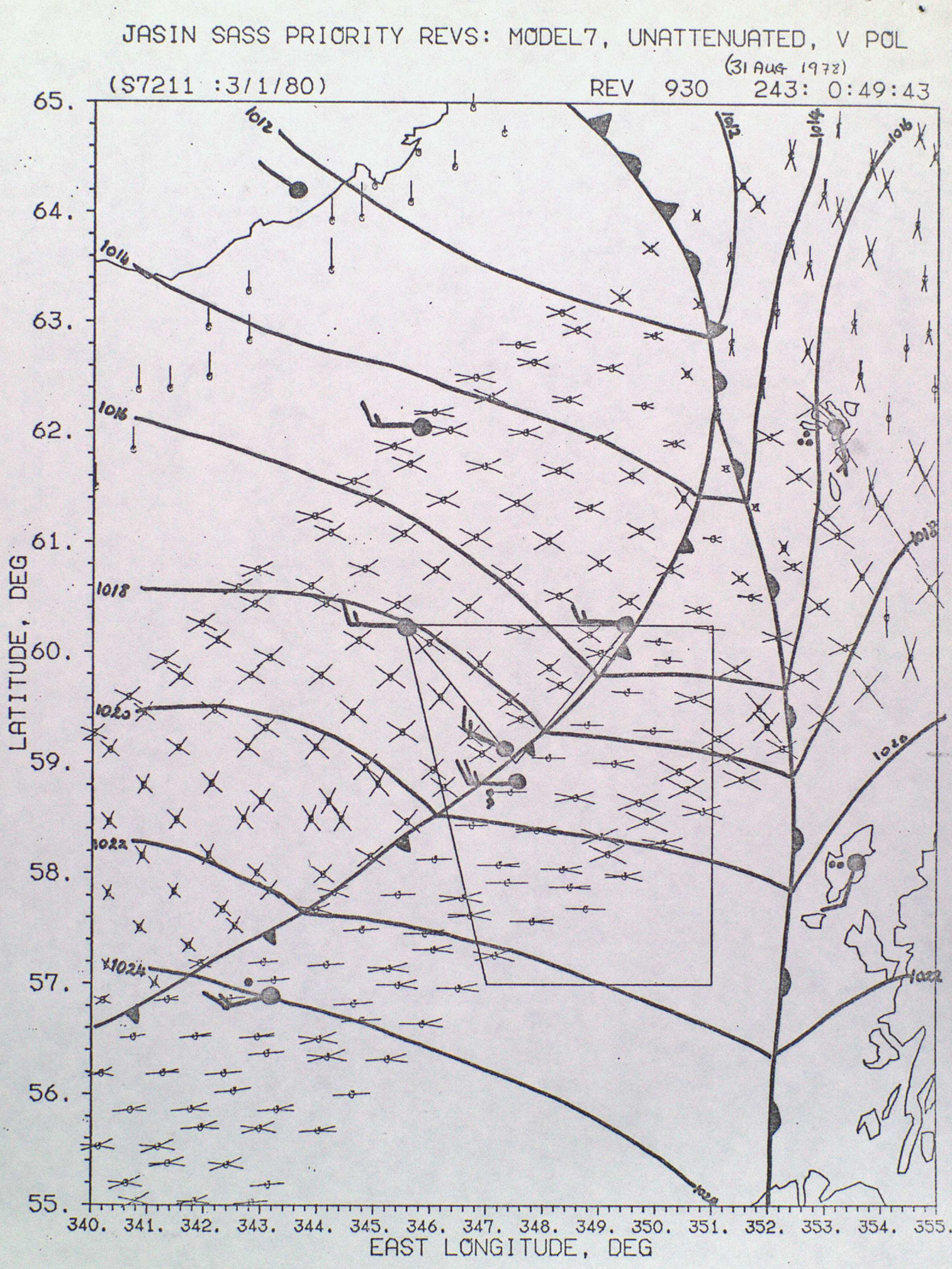
JASIN SASS PRIORITY REVS: MODEL7, UNATTENUATED, V POL
(31 AUG 1978)
(S7211 :3/1/80)
REV 930 243: 0:49:43
1012
1012
1014
1014
1016
1016
1018
1018
1020
1020
1022
1022
1024
1024
1028
LATITUDE, DEG
65.
64.
63.
62.
61.
60.
59.
58.
57.
56.
55.
340. 341. 342. 343. 344. 345. 346. 347. 348. 349. 350. 351. 352. 353. 354. 355.
EAST LONGITUDE, DEG

Figure 14.

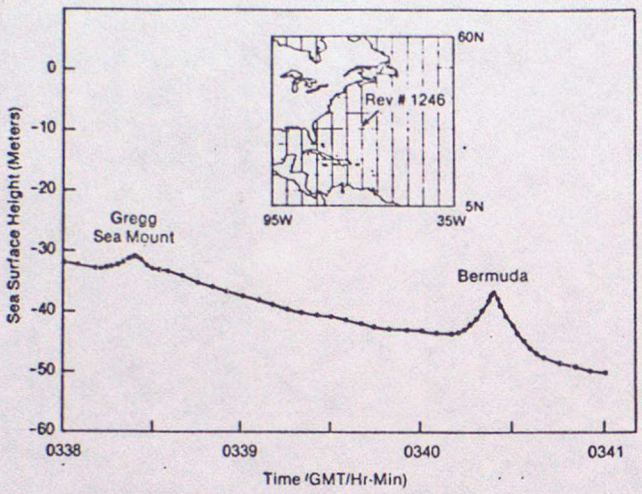

Fig. 15 Sea surface height over sea mount-type features.

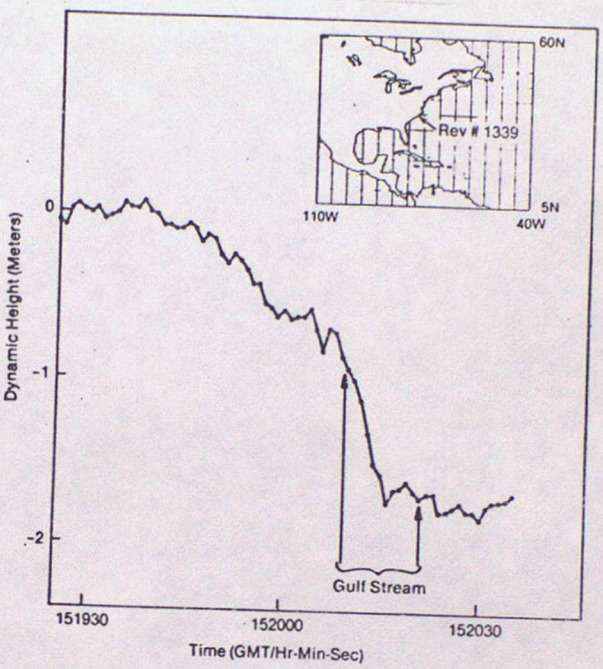

Fig. 16 Dynamic height over Gulf Stream [12].

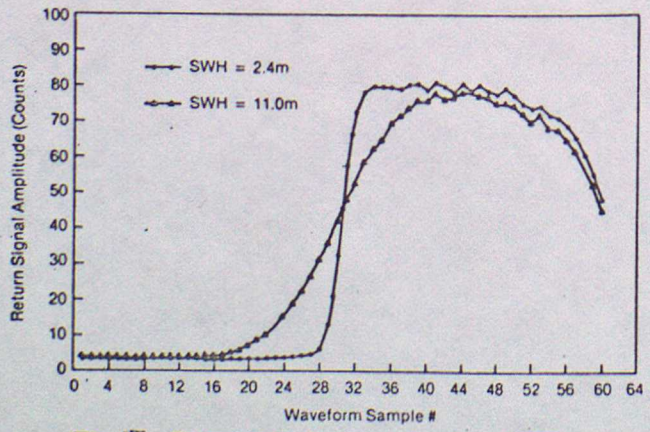

Fig. 17 Return pulse shape as a function of SWH.

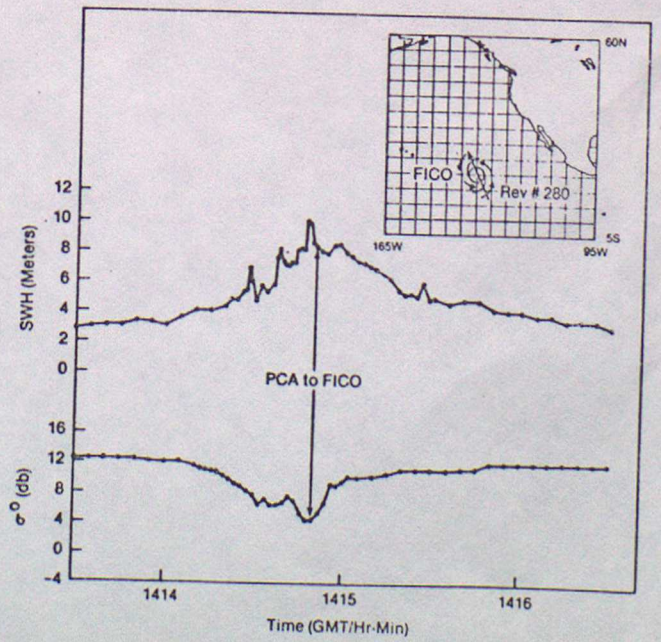

Fig. 18 Altimeter measurements over Hurricane Fico.

ADVANCED LECTURES - 1981

Satellite Meteorology

9 RESEARCH AND FUTURE POSSIBILITIES (Miller)

1 Satellite observations for meteorological research

This section provides brief reviews of two areas in which satellite observational techniques are important.

A Radiation Balance

Satellites can provide observations of the three main components of the radiation budget of the earth-atmosphere system: the solar input, outgoing (reflected) short-wave radiation and emitted longwave radiation. Instruments on satellites can monitor in-coming solar radiation un-impeded by the variability of the atmosphere, and could provide long continuous series of observations from which the "solar constant" can be studied. Heath (1973) reported observations in various spectral passbands in the ultraviolet; he detected significant variability at wavelengths below 200 nm. However, measurements on the total solar spectrum require a precision of 0.1%, and comparable long-term stability. Achievement of this performance has proved very difficult, but various cavity radiometers are now available (eg Smith et al, 1977).

The out-going components of the radiation balance are variable in both time and space because of clouds and the diurnal cycle of solar illumination. The reflectivity of the earth's surface varies with wavelength, according to the surface, is non-isotropic and depends on solar zenith angle. Satellite instruments can only sample the outward flux through the spherical shell at orbital radius, whereas our interest is generally in averages over days or weeks and in spatial scales of a few hundred kilometers within the earth's atmosphere. One must design any instrumentation (and select the orbits of the satellites on which they are mounted) in such a way as to obtain a representative sample of the outgoing fluxes. Earliest observations were made with spectrally non-selective wide-angle field-of-view sensors (see Ellis et al, 1978, for a review). However, these have in-adequate spatial resolution ($\sim$ 2000km). Visible and infra-red imagery from operational polar-orbiting meteorological satellites is being used for radiation budget studies (eg Gruber, 1977). In this case wavelength dependence of the fluxes must also be parameterized in order to infer total fluxes from measurements made in rather narrow spectral bands. The Earth Radiation Budget (ERB) experiment flown on Nimbus-6 and 7, incorporating a multi-spectral scanner of modest spatial resolution as well as radiometers, designed to obtain information on angular scattering properties of typical clouds and to investigate spectral parameterisation schemes (Smith et al, 1977). First results from ERB, in terms of planetary radiation budget, were given by Jacobowitz et al (1979).

However, observations from sun-synchronous orbit provide a poor sample of the range of solar zenith angles and of diurnal fluctuations in cloudiness (convection over land) and land surface temperature. The latter may be investigated using observations from geosynchronous satellites (Saunders and Hunt, 1980).

An experiment is to be mounted, starting around 1984, in which ERB packages are to be flown simultaneously on two Tiros-N series operational spacecraft (in sun-synchronous orbits, about 6 hours apart) and on a special spacecraft (ERBS). The latter will be in an orbit of inclination about 55°, so the orbital plane will precess (see Lecture 1) allowing the full range of local solar time to be explored several times during the course of a year. This venture is known as the Earth Radiation Budget Experiment (ERBE). (For further information, contact Dr G E Hunt, UCL, who is on the Experiment Team for ERBE. Also see Vonder Haar & Wallschlaeger (1978).)

Satellite data may also be used to estimate radiation at the ground, particularly by providing a measure of cloudiness. Tarpley (1979) and Gautier et al (1980) have used visible GOES imagery and demonstrated accuracies of about 10% in daily cumulative insolation by comparison with surface pyranometer observations. Areas of difficulty include estimation of radiation under overcast skies (joint use of infra-red data may give a partial indicator of cloud thickness). The schemes will not work when the ground is snow-covered.

B Composition and temperature of stratosphere/mesosphere

Earlier lectures have described the basis of the temperature sounding technique as applied to operational meteorology and its extension to humidity sounding. These techniques can be applied at higher levels in the atmosphere and to gases whose mixing ratios are $< 10^{-6}$ by directing the instrument's view at the earth's limb (see Fig 1). The instrumental view must be defined by a narrow slit, aligned parallel to the local horizon. Vertical profile information may be obtained by scanning this slit in the direction normal to the horizon. The 'weighting functions' for each position of the slit can be derived by convolving:

- the distribution of absorber density with height;
- the geometrical weighting, (which is zero below the tangent height, increases to its peak at the tangent height and decreases above);
- the height smoothing caused by the width of the slit.

A set of typical weighting functions are shown in Figure 2. The large increase in geometrical path within atmospheric layers above the tangent height serves to enhance the emission (and so minimum detectable mixing ratio). The cold space background, against which the emission is viewed, is also beneficial. Geometrical weighting provides a sharpening of the weighting function relative to those obtained by conventional "vertical" sounding. However, limb geometry produces horizontal averaging, over 500-1000 km and a much poorer coverage of observations. The view is normally from one side of the satellite, at 90° to the orbital velocity vector (to minimise Doppler shift of spectral features in atmosphere and instrumental absorption cells). Determination of scan position relative to the horizon places stringent requirements ($\sim .01°$) on roll stability of the spacecraft, which are not achieved by the Nimbus spacecraft on which these instruments have been flown.

Gille, Bailey and Russell (1980) have described their Limb Infra-red Monitor of the Stratosphere (LIMS) experiment which was flown on Nimbus-7 and designed to measure temperature and profiles of O_3, H_2O, NO_2 and HNO_3. Drummond et al (1980) have described the Oxford University Stratospheric and Mesospheric Sounder (SAMS)

which also flew on Nimbus-7, to measure T, CO, CH_4, NO, N_2O and H_2O. In both cases, data analysis has been hampered and ultimate accuracy will be dictated, by roll performance of the spacecraft.

Limb-measurements of atmospheric attenuation, made using the Sun as source, have also been used to measure profiles of aerosol and ozone. This "occultation geometry" confines observations to sunrise and sunset, so that only about 15 atmospheric profiles are obtained each day. A modern experiment of this type has been described by McCormick et al (1979).

2. The Future

A Extended use of existing products and data

The degree of exploitation of existing satellite products varies very much from Met Service to Service. Those which operate satellites have most incentive to get a return on the cost of the satellites. With the Meteosat programme, the Office has moved into the operator category. Full exploitation of data involves substantial investment in facilities; this is difficult to justify without assurance of continuity of the satellites. For imagery the Office is steadily extending its distribution network (SATFAX) to out-stations. Facilities now exist in CFO for display of imagery on a TV screen, permitting a number of images to be viewed in sequence (particularly important for Meteosat imagery). The FRONTIERS project is using satellite imagery to supplement networked radar data in short period forecasting of rainfall (Browning, 1979).

With regard to soundings, the new numerical forecast model will have a 6 hourly analysis cycle, enabling more of these asynoptic data to be exploited. It has recently been proposed that locally-received radiances should be processed at Bracknell, to generate higher spatial resolution soundings.

B Plans for satellites

i) Polar-orbiters

NOAA/NESS have indicated that they propose to continue the TIROS-N series of polar-orbiting satellites, with declared launchings extending to at least 1987. No major changes of operational instrumentation are expected before 1987, but an improved multi-channel microwave sounding unit (AMSU), which would replace the present MSU and SSU, may be developed by NOAA. From about 1984 the satellite will be lengthened, to carry other instruments for atmospheric monitoring (eg ERB, see 1 A above, and SBUV for ozone). The spacecraft will then be known as the Advanced TIROS-N (ATN).

Various oceanic monitoring satellites are being planned. These should provide semi-operational observational services of surface winds, significant wave height and perhaps other wave data. Such information may be useful for off-shore forecasting activities. The US National Oceanic Satellite System (NOSS) was the most ambitious of these proposals, but following budget revisions its status is doubtful. It could not be available before 1987. The European Space Agency are proposing ERS-1, but the decision on whether to proceed will not be made until autumn 1981. The Japanese are working on a rather simpler satellite (MOS) for similar purposes.

On the research side, mention has already been made of ERBS. The Nimbus series is now complete, although several experiments continue to provide data. The Upper Atmosphere Research Satellite (UARS) is likely to carry advanced limb-sounding radiometers and perhaps experiments to measure upper winds. It is due to be launched in 1986-7 and the Office (Met O 20) expects to be involved in data analysis and interpretation. Shuttle/Spacelab will be used to provide short period "Test flights" of new instruments and to fly heavy power-hungry instruments (eg lidar systems). The Office (Met O 15, Dr Tuck) are involved in an experiment to measure minor constituent profiles (HALOE). One element of the Shuttle system is TDRSS, a telecommunications satellite system which will be used to relay data in real-time from polar orbiters to the USA. This system will ultimately remove the need for on-board data storage and the associated delay in recovery of data for processing.

ii) geosynchronous satellites.

The US have recently launched GOES-4 and at least two more similar spacecraft are being prepared. These spacecraft are compatible with earlier GOES spacecraft, but have more complex spin-scan radiometers known as VAS with multiple detectors and spectral channels. These can be used either to provide high spatial and temporal resolution soundings or normal imagery. Soundings are at present a research activity. A second Meteosat is to be launched in June 1981. Discussions are underway aimed at establishing an operational series of Meteosats from 1986. This will involve heavy financial support from the Office (~ £2½M/year). The Japanese will launch GMS-2 this year to continue their observations from 140°E. An Indian telecommunications satellite, INSAT-1 will carry an imaging system (at 74°E), probably within the next year. An ESA telecommunications satellite, SIRIO-2 will be used to demonstrate telecommunications links between regional and national Met centres in Africa.

C New instrumental techniques

Proposals now exist for instruments to measure two parameters of meteorological importance which have previously been out of reach; surface pressure and winds (in clear air). In both cases, one of the methods is being investigated in the UK.

Flower and Peckham (1980) of Heriot-Watt University propose to measure surface pressure by determining the attenuation of microwave radiation, transmitted from the satellite and reflected back by the ocean surface. The primary measurement would be made in the absorption band of molecular oxygen, at about 52 GHz. Measurements at about 5 other frequencies between 30 and 70 GHz would provide corrections for reflectivity of the ocean surface, atmospheric water (vapour and liquid) and temperature distribution. Simulation of performance under cloud-free and total cloud conditions indicates an rms error of about 1.5 mbar. A simplified form of the experiment is being tried out by NASA from an aircraft later this year. Supporting experimental and theoretical work is being done at the Appleton Laboratory and in Met O 19. Our own studies are exploring the probable accuracy under meteorologically active conditions and the possible impact of the measurements on

operational meteorology. Coverage of observations will be rather sparse, since measurements are possible only within about 14° of the nadir.

An alternative form of the experiment exploits narrow absorption lines of oxygen at around 0.7 micron, (Smith and Platt, 1977), a laser would be used to generate radiation at two wavelengths, one in an absorption line, the other alongside it. Naturally this technique could not work through continuous cloud cover (although pressure at the cloud top would be a useful by-product).

Both techniques for measuring winds depend on measuring the Doppler shift associated with the velocity of the scatterer. Rees (1980) at UCL proposes to detect shifts of atmospheric absorption lines (mainly due to H_2O or O_2) or Fraunhofer lines in sunlight scattered by air molecules, aerosol or clouds. He anticipates accuracies of 3-5 ms^{-1} with spatial resolution about half a scale-height and 300km horizontally. The instrument involves very high spectral resolution Fabry-Perot interferometers. The technique has been used to study winds in the thermosphere. Being a passive device, its power requirements are small and the experiment has been proposed for the Upper Atmosphere Research Satellite.

The alternative proposal, by Huffaker et al (1979) again exploits a laser; radiation would be scattered by natural aerosol including clouds. Accuarcies of order 1 m/s with good vertical resolution are promised. This experiment demands substantial power and weight and is not a candidate for a free-flying satellite during this decade.

3 Availablity of satellite data

Satellite imagery is useful to many research projects. This section identifies the main sources for past data. For TIROS-N imagery, low-resolution data is stored on the spacecraft and global mosaics are compiled by NOAA/NESS. Such data is available as photographsor on tape, through NOAA's Environmental Data and Information Service (EDIS). The Visual Aids Librarian and Met O 19 hold bulletins which list EDIS stocks. A monthly NOAA publication (EDIS, Key to Met Records Documentation No 5.4, Environmental Satellite imagery) shows the daily mosaics and is a useful check on completeness of coverage on the required date. The Library (Visual Aids) keeps copies of one of the AUTOSAT mosaics for each day, on 35mm film.

High resolution polar-orbiter imagery is not generally available from NOAA, since this is essentially a direct broadcast product. The University of Dundee (funded by NERC) receive and archive AVHRR imagery for the UK and surrounding area, (and also VHRR prior to 1978). They can provide high quality photos and magnetic tapes. Met O 15 (Tom Oliver) can assist with arrangements to acquire data from Dundee. AVHRR data can also be obtained by prior arrangement from the Remote Sensing Centre (RAE Farnborough). The Remote Sensing Centre has powerful image display facilities, which can be used to explore the imagery. Dr Brownscombe, Met O 19, can provide further information on this facility. Geostationary satellite imagery is available from satellite operators. In some cases their archives may be incomplete, or only available in photographic formats. Data from US satellites can be obtained from EDIS. Met O 19 (John Bedford Smith) can assist in acquiring

Meteosat data from ESA. ESA issue a monthly Image Bulletin, showing the midday images in three spectral channels, and identifying images available in their archive. The Japanese Met Satellite Centre issue a Monthly Report, listing products (nephanalyses, winds etc) extracted from GMS images and the images which have been archived.

Information on the various satellite systems can be found in the references to Lecture 1. Met O 19 will endeavour to provide or obtain such further details as users may require.

4 Conclusion

In this series of lectures we have tried to show some of the ways in which satellites can and are serving meteorology. Inevitably, some areas have had to be left out. Recent review papers listed at the end of Lecture 1, and some more specific papers, listed at (d) below, may help to fill these gaps.

In introducing this series I set out the major advantages which satellite techniques have brought:

- new types of information, through essentially simultaneous observation of large areas;
- more observations, particularly important in data sparse ocean areas;
- more consistent observations, through use of a single instrument to observe over wide areas;
- rapid means of collecting and distributing observations, which can be rather economic when such facilities are a small addition to an operational meteorological satellite.

I hope the lectures have given you some appreciation of these advantages.

Equally, the lectures should have given you a feel for the principal limitations of satellite techniques, which must be borne in mind when using satellite products. Particularly, you will recall that:

- satellite observations generally are averages over substantial areas and depths of the atmosphere, and smooth those smaller structures which in-situ techniques reveal. In some cases one may argue that this is an advantage (eg for input to global numerical forecast models); in others (eg location of inversions) it is a great disadvantage. Parameters which display substantial spatial variability (eg rain) will be very difficult to measure with useful precision because of practical problems related to instrumental resolution.

- observations made from polar-orbiting satellites have limited time resolution, and cannot detect fluctuations on scales below about 12 hours. Conventional observations often provide little better resolution, but parameters with large time variability (eg rain, surface radiation) will remain difficult to investigate. Of course, more satellites in orbit would reduce this problem.

- observations from polar-orbiting satellites are asynoptic, and so their effective assimilation presents special difficulties to the analyst.

- the atmosphere must be viewed from above, so clouds have a major impact on coverage and information is not available on cloud-base (or cloud layers below a complete upper layer of cloud).

- many satellite techniques contain an empirical element, which can be "tuned" to give best performance but remains a potential source of error in un-usual (and often meteorologically important) situations.

Satellite techniques have advanced rapidly and will continue to do so. We must learn to make best use of satellite products alongside conventional observations, with an awareness of their respective strengths and weaknesses.

REFERENCES

a) Radiation Budget

Heath, D "Space observations of the variability of solar irradiance in the near and far ultraviolet" J Geophys.Res (1973) 78, 2779-2792

Smith W L et al "Nimbus 6 earth radiation budget experiment" Applied Optics (1977) 16, 306-318

Ellis, J S et al "The annual variation in the global heat balance of the earth" J Geophys Res (1978) 83, 1958-1962

Gruber, A "Determination of the Earth-Atmosphere radiation budget from NOAA satellite data" NOAA Tech Rept NESS 76 (1977)

Saunders R W & Hunt G E "Meteosat observations of diurnal variation of radiation budget parameters" Nature (1980) 283, 645-7

Jacobowitz et al "The first 18 months of planetary radiation budget measurements from the Nimbus-6 ERB experiment", J Atmos Sci (1979) 36, 501-7

Vonder Haar T & Wallschlaeger "Design definition study of the ERBSS" NASA Contract Rept CR-158934 (1978)

Tarpley, J D "Estimating incident solar radiation at the surface from geostationary satellite data" J Appl Met (1978), 18, 1172-1181

Gautier C, Diak G & Masse S "A simple physical model to estimate incident solar radiation at the surface from GOES Satellite Data" J Appl Met (1980) 19, 1005-1012

b) Temperature and composition of upper atmosphere

Gille J C, Bailey P L & Russell J M "Temperature and composition measurements from the LRIR and LIMS experiments on Nimbus 6 and 7" Phil Trans R Soc (1980) A296, 205-218

Drummond J R et al "The stratospheric and mesospheric sounder on Nimbus 7" ibid pp 219-241

McCormick M P et al "Satellite studies of the stratospheric aerosol" Bull Amer Met Soc (1979) 60, 1038-1046

c) New instrumental techniques

Flower D A & Peckham G E "A microwave pressure sounder for the remote measurement of atmospheric surface pressure", Proceedings of CHARM WORKSHOP, ESA-SP 150 pp 189-192 (1980)

Rees,D "Global wind determination by interferometric techniques in the troposphere, stratosphere and mesosphere" ibid pp 193-206 (1980)

Smith,W L & Platt C M R "A laser method of observing surface pressure and pressure-altitude and temperature profiles of the troposphere from satellites" NOAA Technical Report NESS 89 (1977)

Huffaker R M et al "Global wind monitoring by satellite-borne coherent lidar" Bellingham, Wash, Soc Photo-Opt Instr Eng Proc (1979) 183, 283-291

d) other areas

Browning K "The FRONTIERS plan....." Met Mag (1979) 108,161-184

Bellon A, Lovejoy S & Austin G L "Combining satellite and radar data for the short-range forecasting of precipitation", MWR (1980) 108, 1554-1566

Lovejoy S & Austin G L "The sources of error in rain amount estimating schemes from GOES visible and IR satellite imagery" MWR (1979) 107, 1048-1054

Lovejoy S & Austin G L "The estimation of rain from satellite borne radiometers" Q J Roy Met Soc (1980) 106, 255-276

NOAA "GOES Data Collection System" NOAA Tech Rpt 78 (1979)

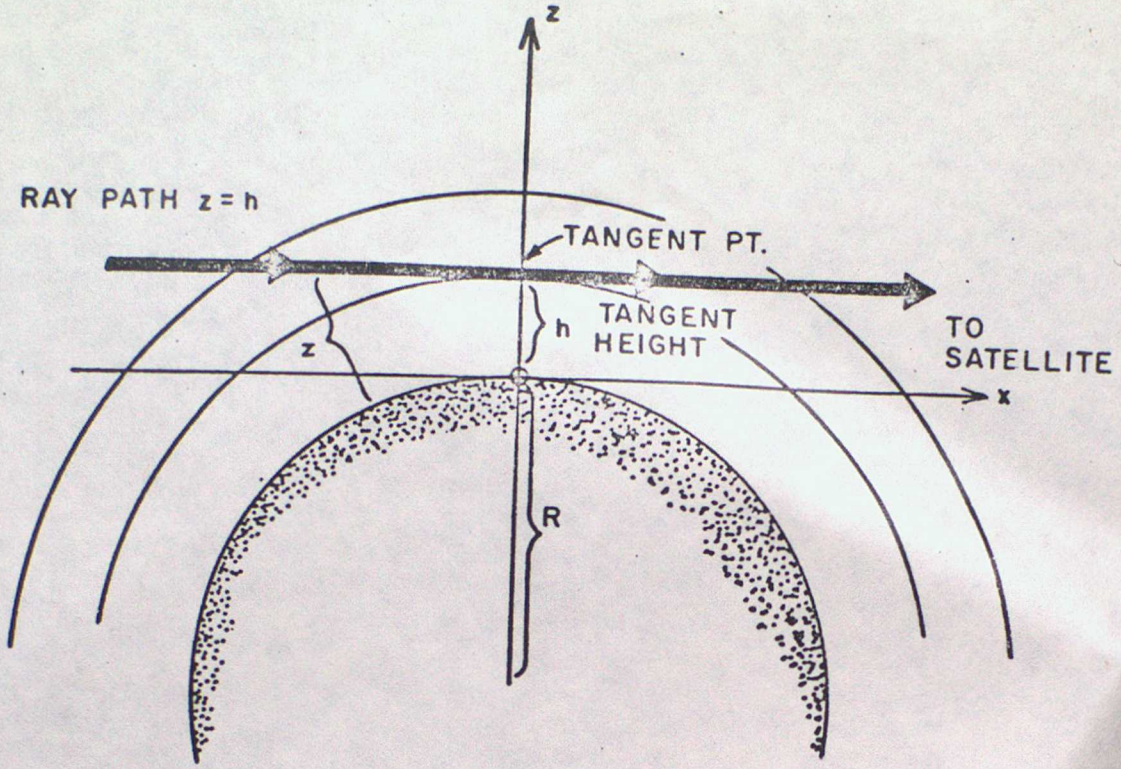

Figure 1. Geometry for limb sounding.

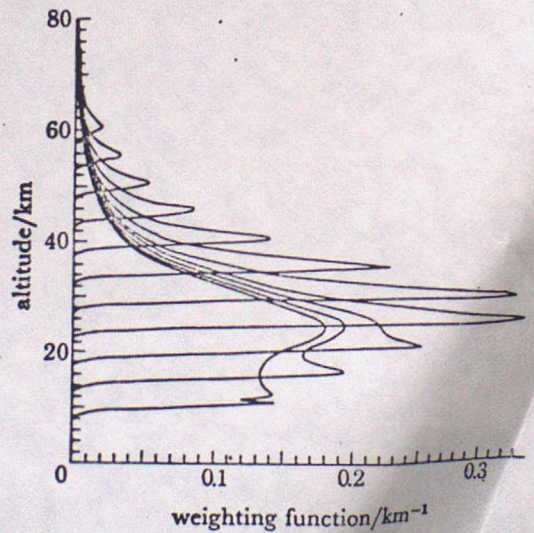

FIGURE 2. Representative weighting functions for the l.r.i.r. wide 15 μm CO_2 channel (WCO_2) used for temperature retrievals. These were calculated by convolving infinitesimal weighting functions (Gille & House 1971) with a nominal 2 km field of view. Actual weighting functions were spaced every 1.5 km in the vertical.

[Taken from Gille, Bailey & Russell, 1980]